UNITED NATIONS EDUCATIONAL, SCIENTIFIC AND CULTURAL ORGANIZATION
INTERNATIONAL CENTRE FOR THEORETICAL PHYSICS
I.C.T.P., P.O. BOX 586, 34100 TRIESTE, ITALY, CABLE: CENTRATOM TRIESTE

SMR.550 -28

SPRING COLLEGE IN MATERIALS SCIENCE ON

"NUCLEATION, GROWTH AND SEGREGATION IN MATERIALS SCIENCE AND ENGINEERING"

(6 May - 7 June 1991)

A STRESS CORROSION CRACKING MECHANISM BASED ON SURFACE MOBILITY

J.R. GALVELE
Gerencia de Desarrollo
Comision Nacional de Energia Atomica
Avda. Libertador 8250
1429 Buenos Aires
Argentina

These are preliminary lecture notes, intended only for distribution to participants.

A STRESS CORROSION CRACKING MECHANISM BASED ON SURFACE MOBILITY

José R. Galvele

Departamento Materiales, Comisión Nacional de Energía Atómica,
Avda. Libertador 8250, Buenos Aires 1429, Argentina

Abstract—A mechanism for stress corrosion cracking (SCC) is developed from simple metallurgical principles and assuming that high surface mobility is present in the process. An equation is found for crack velocity as a function of surface mobility and stress concentration at the tip of the crack. This mechanism is shown to predict SCC specificity, as well as the effect of temperature on SCC, and the enhancement of crack velocity by hydrogen. A correlation between SCC, liquid metal embrittlement and hydrogen embrittlement of non-hydride forming metals is established.

INTRODUCTION

The problem of environment-sensitive fracture which is over a century old,[1,2] is of great technological and scientific interest, and has given place to many thorough reviews, meetings and publications.[3–11] Numerous mechanisms have been proposed to explain stress corrosion cracking (SCC), hydrogen embrittlement (HE) and liquid metal embrittlement (LME).[1–10] One of the big limitations of most of the available mechanisms is that, as pointed out by various authors,[12–14] great similarities are to be found in the embrittlement phenomena, but none of the available mechanisms seems to give a satisfactory explanation of such similarities. Another serious limitation[1,2] is that with the available mechanisms we are still unable to predict new cases of environment-sensitive fracture.

The purpose of the present paper is to discuss a new mechanism of environmental embrittlement which, although still very speculative in nature, has the following attractive qualities:

(1) it gives account of most experimental observations in SCC and LME;
(2) it joins SCC, LME and some cases of HE in just one mechanism;
(3) it can be extended to non-metallic solids;
(4) it allows the prediction of new cases of environment embrittlement; and
(5) it is susceptible of simple experimental verification.

As suggested in two recent publications,[15,16] high surface mobility would be the only common factor to be found in SCC in liquid environment, SCC in gaseous environments and LME. A solid material subjected to a tensile stress can relax that stress either by glide motion of dislocations, by dislocation creep, by diffusional flow or by developing cracks perpendicular to the direction of the tensile stress. If the stress is lower than the flow stress no dislocation glide will be observed.[17] If, at the same time, the temperature is below 0.5 T_m, T_m being the melting point of the material in K, dislocation creep and diffusional flow will be too slow to be detected.[17] The present mechanism[16] suggests that under those conditions, if a sufficiently high

Manuscript submitted 20 June 1986.

surface mobility is induced by the environment, the stresses will be relaxed by cracks growing into the material. In the present paper such a mechanism is developed, assuming that cracks will grow by the arrival of surface vacancies to, or emission of adatoms from, the bottom of the crack. According to Rhead[18] high surface mobility is produced by low melting point contaminants on the metal surface. In this way specificity in producing SCC can be explained, and compounds capable of inhibiting SCC can be detected. The presence of hydrogen, by interaction with vacancies, will accelerate the cracking process.

THE CRACK PROPAGATION MECHANISM

When a crystal is stressed, the equilibrium concentration of vacancies is different from that in the absence of stresses.[19] The concentration will be higher than thermal equilibrium if the stresses are tensile, and lower if they are compressive. At high temperatures, close to the metal melting point these changes in vacancy concentration are responsible for the Nabarro–Herring creep.[20] Under higher stresses, and with high surface mobilities, intergranular creep cracks, growing by surface diffusion, are also observed.[21-23]

At temperatures at which SCC is usually found, below 0.5 T_m, the above processes become so slow that they are of little practical interest.[17,23] Attention will now focus on what happens at these low temperatures if the surface diffusivity becomes abnormally high. Figure 1 shows schematically the atom distribution at the bottom of a stressed crack. For didactical purposes the atom distribution in Fig. 1 follows the crack tip geometry found by deCelis and coworkers[24] through molecular dynamics simulation of crack tips in alpha-iron. Usually, as a result of the emission of dislocations from the bottom of the crack, the growing cracks will be wider than those of Fig. 1. Nevertheless, as shown by Paskin *et al.*,[25] the width of the cracks, at an atomic level, has little effect on the stress concentration at the bottom of the crack, and the conclusions to be drawn from Fig. 1 will be valid also for cracks of different shape.

Following the reasoning used by Nabarro for creep,[19] an energy U_v is required to form a vacancy in a stress free region. If the area exposed by each atom to the stress σ is a^2, then the work done by the stress on removing the atom is σa^3, and the effective energy of formation has become $U_v - \sigma a^3$. In thermal equilibrium, the concentration of vacancies, C, on a tensile region will be:

$$C = C_0 \exp\left(\frac{\sigma a^3}{kT}\right) \tag{1}$$

C_0 being the thermal equilibrium concentration of vacancies in the stress free region; T the temperature in degrees K; and k the Boltzmann constant. The equilibrium concentration, C, will be reached by interaction of the lattice with the most common sinks and sources of point defects, like surfaces, dislocations, grain boundaries, etc.[26] This interaction will involve surface, grain boundary and volume diffusion. Nevertheless, at the temperatures considered, the volume and grain boundary diffusion coefficients are so low that no significant changes are observed.

The transition A–B, in Fig. 1, introduces a vacancy into the lattice site A, and will be favoured by the tensile stresses. But again, in the presence of an atomically clean surface, and at the temperatures considered, the surface diffusion coefficient, D_s, is so low that this effect will remain undetectable.

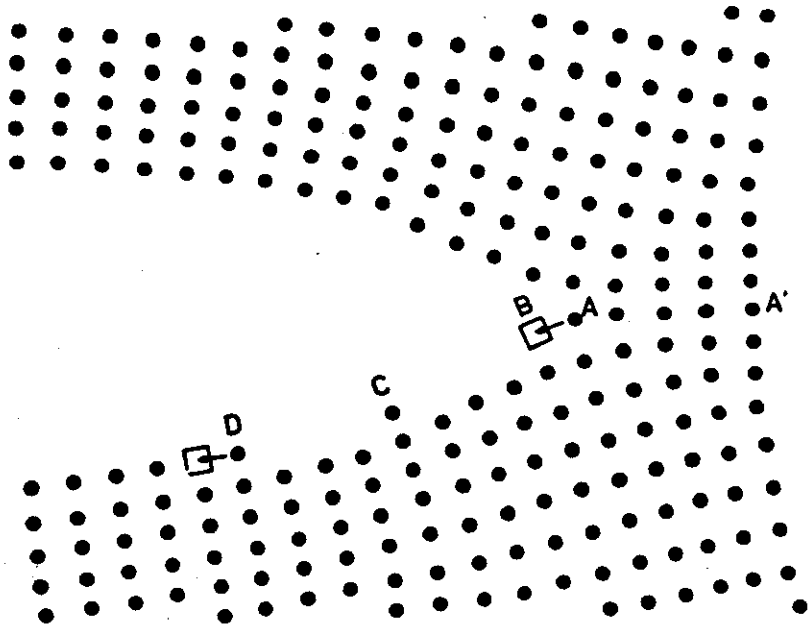

FIG. 1. A schematic description of the surface mobility cracking mechanism. Stresses, at the tip of the crack, will favor the A–B exchange, introducing a vacancy at the tip of the crack, and advancing the crack one atomic distance. The rate determining step will be the rate at which the excess atoms, C, are transported, by surface diffusion, from the tip of the crack to a new lattice site: B–D. (Atoms distribution from de Celis *et al.*[24]).

If, on the other hand, the surface diffusion coefficient, D_s, is high, the adatom produced by the exchange A–B will move along the crack surface, B–C–D, giving way to new A–B exchanges. These A–B exchanges will introduce an excessive concentration of adatoms on the crack surface, C, that will be annealed out as soon as those adatoms reach kink sites on the surface, D. If instead of using a description of surface diffusion based on adatoms, surface vacancies are considered, the above description is still valid.

During the A–B exchanges when a vacancy takes its place at A, the stressed lattice will partially relax, and the crack will advance one atomic step. This will lead to the crack propagation process, that in Fig. 1 will be equivalent to the relocation of the atoms in the plane A–A'. Figure 1 shows the propagation of a transgranular crack, but the same reasoning is valid if a grain boundary is present along A–A'.

It is possible to calculate crack velocity, V_p, when propagation occurs by this mechanism. The difference in vacancy concentration between the stressed and the stress-free region will be:

$$C - C_0 = C_0 \left[\exp\left(\frac{\sigma a^3}{kT}\right) - 1 \right]. \tag{2}$$

To calculate the vacancy concentration gradient, the distance L between the stressed and the stress free regions must be found. Under high surface mobility conditions the surface layers will be expected to be in equilibrium with the lattice atoms close to the surface, and any gradient in vacancies between stressed and stress-free regions should be reflected by an equal gradient in the surface defect concentration. The present mechanism is only concerned with stresses that reach the surface. In a crack there will be a high stress concentration on the surface at the tip of the crack.[27] This will not be the case with the surfaces at the sides of the crack. From atomic crack

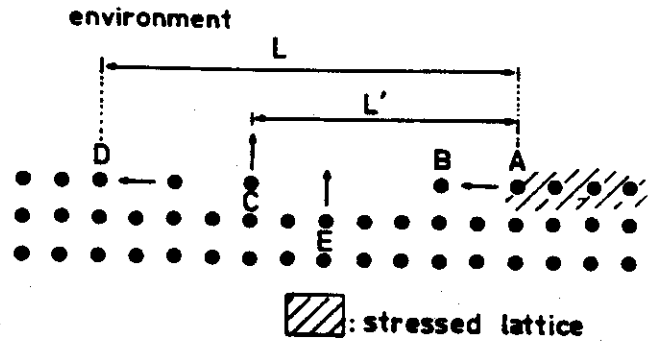

FIG. 2. The distance (L) that the excess atoms have to travel from the tip of the crack to a kink site on the crack surface. The distance will be smaller (L') if the excess atoms are dissolved by reaction with the environment (C), or if selective dissolution of the alloy is taking place (E). In both cases empirical correlations between crack velocities and anodic dissolution will be found.

models[24] the stresses on the side surfaces of the cracks are found to drop substantially after only 5–7 atomic distances away from the tip of the crack.

Since the surface stressed region is very small, the value of L will be determined mainly by the distance the adatom has to travel before it reaches a kink, A–D in Fig. 1. This distance will be a function of the crystallographic orientation of that surface. In most of the SCC cases the diffusion distance, L', will be smaller than L (Fig. 2) because of the reaction with the environment. The environment will act by dissolving the excess of adatoms, C, or by introducing surface vacancies, E, as in the de-alloying of Cu–Zn alloys. In this case the higher the content of Zn in the alloy, the lower L' should be expected to be.

Reactions C and E, in aqueous solutions under anodic polarization conditions, will involve charge transfer, and the rate of exchange will be proportional to the rate of crack propagation, the transition process A–B. This would explain why numerous authors reported a proportionality between current densities on straining metals and crack velocities.[1,2,8,28–31]

The vacancy concentration gradient will be given by

$$\frac{dC}{dx} = \frac{C_0}{L}\left[\exp\left(\frac{\sigma a^3}{kT}\right) - 1\right] \tag{3}$$

and the vacancy flow, per unit of time, will be:

$$J_v = D_v \frac{dC}{dx}. \tag{4}$$

For the sake of convenience, instead of the coefficient of surface diffusion of vacancies, D_v, the coefficient of surface self-diffusion, D_s/C_0, will be used.[32] In addition, the concentration of vacancies, given in equation (2) as the number of vacancies per unit of site, will be given in vacancies per unit of volume. The flow of vacancies, per unit of area and unit of time will then be given by:

$$J_v = \frac{D_s}{La^3}\left[\exp\left(\frac{\sigma a^3}{kT}\right) - 1\right]. \tag{5}$$

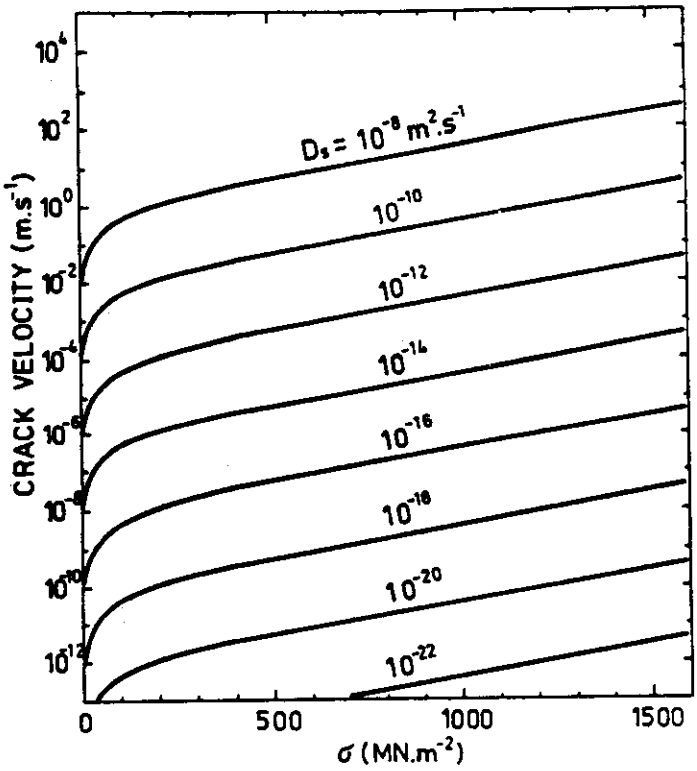

FIG. 3. Crack velocities as a function of the stress at the tip of the crack (σ) and the surface self-diffusion coefficient (D_s), calculated with equation (6), for $L = 10^{-8}$ m; $a = 2.5 \times 10^{-10}$ m; and temperature, 25°C.

If $\nu = a^{-2}$ is the number of atoms per unit of area, then every time that ν vacancies move to the tip of the crack, the crack will advance a distance a. The crack velocity, V_p, will be given by:

$$V_p = \frac{D_s}{L}\left[\exp\left(\frac{\sigma a^3}{kT}\right) - 1\right] \tag{6}$$

V_p being the crack velocity, in m s^{-1}; D_s the surface self-diffusion coefficient, in m^2 s^{-1}; L the diffusion distance of the adatoms or vacancies, in m; σ the elastic surface stress at the tip of the crack, in N m^{-2}; a the atom size, in m; k the Boltzmann constant in J K^{-1}; and T the temperature in K.

At very low stress values, when $\sigma a^3 \ll kT$, equation (6) can be approximated by:

$$V_p = \frac{D_s}{L}\frac{\sigma a^3}{kT}. \tag{7}$$

Figure 3 shows the crack velocity values calculated with equation (6), for different surface diffusion coefficient values. Figure 4 shows the region of stress values where equation (7) is valid. For the above calculations we use the following values: L: 10^{-8} m; a: 2.5×10^{-10} m; k: 1.380662×10^{-23} J K^{-1}; and T: 298 K (25°C).

To evaluate the effect of a and L on V_p, each one of these parameters was changed, keeping the other at the values given above, and assuming a surface diffusion coefficient of $D_s = 10^{-14}$ m^2 s^{-1}.

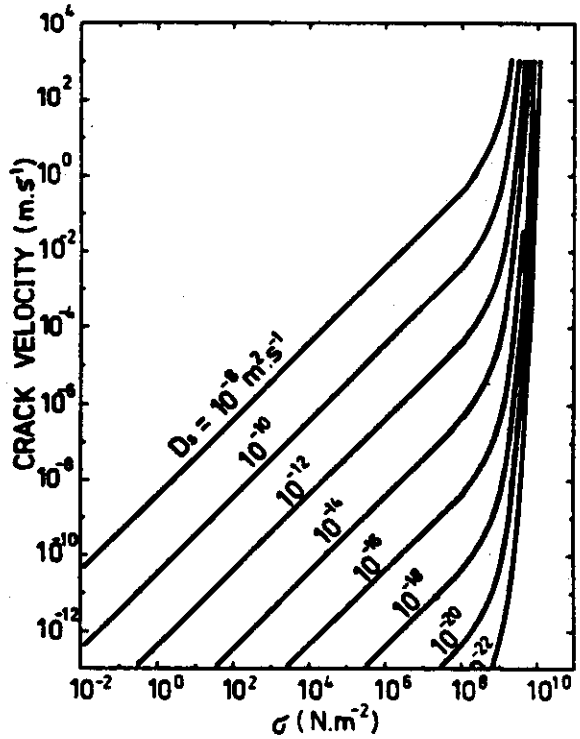

FIG. 4. Crack velocities, as in Fig. 3, showing the low stress region where equation (7) is valid.

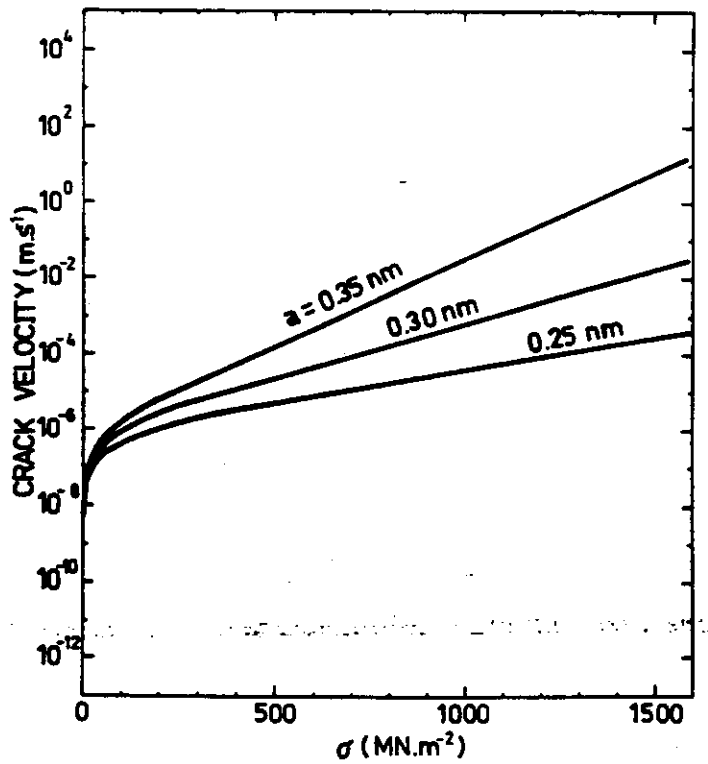

FIG. 5. The effect of the value of a on the crack velocities calculated with equation (6). $D_0 = 10^{-14}\ m^2\ s^{-1}$; $L = 10^{-8}$ m; temperature: 25°C.

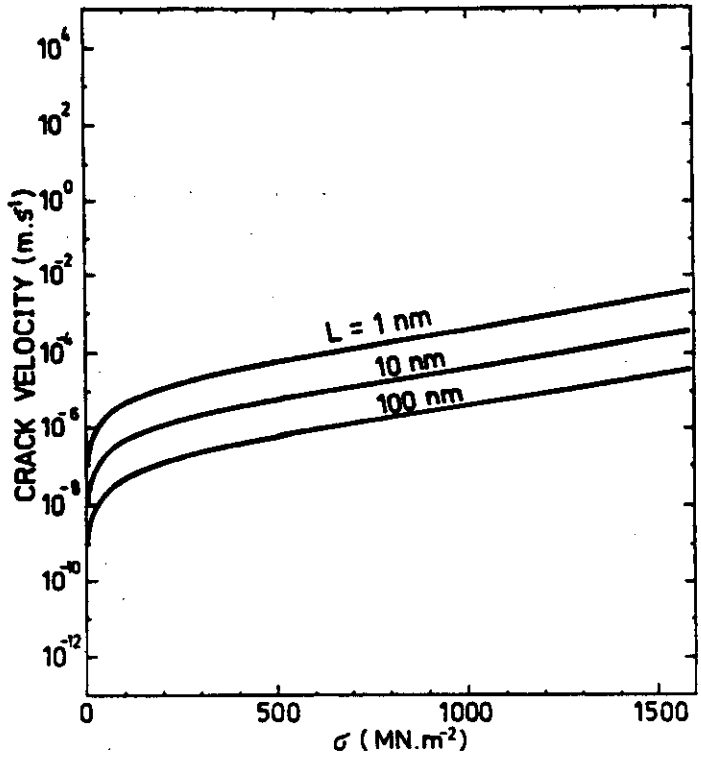

FIG. 6. The effect of the value of L on the crack velocities calculated with equation (6). $D_s = 10^{-14}\ m^2\ s^{-1}$; $a = 2.5 \times 10^{-10}$ m; temperature: 25°C.

As shown in Fig. 5, small changes in the value of a have a strong effect on the predicted V_p value. The interatomic distance, a, for most of the common metals (Fe, Co, Cr, Ni, Cu) is of the order of 2.5×10^{-10} m.[33] For most of the other metals the values of a are higher, reaching 3.18×10^{-10} m for zirconium and 3.50×10^{-10} m for lead. To determine the precise value is difficult because, according to Quéré,[26] there is a volume shrinkage in vacancies, so the a^3 value should be reduced by 10%. On the other hand, Wynblatt and Gjostein[34] showed that the lattice interplanar spacing near the surface is higher than that in the bulk, and this would lead to higher a^3 values.

Figure 6 shows how V_p is modified when different L values are used. The value of L, on a given crystallographic plane, will be smaller than the distance between two ledges on the surface terraces, point D in Fig. 2. Such a distance is frequently used in the studies of electrocrystallization, when the effect of surface diffusion is considered. In the literature of electrocrystallization[35,36] values of 10^{-8} m, for the distance between ledges, were assumed. In this case, the effective diffusion distance, L' in Fig. 2, could be even smaller, so a value of $L = 10^{-8}$ m as used in the present work is considered as a conservative approximation.

SURFACE SELF-DIFFUSION COEFFICIENTS (D_s)

Surface self-diffusion of metals is a subject of high theoretical and practical interest, and a lot of work and extensive reviews on it have been published.[37–39] Several experimental techniques were used in the measurement of D_s on metals.[37,38] Some of them, like grain-boundary grooving or surface-scratch smoothing, are mass-transfer techniques. They were applied to a wide variety of metals, but they usually require high temperatures, above 400°C. Other techniques, such as field ion microscopy[39,40] can be used at low temperatures, even below room temperature, but

they are restricted to refractory metals, like tungsten, platinum, etc. With this last technique the movement of individual atoms can be followed.[39,40]

All the above measurements were made either in vacuum or in the presence of a gas, like hydrogen, argon or helium. The results were systematized by Gjostein,[34,37] but he pointed out that strong deviations were observed in the presence of contaminants. The effect of contaminants was studied by Rhead and coworkers,[41–46] who were able to include the effect of contaminants in the systematization made by Gjostein.

Gjostein[37] has shown that a plot of log D_s versus T_m/T (T_m: melting point; T: temperature; both in K) correlates the surface diffusion data for most fcc metals. The plot is non-linear and can be represented by the sum of two Arrhenius factors. At high and low temperatures, respectively the Arrhenius constants are given approximately by:

$$\left.\begin{aligned} Q_s &= 30\ T_m \text{ cal mole}^{-1} \\ D_0 &= 740 \text{ cm}^2 \text{ s}^{-1} \end{aligned}\right\} T/T_m \geq 0.75 \tag{8}$$

$$\left.\begin{aligned} Q_s &= 13\ T_m \text{ cal mole}^{-1} \\ D_0 &= 0.014 \text{ cm}^2 \text{ s}^{-1} \end{aligned}\right\} T/T_m \leq 0.75 \tag{9}$$

where Q_s is the activation energy, and D_0 is the Arrhenius pre-exponential factor.

Strong deviations were observed from the predictions of equations (8) and (9) when impurities were present. It was found that while some impurities led to D_s values lower than those predicted, others gave much higher values.

Rhead[41,42] rationalized the effect of impurities by postulating that a constant value of D_s, ap. 3×10^{-8} m^2 s^{-1}, was found at the melting point. Rhead found that the results obtained in the presence of impurities followed equations (8) and (9) if instead of the melting point of the bulk metal, the melting point of the surface-adsorbed product was used for T_m. This conclusion was supported by measurements on the following systems: Ag–S, Cu–Pb, Cu–Tl, Cu–Bi and Au–Pb. The melting of lead adsorbed on copper[45] and of adsorbed monolayers of bismuth on copper[46] were confirmed by low-energy electron diffraction (LEED) by Rhead and coworkers. The above correlations were later extended by Delamare and Rhead[43] to Cu–Cl, Cu–Br, and Cu–I, by Pichaud and Drechsler[47] to W–Ni, and by Oda and Rhead[44] to Ni–Cl, Ni–Br and Ni–I.

Surface self-diffusion of metals is also important in electrochemistry and corrosion, since it is an important step in the processes of dissolution and electrocrystallization. The theoretical aspects for this second process have been developed in great detail.[48,49] Unfortunately the experimental measurement of D_s, in the presence of electrolytes, has proved to be very difficult[50] and no D_s values for metals in the presence of electrolytes are found in the literature. This is particularly bad in our case since it is precisely the kind of information we need for SCC in aqueous environments.

In environmentally assisted cracking metal surfaces are always contaminated by impurities. There are no atomically clean surfaces. To estimate the most probable D_s values the following assumption must be made. It is assumed that in all cases of environmentally assisted cracking D_s will be given by equations (8) and (9), with the modification introduced by Rhead:

$$D_s\ (\mathrm{m^2\ s^{-1}}) = 740 \times 10^{-4} \exp - (30\ T_m/RT) + 0.014 \times 10^{-4} \exp - (13T_m/RT) \quad (10)$$

R being the gas constant ($R = 1.987$ cal mole^{-1} K^{-1}), T the absolute temperature in K, and T_m the melting point of the surface adsorbed impurity in K. In the work of Rhead *et al.*, the T_m values used were the melting point of Ag_2S for the Ag–S system, CuCl for Cu–Cl, CuBr for Cu–Br, CuI for Cu–I, NiI_2 for Ni–I, $NiBr_2$ for Ni–Br, etc.

In our case for SCC of aluminium in NaCl solutions we will consider the melting point of $AlCl_3$; for copper alloys in perchlorate solutions, the melting point of $Cu(ClO_4)_2$; for Zr–I_2, the melting point of ZrI_4; etc. Gjostein's equations (8) and (9) were found from experimental data from fcc metals, while Rhead made no reference to the crystal structure of the adsorbed products. In the use of equation (10), no distinction is made between the crystalline structures of the bulk metal or the surface product.

The above approach to the calculation of D_s for SCC processes may seem very crude, but it is the best one possible at present, and it gives correct predictions when dealing with the phenomenon of specificity in SCC. It will be seen that low melting compounds are those that lead to fast SCC, while high melting point products are those that inhibit SCC. Empirical equations, like (8) and (9), using the melting temperature as a correlating parameter, have been frequently used for properties of materials in chemistry and physical metallurgy.[51] They were successfully used in the prediction of unknown parameters and in mastering large amounts of data. No conspicuous differences were observed between bcc structures and close-packed structures on any of the properties correlated by this kind of empirical equations.[51]

Equation (10) was used to calculate the self-diffusion coefficient for a variety of surface contaminants. The calculations were made for temperatures between 0 and 200°C. The T_m values used ranged from 373 K, for a surface compound melting at 100°C, up to 2073 K, for a surface compound melting at 1800°C. The results are shown in Fig. 7. For the sake of comparison the D_s values for aluminium, copper, nickel and iron, predicted by equation (10), have also been included.

If we take for a minimum crack velocity, V_p, a value of 10^{-11} m s^{-1} (roughly 1 mm in 3 years), Fig. 3 shows that for an intermediate stress value of 600 MN m^{-2}, a surface diffusion coefficient of 10^{-20} m^2 s^{-1} will be required. This D_s value was chosen in Fig. 7 as the safety limit. For room temperature, 25°C, it can be seen that this safety limit is reached by surface compounds melting at 1200°C. Compounds melting at this temperature, and above, can be considered protective, since they will allow very low surface mobility. It is important to point out that, at 25°C, copper and aluminium show predicted D_s values above the safety limit. In the case of copper the predicted D_s value is about 10^{-19} m^2 s^{-1}, which for 600 MN m^{-2} would give a crack velocity of 10^{-10} m s^{-1}. In the case of aluminium, the predicted D_s value is about 10^{-15} m^2 s^{-1}, and the crack velocity 10^{-6} m s^{-1}. On the other hand, aluminium oxide, with a melting point of 2045°C, will be an excellent inhibitor for SCC of aluminium. The above observations would explain why Speidel[52] reported SCC of Al–Mg–Zn alloys even in high purity water. Any environmental condition interfering with the immediate formation of Al_2O_3 inside the cracks, e.g. localized alkalinization due to dissolution of magnesium from the alloy, will lead to SCC even in the absence of specifically corrosive anions. A similar situation, though with lower crack velocities, is found with copper. Parkins *et al.*[53] reported that slow SCC of brass was found in a

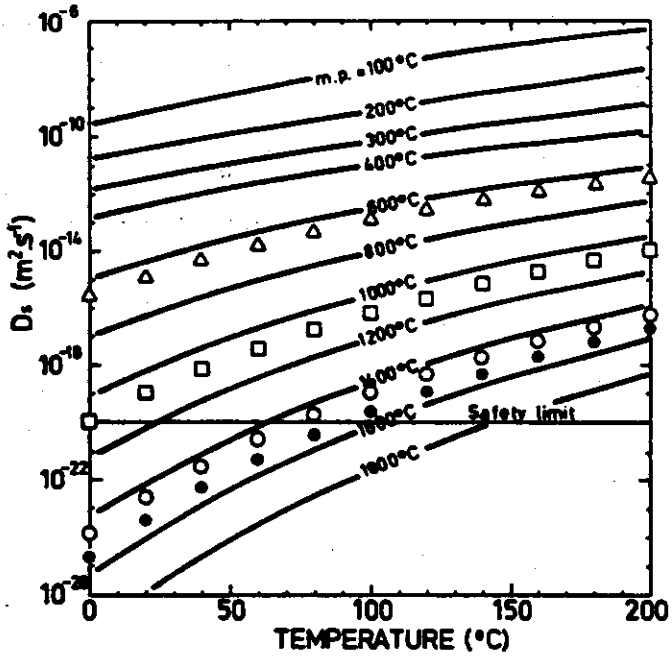

FIG. 7. Surface self-diffusion coefficients (D_s) for metals, at various temperatures, and as a function of the metal melting point, calculated with equation (10), based on the work of Gjostein.[37] For SCC and LME, where surface contaminants are present, it will be assumed, following Rhead,[41,42] that the value of D_s is a function, not of the metal melting point, but of the surface contaminant melting point. For the sake of comparison the calculated D_s values for clean aluminium (△), copper (□), nickel (○) and iron (●) have also been included. The safety limit indicates the D_s value that, with a crack tip stress of 600 MPa, will give a crack velocity of 10^{-11} m s^{-1}.

wide variety of environments, including pure water. The same happens with iron and nickel when the environment temperature is above 100°C. In this case, impurities segregated to the grain boundaries, and with melting points only slightly lower than those for the bulk metal, could lead to SCC, as found for steam turbine rotors.[54]

The above observations on aluminium, copper, iron and nickel show that for the present mechanism we have to distinguish between *intrinsic SCC susceptibility* and *specific SCC susceptibility*. In the first case the metal, or its impurities, can exhibit D_s values big enough to account for SCC. In the second, the environment has ions that, by adsorption to the metal surface, can lead to higher surface mobility and SCC velocity. In the case of aluminium, its low melting point, 660°C, allows for D_s values high enough to produce SCC, but in the presence of NaCl solutions, at appropriate electrode potentials, $AlCl_3$ will be adsorbed on the metal, and this compound with a melting point of 190°C, will lead to crack velocities several orders of magnitude higher.[52]

From Figs 3 and 7 we find that, at room temperature, a D_s value of 10^{-20} m^2s^{-1} is a safe limit, and that it is related to a melting point of 1200°C. To evaluate compounds that could be formed on the metal by reaction with the environment, we will regard as protective any compound having a melting point equal to or higher than 1200°C. With lower melting point products SCC could be expected, but the crack velocity will be function of the D_s value.

The D_s values predicted by Rhead for contaminated surfaces are for full coverage of the metal surface.[41,42] In gaseous environments, this means that the partial pressure of the contaminant is equal to the equilibrium pressure of the compound at

that temperature. If the partial pressure is lower the D_s value will also be lower. For example, for copper at 900°C, in the presence of CuCl vapor at the equilibrium pressure, Delamare and Rhead[43] found a D_s value of *ca* 10^{-5} m^2 s^{-1}, but if the vapor pressure of CuCl was only one half of the equilibrium value, D_s dropped to *ca* 10^{-8} m^2 s^{-1}. Similar observations were reported for Au–Bi,[18] Ag–S,[18] Cu–Bi[18] and Ni–I.[44] In liquid metals, or in gaseous environments with sufficiently high vapor pressure of the aggressive compounds, crack velocities of the order of those predicted by Figs 3 and 7 could be expected. In aqueous environments, on the other hand, the D_s value will be a function of the degree of surface coverage by the contaminant, which will be, in turn, a function of the electrode processes on the metal surface. Oxides usually have very high melting points and if they are formed by direct reaction with the metal, they will protect against SCC. Cracking will be found under conditions where thick tarnish films are found if in these cases a mechanism of dissolution and precipitation occurs in the film formation process,[55] since time will be available for surface mobility and thus SCC. Cracking will also be found in those potential regions where the oxide film is partly unstable, as in the active–passive transition or in the passive–pitting transition.[56] In those regions the low melting point compounds can compete with the oxide film in the coverage of the metal surface, and can lead to SCC. Anodic potentials will favor the formation of the low melting point compounds, thus accelerating SCC, but the degree of coverage could be limited by competing anodic reactions. If the low melting point compound is very soluble, high coverages will be followed by fast metal dissolution, and a general corrosion process will compete with the nucleation of SCC. Then, in aqueous environments we will expect that D_s will be a function of the electrode potential, and that it will be usually lower than the maximum values predicted by equation (10).

Going back to Fig. 7, at melting points below 1200°C SCC will be possible, but with various degrees of aggressiveness. For a compound with a melting point of 800°C, D_s at 25°C will be *ca* 10^{-16} m^2 s^{-1} for full coverage, or 10^{-19} m^2 s^{-1} for a lower coverage. In that case, depending on the degree of coverage, it could be either a dangerous or an innocuous compound. According to this, we will label those compounds with melting points between 1200° and 800°C as unsafe compounds. Finally all the compounds with melting points lower than 800°C will be labeled as dangerous compounds. It is with these criteria that Table 1 was prepared. In most cases only anhydrous compounds were considered. This was done on the assumption that the reaction of the metal with water, leading to oxide films, will compete with SCC. There are cases, particularly with noble metals, where the metal is thermodynamically stable in contact with water and hydrated salts will not lead to oxide formation. For this reason hydrated salts were also tabulated for platinum and copper. As for the case of iron and nickel nitrates, only the melting points of the hydrated salts were found[57] and are reported in Table 1. Some organic acid salts, like palmitates, stearates and oleates of nickel, copper, etc. have low melting points, but they were not included in Table 1, because it is not clear if equation (10) will be valid for these large organic molecules. This point, as well as that of the hydrated salts, will require experimental confirmation.

Table 1 shows a good correlation with the available information of SCC susceptibility. Aluminium, as seen above, is intrinsically susceptible to SCC, and cracking will be accelerated by chlorides, bromides and iodides. Fluorides have no accelerating effects, as shown by Speidel.[52]

TABLE 1. THE CLASSIFICATION OF THE SCC ACTIVITY OF METAL COMPOUNDS, BASED ON THE RATE OF SURFACE SELF-DIFFUSIVITY THEY CAN INDUCE ON THE BASE METAL. DERIVED FROM THEIR MELTING POINTS

Dangerous compounds			Unsafe compounds			Protective compounds		
Compound	m.p. (°C)	Ref.	Compound	m.p. (°C)	Ref.	Compound	m.p. (°C)	Ref.
Aluminium (0.5 T_m = 193°C):								
$AlBr_3$ (or Al_2Br_6)	97.5	57						
$AlCl_3$	190	57				AlF_3	1291 subl	57
AlI_3	191	57				$3Al_2O_3 \cdot 2SiO_2$	1920	57
						Al_2O_3	2045	57
Beryllium (0.5 T_m = 502°C):								
$BeO(C_2H_3O_2)_2$*	284	57	BeF_2	803	58	BeO	2530	57
$BeCl_2$	405	57						
$BeBr_2$	490	57						
BeI_2	510	57						
Bismuth (0.5 T_m = −1°C):								
$BiBr_3$	218	57	Bi_2O_3	820	57	BiOBr	d red ht	57
$BiCl_4$	226	57				BiOCl	red ht	57
$BiCl_3$	231	57				BiOF	d red ht	57
BiI_3	408	57				BiOI	d red ht	57
BiF_3	727	57						
Cadmium (0.5 T_m = 23°C):								
$Cd(C_2H_3O_2)_2$†	256	57	$CdSO_4$	1000	57	CdO	1400	57
$CdCl_2NH_4Cl$	289	57	CdF_2	1100	57	$Cd_3(PO_4)_2$	1500	57
$Cd(NO_3)_2$	350	57				CdS	1750	57
CdI_2	387	57						
$CdBr_2$	567	57						
$CdCl_2$	568	57						
Chromium (0.5 T_m = 792°C):								
CrO_2Cl_2	−96.5	57	$CrCl_3$	824	57	CrF_3	1404	48
CrO_3	196	57	$CrBr_3$	842	57	CrS	1550	57
CrI_3	>600	57	CrI_2	856	57	Cr_2O_3	2435	57
			CrF_2	1100	57			
			$CrCl_3$	1150	57			

12

Cobalt (0.5 T_m = 611°C):								
$CoI_2 \cdot 6NH_3$	141	57				CoF_2	1250	58
$CoCl_2 \cdot 2NH_3$	273	57				Co_2SiO_4	1345	57
CoI_2	515	57				CoO	1935	57
$CoBr_2$	678	57						
$CoCl_2$	724	57						
Copper (0.5 T_m = 405°C):								
$Cu(ClO_3)_2 \cdot 6H_2O$	65	57	CuF (or Cu_2F_2)	908	57	Cu_2O	1235	57
$Cu(ClO_4)_2 \cdot 6H_2O$	82	57	CuF_2	950	58	CuO	1326	57
$Cu(ClO_4)_2$	82.3	57	CuSCN	1084	57			
$(Cu(NH_3)_4)(NO_2)_2$	$-2NH_3$, 97	57	Cu_2S	1100	57			
$Cu(NO_3)_2 \cdot 3H_2O$	114.5	57						
$Cu(C_2H_3O_2)_2 \cdot H_2O$‡	115	57						
$CuCl \cdot 3(CS(NH_2)_2)$§	168	57						
$Cu(NH_3)_2Cl_2$	260	57						
CuCl (or Cu_2Cl_2)	430	57						
CuBr (or Cu_2Br_2)	492	57						
$CuBr_2$	498	57						
CuI (or Cu_2I_2)	605	57						
$CuCl_2$	620	57						
Gold (0.5 T_m = 395°C):								
$AuBr_3$	97.5-Br, 160	57						
$AuCl_3$ (or Au_2Cl_6)	d 254	57						
$AuTe_2$	d 472	57						
Hafnium (0.5 T_m = 977°C):								
$HfBr_4$	424	58				HfO_2	2812	57
$HfCl_4$	434	58						
Iridium (0.5 T_m = 1068°C):								
IrF_6	44.4	57						
Iron (0.5 T_m = 631°C):								
$Fe(NO_3)_2 \cdot 6H_2O$	60.5	57	FeF_2	1020	58	FeS	1199	57
$Fe(ClO_4)_2$	$d > 100$	57	FeF_3	1027	58	FeO	1420	57

(*continued*)

TABLE 1. CONTINUED

Dangerous compounds			Unsafe compounds			Protective compounds		
Compound	m.p. (°C)	Ref.	Compound	m.p. (°C)	Ref.	Compound	m.p. (°C)	Ref.
Iron (*continued*)								
$FeCl_3$ (or Fe_2Cl_6)	306	57	$FeSiO_3$	1146	57	Fe_2SiO_4	1503	57
FeI_2	594	59	FeS_2	1171	57	Fe_3O_4	1597	59
$FeCl_2$	670	57				Fe_2O_3	1565	57
$FeBr_2$	689	58						
Lead (0.5 T_m = 27°C):								
$PbCl_4$	−15	58	$Pb_2P_2O_7$‖	824	57			
$Pb(C_2H_3O_2)_4$¶	175	57	$PbCrO_4$	844	57			
$Pb(C_2H_3O_2)_2$**	280	57	PbF_2	855	57			
$PbBr_2$	373	57	PbO	888	57			
PbI_2	402	57	$Pb_2(OH)_2CrO_4$	920	57			
$Pb(NO_3)_2$	d 470	57	$PbSO_4 \cdot PbO$	977	57			
$PbCl_2$	501	57	$Pb_3(PO_4)_2$	1014	57			
PbF_4	600	58	PbS	1114	57			
PbFCl	601	57	$PbSO_4$	1170	57			
$PbCl_2 \cdot 2PbO$	693	57						
$PbSiO_3$	766	57						
Magnesium (0.5 T_m = 187°C):								
$Mg(C_2H_3O_2)_2$††	323 d	57	$MgSO_4$	d 1124	57	$Mg_3(PO_4)_2$	1184	57
MgI_2	650	58				MgF_2	1266	57
$MgBr_2$	700	57				$Mg_2P_2O_7$‡‡	1383	57
$MgCl_2$	708	57				Mg_2SiO_4	1910	57
						MgO	2800	57
Molybdenum (0.5 T_m = 1172°C):								
MoF_6	17	58				MoS_2	1185	57
MoF_5	64	58						
$MoOF_4$	98	57						
$MoCl_5$	194	57						
MoO_3	795	57						

Nickel (0.5 T_m = 590°C):

$Ni(NO_3)_2 \cdot 6H_2O$	56.7	57
$(Ni(NH_3)_6)(ClO_3)_2$	180	57
Ni_3S_2	790	57
NiI_2	797	57
NiS	797	57
$NiBr_2$	963	57
NiF_2	subl 1000	57
$NiCl_2$	1001	57
NiO	1990	57

Niobium (0.5 T_m = 1097°C):

NbF_5	72	57
$NbCl_5$	204.7	57
$NbBr_5$	265.2	57
$NbOCl_3$	subl 400	57
$NbOBr_3$	subl	57
NbI_4	503	58
Nb_2O_5	1460	57
Nb_2O_3	1780	57

Platinum (0.5 T_m = 749°C):

PtF_6	57.6	57
$H_2PtCl_6 \cdot 6H_2O$	60	57
$(Pt(NH_3)_2)Cl_4$	200	57
$(Pt(NH_3)_4Cl_2 \cdot H_2O$	250	57
$PtCl_3$	435	57
PtO_2	450	57
PtF_4	d red heat	57
$PtTe_2$	1200	57

Silver (0.5 T_m = 344°C):

$AgIO_3$	>200	57
$AgNO_3$	212	57
$AgClO_3$	230	57
AgBr	432	57
AgF	435	57
AgCl	455	57
AgI	558	57
$Ag_4P_2O_7$§§	585	57
Ag_2SO_4	652	57
AgF_2	690	57
Ag_2S	825	57
Ag_3PO_4	849	57

Tantalum (0.5 T_m = 1361°C):

TaF_5	96.8	57
$TaCl_5$	216	57
$TaBr_5$	265	57
$TaBr_4$	392	58
TaI_5	497	59
Ta_2S_4 (or TaS_2)	>1300	57
Ta_2O_5	1800	57

(*continued*)

TABLE 1. CONTINUED

Dangerous compounds			Unsafe compounds			Protective compounds		
Compound	m.p. (°C)	Ref.	Compound	m.p. (°C)	Ref.	Compound	m.p. (°C)	Ref.
Tin (0.5 T_m = −21°C):								
$SnCl_4$	−33	57	SnS	882	57			
$SnBrCl_3$	−31	57	SnO_2	1127	57			
$SnCl_2Br_2$	−20	57						
$SnBr_4$	31	57						
$SnBr_2I_2$	50	57						
SnI_4	144.5	57						
$Sn(C_2H_3O_2)_2$	182	57						
SnF_2	212	58						
$SnBr_2$	215.5	57						
$SnCl_2$	246	57						
SnI_2	320	57						
SnF_4	705 subl	57						
Titanium (0.5 T_m = 693°C):								
$TiCl_4$	−25	57	$TiCl_2$	1025	58	TiF_3	1200	57
$TiBr_4$	39	57				TiO	1750	57
TiI_4	150	57				TiO_2	1830	57
TiF_4	>400	57				Ti_2O_3	2130 d	57
$TiCl_3$	d 440	57						
$TiBr_2$	d > 500	57						
TiI_2	600	57						
Tungsten (0.5 T_m = 1568°C):								
WF_6	2.5	57	W_2O_5	subl 800	57	WO_3	1473	57
WOF_4	110	57						
$WOCl_4$	211	57						
WBr_6	232	57						
WCl_5	248	57						
WO_2Cl_2	266	57						
WCl_6	275	57						
WBr_5	276	57						
$WOBr_4$	277	57						

Uranium (0.5 T_m = 429°C):								
UF_6	64.5	57	UCl_3	842	57	UO_2	2500	57
UBr_4	516	57	UF_4	960	57			
UO_2Cl_2	578	57	UF_3	d > 1000	57			
UCl_4	590	57						
UBr_3	730	57						
Vanadium (0.5 T_m = 808°C):								
$VOCl_3$	−77	57	VI_2	750	57	VCl_2	1350	58
VCl_4	−28	57				VF_3	1400	58
VF_5	19	58				VO_2 (or V_2O_4)	1967	57
VOF_3	300	57				V_2O_3	1970	57
V_2O_5	690	57						
Zinc (0.5 T_m = 73°C):								
$(Zn(NH_3)_2)Cl_2$	210.8	57	ZnF_2	872	57	$ZnSiO_3$	1437	57
$ZnCl_2$	283	57	$Zn_3(PO_4)_2$	900	57	Zn_2SiO_4	1509	57
$ZnBr_2$	394	57	$3ZnO{\cdot}2B_2O_3$	980	57	ZnS	1700	57
ZnI_2	446	57				ZnO	1975	57
Zirconium (0.5 T_m = 789°C):								
$ZrCl_4$	437	57	ZrF_4	932	58	ZrO_2	2715	57
$ZrBr_4$	450	57				$ZrBr_2$	*ca* 3000	57
ZrI_4	499	57						

* Beryllium acetate, basic; † cadmium acetate; ‡ copper(II) acetate; § copper chloride, thioureate; ‖ lead pyrophosphate; ¶ lead tetraacetate; ** lead acetate; †† magnesium acetate, ‡‡ magnesium pyrophosphate; §§ silver pyrophosphate; ‖‖ tin acetate. Notice that, for the sake of simplicity, the values of 0.5 T_m are not given in K but in °C.

For beryllium, acetates appear, together with halides, as dangerous compounds. Bismuth should not be susceptible to SCC because of its low 0.5 T_m value. For cadmium, we should expect SCC susceptibility in chlorides, bromides, iodides, nitrates and acetates, but because of its low melting point what we called above intrinsic SCC will most probably predominate.

In the case of Fe–Cr–Ni alloys, like austenitic stainless steels, Table 1 shows that in the presence of halide ions the susceptibility to SCC would be due to the iron halide compounds, with melting points lower than 700°C. On the other hand, at high potentials, in the transpassive region, SCC should be expected, as it is the case,[60] because of the formation of CrO_3 with a melting point of only 196°C.

Cobalt alloys should show SCC susceptibility in chlorides, bromides and iodides, at those experimental conditions where cobalt halides are formed on the metal surface.

Copper forms very low melting point compounds with chlorates, perchlorates, nitrates, etc., all of them highly aggressive from the SCC point of view.[61,62] Gold alloys are known to show SCC susceptibility in $FeCl_3$;[63] gold oxide, Au_2O_3, decomposes at low temperatures, 160–250°C, and could explain the susceptibility of these alloys in strongly oxidizing solutions like chromates. From Table 1 it is predicted that gold alloys should be susceptible to SCC in the presence of tellurium vapor. No information was found for hafnium, but behaviour similar to that of zirconium should be expected.

The susceptibility to SCC of hydrated iron in nitrates is very well known[64,65] and it is consistent with the low melting point of iron nitrate. Susceptibility to SCC in caustic solutions[66,67] is probably due to what is above called intrinsic SCC, and the function of the alkali would be to dissolve the oxide film and interfere with the passivation of iron, thus allowing for surface mobility. In these conditions magnetite is formed by a dissolution and precipitation mechanism[55] which agrees with the above explanation. Iron silicates could inhibit SCC.[66] In the case of lead, as expected from Table 1, SCC has been reported in solutions containing lead acetate and nitrate ions.[3,4] Other possible aggressive environments are shown in Table 1, nevertheless, the low flow stress of lead will limit the level of stresses available for SCC.

For magnesium, besides the specific SCC predicted in halides and acetates, intrinsic SCC should be expected. In the case of nickel, besides the intrinsic SCC, in high temperature water discussed above, susceptibility should be expected in the presence of sulphides and iodides. As for nitrates, the behaviour of nickel should be close to that of iron. Unfortunately, no melting point data was available for the anhydrous nickel nitrate. The hexahydrate has a very low melting point, 56.7°C, but the anhydrous salt decomposes above 105°C,[68] and the melting point is not reported.

Silver is attractive from an academic point of view because of the high number of low melting point compounds reported. No information was found for SCC of tantalum, except for hydrogen susceptibility.[69] Nevertheless, tantalum is susceptible to pitting in halide solutions[70] and SCC susceptibility should be expected near the pitting potential.

Tin could be susceptible to SCC in a wide variety of environments, but its low 0.5 T_m value suggests that no SCC should be found at room temperature. For titanium SCC chloride, bromide and iodide ions have been reported[71] as accelerators of SCC while fluoride ions are inhibitors, in good concordance with their respective melting points. Tungsten could be susceptible to SCC in the presence of halogen vapors. Uranium is very reactive, and easily produces hydrides that will compete

with the present mechanism. Nevertheless, under appropriate conditions, uranium should be expected to show SCC in halogen vapor.

Vanadium, the same as chromium, should be susceptible to SCC in the transpassive region, where V_2O_5 could be formed. Zinc should show SCC in halide solutions, and also intrinsic SCC susceptibility.

Zirconium alloys are susceptible to SCC in the presence of halogens, because of the low melting point of its halides, all of them lower than 500°C. So far no contradictions have been found between the predictions of Table 1 and what is reported in the literature. On the other hand, the good coincidence between prediction and experience gives a strong support to the mechanism proposed in the present paper.

Table 1 is not exhaustive as the melting points of some important compounds were not available.[57] Approximate melting point values of those compounds could be evaluated from their crystal structure.[72]

EFFECT OF HYDROGEN

The hydrogen-related failure of metals involves a variety of failure modes[73] and its discussion falls outside the scope of the present paper. Nevertheless, frequent references to similarities between LME and HE[14,74] and between SCC and HE[75,76] have been found in the literature. In the second case examples were found where the distinction between SCC and HE is subtle, and sometimes unconvincing. We will analyse now what effect the hydrogen, present in the lattice or evolving on the metal surface, could have on the mechanism of crack propagation proposed in the present paper.

Hydrogen could accelerate crack propagation in two main ways. The first and most straightforward one is by reduction of the oxide films present on the metal surface. The removal of these high melting point products will aid surface mobility, and allow for intrinsic SCC. This process could be important in low melting point metals that have easily reducible oxide films. In the case of nickel on steels at room temperature, as observed in Figs 3 and 7, this could only account for very low crack velocities.

The second, and most important one, is related to the hydrogen–vacancy interaction. Recent work[77,78] has shown that vacancies act as deep trap sites for hydrogen at room temperature. The binding energy reported[77] for H-monovacancies, in nickel was $E_b = 0.43$ eV. As for iron, the values reported were $E_b = 0.53$ eV for H-monovacancies and $E_b = 0.71$ eV for small vacancy clusters.

By comparison with carbon interstitials, which increase the self diffusion in γ-iron, Gibala[79] suggested that hydrogen, interacting with vacancies, should also increase the self-diffusion of the metal. According to this author, the activation enthalpy for self-diffusion is reduced by an amount equal to the binding enthalpy of a vacancy-interstitial. Similar effects should be expected for surface self-diffusion. In any case, the presence of low hydrogen concentrations in the metal lattice should induce only a moderate increase in the D_s value. Nevertheless, very large hydrogen concentrations are expected in elastically strained regions, like the tip of a crack.[73,80–83] The high difference in hydrogen concentrations, between the tip and the sides of the cracks should lead to an effect similar to that described above for vacancies in stressed crystals. To account for the influence of hydrogen in a crack the following change in equation (6) is suggested:

$$V_p = \frac{D_s}{L}\left[\exp\left(\frac{\sigma a^3 + \alpha E_b}{kT}\right) - 1\right] \quad (11)$$

where α is a dimensionless function that measures the difference in degree of saturation with hydrogen of the vacancies, between the stressed and the stress-free regions. The value of α should range between 0 and 1, and will be function of stress. In the case of carbon in γ-iron (see Fig. 4 in Ref. 79), saturation of the vacancies is reached for a content of 2 atomic percent of carbon in the metal. We have no equivalent information for hydrogen in metals.

According to equation (11), under maximum hydrogen availability ($\alpha = 1$), the H-vacancy binding energy for nickel could account for a crack velocity increase by a factor of 2.2×10^7, while in the case of iron the increment could be as much as 1.1×10^9 times. So far it has been assumed that there is at least a minimum of surface mobility even in the absence of hydrogen. This could explain why the presence of segregated impurities is so important in the HE of nickel and high strength steels.[73,83] HE of nickel is strongly related to the segregation of sulphur to the grain boundaries.[84] From Table 1 we see that T_m for either Ni_3S_2 or NiS is close to 800°C. From Fig. 7 we find that the predicted diffusion coefficient will be $D_s = 5.6 \times 10^{-17}\,m^2\,s^{-1}$. Even if there is no full coverage by the nickel sulphide on the grain boundaries, the diffusion coefficient can be expected to be $>10^{-20}\,m^2\,s^{-1}$. As will be shown, even this very low surface diffusion coefficient is high enough to account for HE of nickel.

The maximum crack velocities ($\alpha = 1$) predicted by equation (11) for nickel and for high strength steels must now be considered. In the case of nickel, using the following values: $D_s = 10^{-20}\,m^2\,s^{-1}$; $T = 298$ K; $E_b(\text{Ni}) = 0.43$ eV; $L = 10^{-8}$ m; $a = 2.5 \times 10^{-10}$ m; $\sigma = 5 \times 10^8\,N\,m^{-2}$; $k = 8.617347 \times 10^{-5}$ eV $K^{-1} = 1.380662 \times 10^{-23}$ J K^{-1}; the crack velocity predicted is:

$$V_p\,(\text{HE–Ni}) = 1.25 \times 10^{-4}\ m\ s^{-1};$$

and for steel, with the above values and $E_b(\text{Fe}) = 0.53$ eV, equation (11) predicts:

$$V_p\,(\text{HE–St}) = 6.14 \times 10^{-3}\ m\ s^{-1}.$$

The maximum values reported by Lynch for HE of nickel[14] and of high strength steel[74] were $V_p = ca\ 10^{-4}\ m\ s^{-1}$. The coincidence between the predicted values and those found in practice is outstanding. Nevertheless, it is important to point out that the present mechanism requires that, in the absence of hydrogen, and without any interference from oxide films or other inhibiting compounds, the cracks in nickel should propagate under stress at a rate of at least $5.7 \times 10^{-12}\,m\,s^{-1}$. In the case of high strength steels, where the predicted value is much higher than the measured one, the crack velocity in the absence of hydrogen could be $ca\ 10^{-13}\ m\ s^{-1}$. These crack propagation rates fall within the range of what we called above intrinsic SCC susceptibility. In this respect, the present mechanism is in the same standing as the decohesion mechanism developed by Oriani and Josephic, when they say[85] that nothing qualitatively new happens in cracking with hydrogen that does not occur in its absence and that hydrogen embrittlement of steels is best termed hydrogen-assisted cracking.

As shown above, the surface mobility crack mechanism developed in the present paper can be assisted by hydrogen. According to this, it is concluded that much of the discussion found in the literature showing anodic dissolution SCC and HE of non-

According to the present mechanism, both processes can be mixed without a clear difference between them. The only point is that the experimental conditions favoring the formation of low melting point anodic films will hinder hydrogen evolution, and vice versa.

Another important conclusion is that no differences should be expected between the fractographic features of anodically assisted failures and those of hydrogen-assisted failures. This puts some doubt on the frequently made assumption[86] that if the fractography of steel, in aqueous solutions, at a high electrode potential is similar to that under hydrogen evolution conditions, both cracks will be due to hydrogen.

In the case of copper where no HE has been reported, the binding energy measured for hydrogen-monovacancies[78] is $E_b = 0.4$ eV, and with $\sigma = 2 \times 10^8$ N m^2 and $\alpha = 1$, equation (11) predicts a crack velocity of 1.24×10^{-5} m s^{-1}. Assuming that the reported value for E_b is correct, the availability of hydrogen, as measured by α, is believed to play a key role in this system. A positive contribution of hydrogen to V_p should not be disregarded, particularly in aged Cu–Be alloys, where high σ values could be reached.

EFFECT OF TEMPERATURE

It is well documented in the literature[52,87–90] that temperature has a strong effect on environmental cracking susceptibility. If the temperature is increased, the crack velocity increases, showing a variety of apparent heat activation energies. When the temperature is further increased, conditions are reached where cracking susceptibility eventually disappears. This is observed in LME[12,91,92] and also in superalloys for turbine components.[93] In this last case several nickel and cobalt alloys were found to crack in sulphate/chloride melts at 704°C, in what was called, for turbine applications, low temperature corrosion. No cracking was observed at higher temperatures.

According to the present mechanism, the high temperature cracking–non cracking transition found in LME and in turbine components should be related to 0.5 T_m. At this temperature dislocation creep and diffusional flow[17] will compete against the high elastic stress necessary for cracking. The exact transition temperature will be a function of the strain rate. With higher strain rates the diffusional process will have less time for stress relaxation, and cracking will be found at higher temperatures. An effect of this type has been observed in numerous cases of LME,[12,91,92] e.g. during the straining of zinc in indium, of 2024-T4 aluminium alloy in mercury, etc.

According to equations (6), (7) and (11) the crack velocity, V_p, should be affected by the temperature in a complex way. Since most of the information available is for high σ values, only equations (6) and (11) will be considered. As shown in equations (8) and (9), the surface self-diffusion coefficient, D_s, is a function of the temperature, with an activation energy, Q_s, ranging from 13 T_m up to 30 T_m cal mole^{-1}. But, according to equations (6) and (11), the apparent activation energy for crack propagation, Q_{cp}, will be lower than Q_s. For high σ values, the activation energy for crack propagation will be:

$$Q_{cp} = Q_s - \sigma a^3 - \alpha E_b. \tag{12}$$

Q_{cp} will then be concluded to be a function of T_m, σ and αE_b. The lower the T_m the lower the activation energy; on the other hand, the higher σ and the higher αE_b, the lower the Q_{cp}.

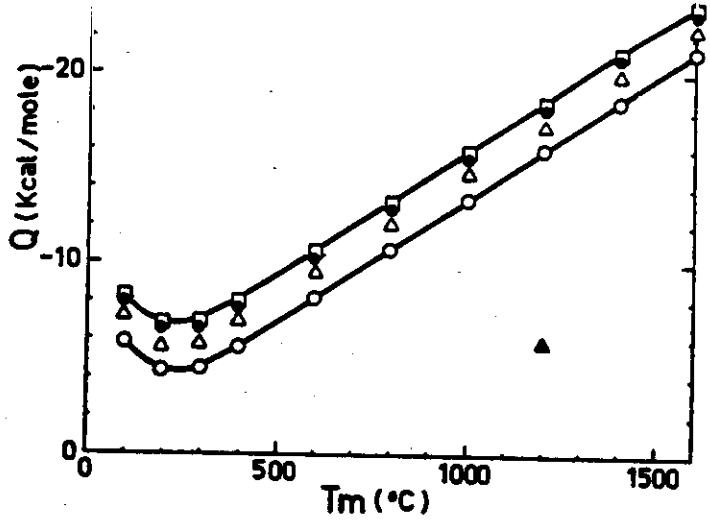

FIG. 8. The apparent activation energies for crack propagation under the surface mobility mechanism, as a function of the surface melting point. Q values were calculated from the V_p values predicted at 0°C and 100°C, in the absence of hydrogen, and with the following stress values at the tip of the crack: □ = 85 MPa; ● = 240 MPa; △ = 800 MPa; and ○ = 1400 MPa. ▲: Example of a Q value calculated in the presence of hydrogen (T_m = 1200°C; σ = 500 MPa; E_b = 0.53 eV).

From equations (6) and (10) the crack velocities for T_m values between 100°C and 1600°C, for σ values from 85 MPa up to 1400 MPa, and for temperatures of 0°C and 100°C, were calculated. With these V_p values, the apparent activation energies were found, and these values are shown in Fig. 8. The present theory predicts that, in the absence of hydrogen and for σ values ranging between 1400 MPa and 85 MPa, the apparent activation energy could span between 4.2 and 23.6 kcal mole^{-1}. In the presence of hydrogen the values will be lower, because of the contribution of αE_b.

The most reliable experimental Q_{cp} values available are those measured by techniques of fracture mechanics. Three regions are usually detected in the log V_p vs stress intensity diagrams, and different Q_{cp} values are found for each region. As we will see later, Region II is the one that most probably relates to the present mechanism. The activation values measured in this region follow closely the values predicted in Fig. 8. For aluminium alloy 7039-T64, in aqueous KI solutions, two values were found for this region,[52] one of 20 kcal mole^{-1} and the other of 4 kcal mole^{-1}. For aluminium alloy 7079-T651, in 3 M aqueous KI solution, for the same region, a value of 3.8 kcal mole^{-1} was reported.[52] For Nimonic 105, steel 300M, 12% chromium steel and aluminium alloy 7039 T061, all of them in distilled water, Speidel[90] reported a value of *ca* 9 kcal mole^{-1}. For Monel 400 in 0.063 M CuF_2 + 0.38 M HF solution an apparent activation energy of *ca* 11 kcal mole^{-1} has been found.[94] For titanium alloys in 1 M HCl and 0.6 M neutral chloride solutions, the activation energy values reported are *ca* 5 kcal mole^{-1}.[71] All these values fall closely in the region predicted by Fig. 7.

Values lower than the minimum in Fig. 7, i.e. 4.2 kcal mole^{-1}, particularly for T_m values higher than 300°C, are most probably due to the contribution of αE_b. For example, in the above studied case of iron, assuming that T_m = 1200°C, $\sigma = 5 \times 10^8$ N m^{-2}, and αE_b = 0.53 eV, in the absence of hydrogen the activation energy would be

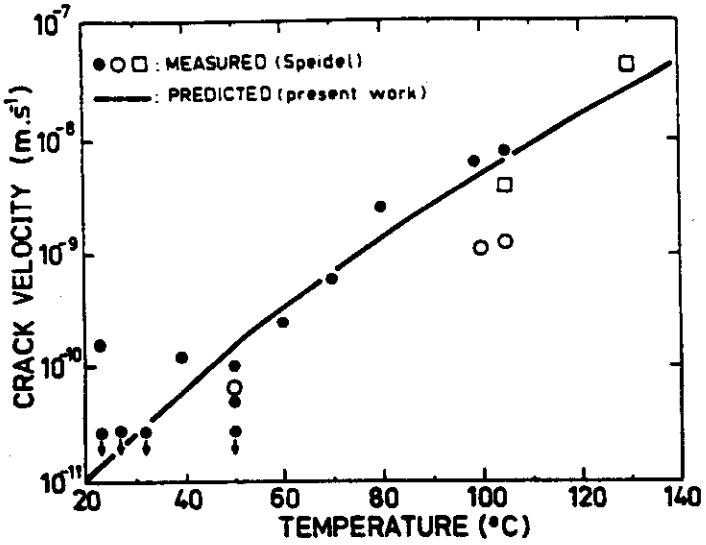

FIG. 9. A comparison between theory and experiment: effect of temperature on the rate of stress corrosion cracks in austenitic stainless steels exposed to chloride solutions; experiments reported by Speidel.[87] ●: 304 sensitized; ○: 304 annealed; □: 304L annealed. Experiment at 130°C in 42% $MgCl_2$; all the other experiments in aerated 22% NaCl solution. For the predicted values the following parameters were used: T_m = 1100°C; σ = 240 MN m^{-2} (yield strength of the samples used by Speidel).

17.8 kcal mole^{-1}, while in the presence of hydrogen it should drop to 5.8 kcal mole^{-1}.

As pointed out above, the exact T_m value of the films formed in aqueous solutions cannot be given at present. But, it is possible at least to see if the predictions of the present mechanism follow the trend of the experimental values. Figure 9 shows the values reported by Speidel[87] for austenitic stainless steels type 304 and 304L in aqueous chloride solutions, as compared with the change in V_p with temperature predicted by the present mechanism. The conclusion to be drawn from Fig. 9 is that if V_p is measured for one temperature, the values at the other temperatures can be predicted with the present mechanism.

It is with the purpose of pointing to this predictive capability that Figs 10, 11 and 12 have been prepared. They show the V_p values predicted by the present mechanism, for σ values of 240, 800 and 1400 MN m^{-2}. For the sake of comparison, the values measured by Speidel on 304 stainless steels in chloride solutions were included in Fig. 10. Figure 11 shows some other experimental values reported by Speidel.[90] In all these cases the measured values follow the trend predicted by the mechanism described in the present paper.

MEASUREMENTS EMPLOYING FRACTURE MECHANICS

The techniques of fracture mechanics are very important in the studies of environmental cracking,[95] and it would be very convenient to find out how the present mechanism fits in with the information obtained through those techniques. For that purpose we have to find a relation of the stress at the tip of the crack, σ, with the stress applied to a pre-cracked specimen, σ_a, and with the stress intensity, K. Paskin *et al.*,[25] using molecular dynamic simulations, investigated the stress distribution, at an atomic level, near the tip of a crack. They found a linear relation

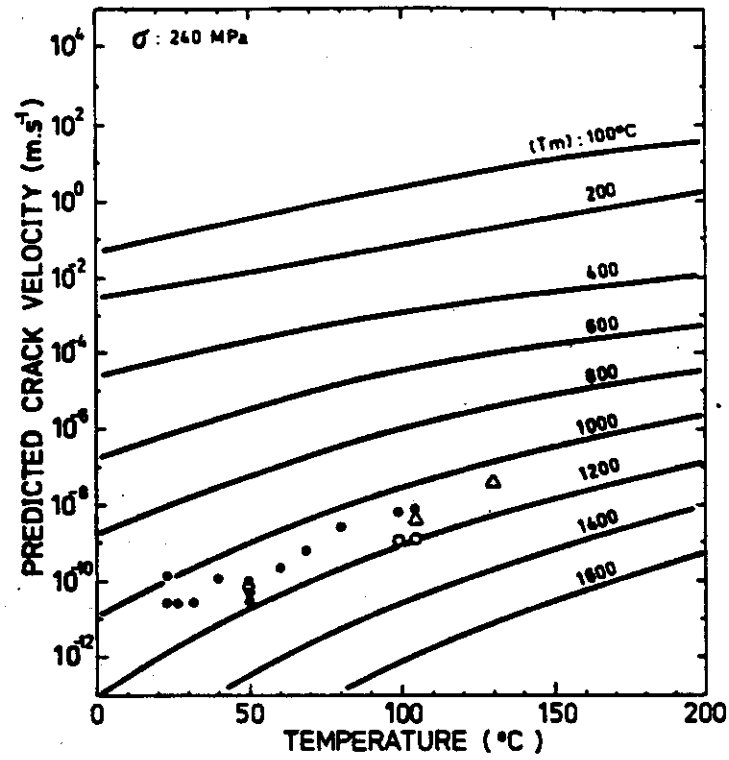

FIG. 10. The prediction of the effect of temperature on the growth rate of stress corrosion cracks, for various T_m values, and with a stress, at the tip of the crack, of 240 MN m^{-2}. The experimental points were reported by Speidel[87] for AISI 304 exposed to chloride solutions.

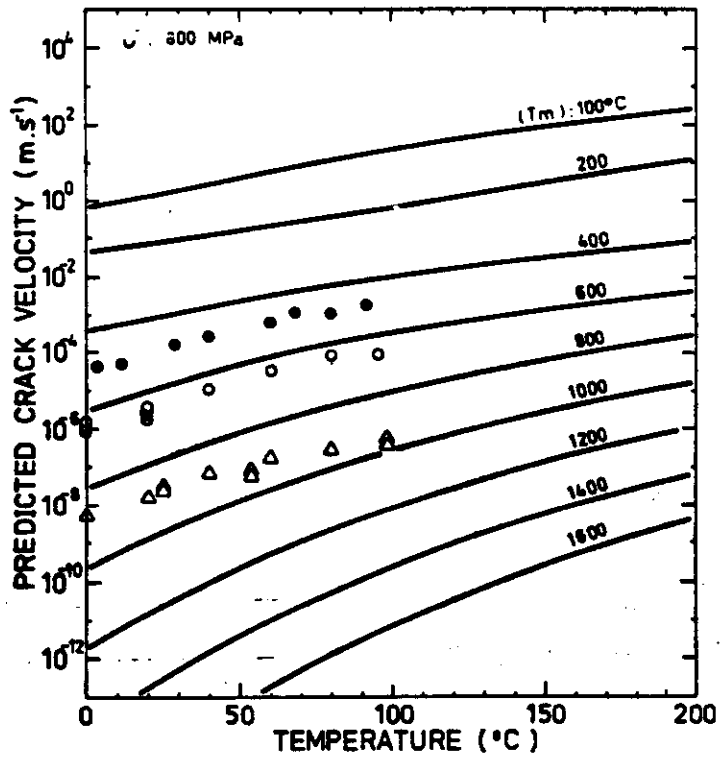

FIG. 11. The prediction of the effect of temperature on the growth rate of stress corrosion cracks, for various T_m values, and with a stress, at the tip of the crack, of 800 MN m^{-2}. Experimental values reported by Speidel:[90] ●: Nimonic 105; ○: steel 300 M; △: 12% chromium steel, all treated in distilled water.

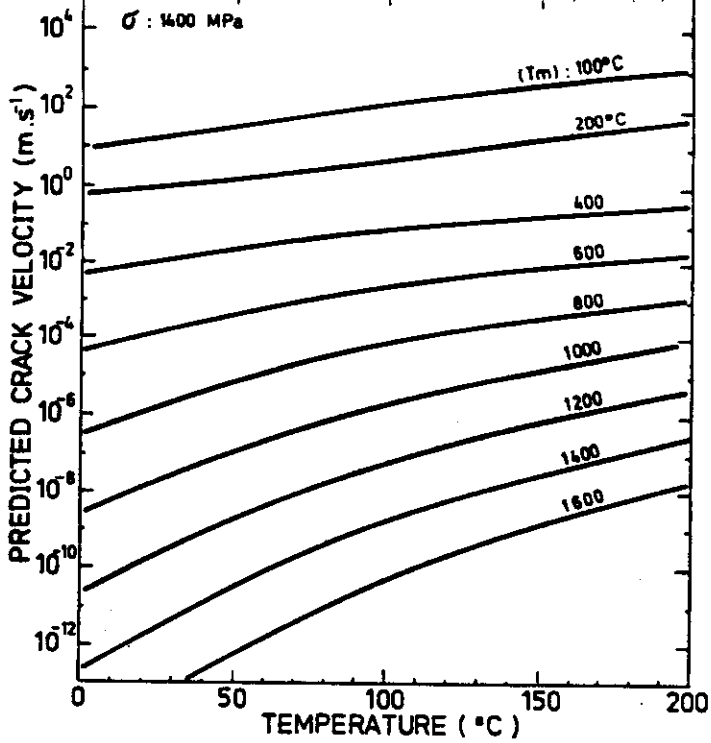

FIG. 12. The prediction of the effect of temperature on the growth rate of stress corrosion cracks, for various T_m values, and with a stress, at the tip of the crack, of 1400 MN m^{-2}.

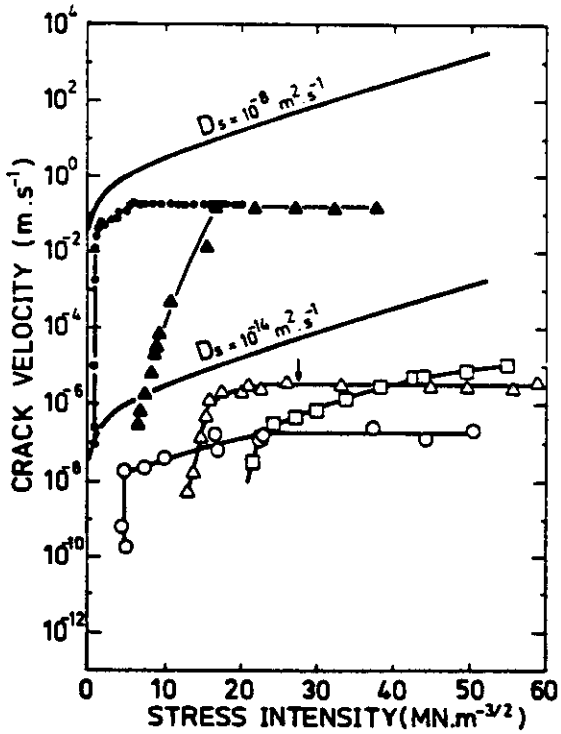

FIG. 13. The predicted effect of stress intensity on stress corrosion crack velocity, for two different surface self-diffusion coefficients, at 25°C. Comparison with experimental values reported in the literature: ●: aluminium alloy 7075-T651 in liquid mercury at 23°C;[52] ▲: titanium alloy (Ti–8Al–1Mo–1V) in liquid mercury at 24°C;[99] ○: yellow brass (Cu–63% Zn) over NH_4OH solution, at room temperature;[97] △: Zircaloy-4 in 1 M KBr + 0.25 M Br_2, open circuit, 23°C;[98] □: Zircaloy-4 in 3 M KI solution at +450 mV(NHE).[98]

between the stress concentration factor $[(\sigma/\sigma_a) - 1]$, at the tip of the crack, and the crack length, d. Their results fit the following equation:

$$\frac{\sigma}{\sigma_a} - 1 = 0.34 \frac{d}{a} \tag{13}$$

where σ is the local stress at the tip of the crack, d is the half crack length and a the interatomic spacing. In the present case, $a = 2.5 \times 10^{-10}$ m. To be coherent with Paskin *et al.*'s work, for the stress intensity factor, K, for mode I behaviour;

$$K_I = \sigma_a(\pi d)^{1/2} \tag{14}$$

which applies to a sharp elliptical crack with major axis length of $2d$.

From equations (6), (13) and (14) the crack velocity, V_p, can be calculated as a function of the stress intensity, K_I. Figure 13 shows the results for two D_s values, assuming a value of $d = 2.5 \times 10^{-3}$ m for the half crack length. The values chosen for the surface self-diffusion coefficients were $D_s = 10^{-8}$ m^2 s^{-1}, and $D_s = 10^{-14}$ m^2 s^{-1}. The first value is expected at the melting point of the metal or the surface contaminant,[41,42] and is the value we expect in LME. The other value, $D_s = 10^{-14}$ m^2 s^{-1}, corresponds to $T_m = 550$°C, and should apply to cases of fast SCC. The same figure shows various experimental curves for LME and SCC.

As was expected, the predicted curves are similar in shape to those in Fig. 3. In the absence of adsorbed substances that could inhibit surface mobility, small stress intensity values will lead to a sharp increase in V_p. In practice this is seldom found. Adsorption of oxygen or water vapor will lead to the surface adsorption of high melting point products that will hinder the crack propagation process. The only exception among the cases reported in Fig. 13 is aluminium–mercury. It is well known that, once mercury wets an aluminium surface,[96] the latter metal loses its ability to form protective films. As shown in Fig. 13, the values measured for 7075 aluminium alloy in mercury[52] follow very closely the predicted values, thus suggesting that the cracks propagate by the mechanism described in the present paper, and that the D_s value chosen is correct. When oxide films are formed, higher K_I values are needed to start cracking, an aspect that was covered by various authors[8] when discussing anodic dissolution and other SCC mechanisms.

After the initial part, Region I, all the experimental curves show variable lengths of curved regions that closely follow the predicted values. Similar curved regions were reported in various other systems, like aluminium alloy 7039-T61 in distilled water at 80 and 99°C;[100] Ti–6Al–4V alloy in 5.0 M KI solution at various potentials;[99] Ti–8Al–1Mo–1V alloy in the following media: 10 M HCl solution at various temperatures,[99] spectrograde methanol and methanol–KI solutions,[99] spectrograde carbon tetrachloride and carbon tetrachloride plus iodine;[99] U–4.5% Nb in wet oxygen,[89] etc.

At higher K_I values a plateau is usually reached, which is called Region II. One frequent explanation for the occurrence of this region is that it is due to environmental limitations to crack propagation.[52,71,91,101] It is assumed that cracks can grow only as fast as the embrittling species can be transported to the crack tip. In SCC this would be related to the maximum rate at which the metal can be solvated, leading to growth by dissolution, or, in HE, the maximum rate at which hydrogen is transported to the region of crack growth. This explanation seems to be correct for LME, where, as shown in Fig. 13, different metals, like aluminium and titanium alloys, reach the

same crack velocity in mercury. It is not, though, as clear in other cases. Crack velocity in Region II is strongly dependent on the electrode potential for aluminium alloys[52] and for titanium alloys.[88] This could be understood in the mechanism described in this paper, because the degree of coverage of the anodic surface film is a function of the potential, and will have a strong effect on the D_s value. On the other hand, it is not so clearly understood how the rate of metal solvation could be so radically changed by the potential.

For the surface mobility mechanism, the presence of a plateau indicates that, provided the corrodent reaches the tip of the crack, the maximum stress at the tip of the crack should reach a constant value, above a certain K_I value. Several indications support this conclusion. Atomic crack modeling[24] shows that, when K_I is increased, in ductile metals, dislocations are emitted from the crack. This will have the effect of crack tip blunting, and will limit the maximum stress value, at the crack tip. If this was correct, V_p, in Region II, should be a function of the yield strength of the material. This type of dependence is observed in some aluminium alloys[52] where overaging produces a decrease in the V_p value. This effect is most noticeable in the case of steels in deaerated water, at 100°C. In this system Speidel[97] found a very strong effect of the yield strength of the steel on the V_p value in Region II. He observed that when the tensile yield strength of the steel increases from 700 to 1600 MN m^{-2}, the Region II crack velocity increases from 10^{-11} m s^{-1} to 10^{-4} m s^{-1}. According to the surface mobility mechanism, the higher the yield strength, the higher the maximum σ value at the crack tip. According to this same mechanism, the activation energies measured in Region II should follow the values predicted in Fig. 8, as seems to be the case.

It would be of interest to determine if the crack microbranching and macrobranching frequently observed in Region II[88,97] have their origin in the same process that limits the maximum value of σ.

FRACTURE MORPHOLOGY

As shown in Fig. 1, in the surface mobility mechanism, crack propagation is equivalent to the relocation of a single layer of atoms, A–A'. If the corrosion rate of the alloy in the environment is low, and if the experimental conditions are such that plastic deformation of the cracked surfaces is minimal, both sides of the crack should match perfectly after cracking, even at very high magnifications. This type of matching crack surfaces has been reported by various authors.[102-106]

According to the present mechanism, the choice between intergranular and transgranular cracking is subtle, and both types of cracks could be present in the same alloy. Grain boundary segregation of low melting point impurities, as in high strength steels,[83] or of low pitting potential phases, as in aluminium alloys,[107] will favour intergranular SCC. On the other hand, thin and adherent passive films can limit crack initiation to slip steps, and transgranular cracking will be found. In this case, cracking will start on the slip steps, but it will break into smaller cracks, perpendicular to the tensile stress direction, as reported for austenitic stainless steels in $MgCl_2$ solutions,[108] and for copper single crystals in sodium nitrite solutions.[109]

According to Fig. 1, the cracks will propagate in a direction perpendicular to the tensile stress direction. The anisotropy of surface diffusion,[38,39] however, suggests that cracks will try to follow those crystallographic planes where D_s is higher. Unfortunately, most of the D_s vs crystal orientation information on those metals that are of interest from an environmental cracking point of view was obtained only at

...in the absence of contaminants. We have not enough experimental information at present to predict the crystallographic planes on which cracks will propagate.

In a recent review[110] it was shown that cracks in bcc metals are very close to {100} planes. Surface diffusion measurements on tungsten[39] show that at room temperature the surface diffusion rate decreases in the following way:

$$\{211\} > \{110\} \simeq \{321\}.$$

Measurements on Fe–Si,[111] at high temperatures, show that at 1400 K D_s for {100} planes is close to that for {110} planes. Extrapolations at lower temperatures give:

$$\{100\} \gg \{110\}.$$

It is not known if this relation can be extrapolated to room temperature.

For fcc metals there is some disagreement in the information[110] reported, but it is found that cracks usually initiate at {111} slip planes and propagate, in non-ferrous metals, along {110} planes. For austenitic stainless steels the cracks propagate close to {100} planes, although {110} and {111} planes were also reported.

As for surface diffusion, for copper at 800°C the following order was reported:[112]

$$\{110\} > \{111\} \gg \{100\}.$$

For surface diffusion on fcc metals, at room temperature, the following information is available:[39]

for rhodium:

$$\{111\} > \{110\} > \{331\} > \{100\}$$

and for platinum:

$$\{110\} > \{311\} \simeq \{331\}.$$

The information available confirms that, as expected, there is anisotropy in crack propagation. As for the exact planes on which cracks should propagate, although coincidences are observed between fracture orientation and surface diffusivity, there is no adequate information on which to make a reliable prediction. It should be pointed out also that the present mechanism applies to LME, SCC, and HE of non-hydride forming metals. It should not be extended to systems where cracking is due to brittle hydrides, where cracks will follow the habit planes of those hydrides.

DISCUSSION AND CONCLUSION

According to the mechanism developed in the present paper, crack velocities should be predictable, provided the composition and the properties of the surface contaminants are known. The results found for aluminium alloys in mercury, Fig. 13, are satisfactory. Another area where reasonable predictions could be expected is in corrosive gaseous environments. Kerns and Staehle[113] reported that high strength steels are susceptible to slow crack growth in chlorine gas environments. In 300 torr dry chlorine, at room temperature, they reported crack velocities between 1.1×10^{-3} and 1.5×10^{-3} m s^{-1}. From the work of Sieradzki and Ficalora[114] it can be assumed that higher crack velocities should be found at higher chlorine pressures.

Daniel and Rapp[58] reported that iron, in the presence of chlorine, forms two chlorides: $FeCl_2$ and $FeCl_3$ (or Fe_2Cl_6), their melting points being, respectively,

675°C and 306°C. The fact that, from X-ray photoelectron spectroscopy (XPS) studies only $FeCl_2$ was reported,[115] could be a source of confusion. But in that work all the effort was applied to demonstrate the presence of an iron halide film. The difference in XPS peaks for $FeCl_2$ and $FeCl_3$ is only 0.7 eV,[116] and no deconvolution of the peak was reported.[115] On the other hand, the shakeup satellite of 4.4 eV quoted by Sieradzki[115] was measured by Vernon *et al.*[117] on $FeCl_3$, not on $FeCl_2$. All seems to indicate that Daniel and Rapp are correct, and that both $FeCl_2$ and $FeCl_3$ are formed. From the point of view of the proposed model, the most aggressive one will be that with the lowest melting point, $FeCl_3$. From Fig. 7 the value of D_s at 20°C, for full coverage with $FeCl_3$, should be $3 \times 10^{-12}\ m^2 s^{-1}$. If the tensile stress, at the bottom of the crack, is of the order of 1000 MPa, Fig. 3 predicts a maximum crack velocity of $1.26 \times 10^{-2}\ m\ s^{-1}$. The predicted and the experimental values show very good agreement, if allowance is made for the fact that the predicted V_p is the maximum value expected, and that the one reported by Kerns and Staehle should be higher for higher chlorine pressures.

If we apply the same reasoning to high strength steels in fluorine, where the melting point of FeF_3 is 1027°C, the present mechanism predicts, for 1000 MPa, a crack velocity of $2 \times 10^{-9}\ m\ s^{-1}$, a point that could be experimentally checked.

In the case of SCC in aqueous environments, although anodic dissolution cannot be sustained as the cause of crack propagation, the concept of repassivation as a critical factor in the propagation of stress corrosion cracks, introduced by Scully[118] and endorsed by many authors,[56,119–123] has to be re-vindicated. As most of the oxide films have a high melting point, they will inhibit surface diffusion. If repassivation is fast and follows a mechanism of the type:[124]

$$Me + H_2O = MeOH_{ad} + H^+ + e^-$$

$$MeOH_{ad} = MeO_{ad} + H^+ + e^-$$

there is no time for the surface diffusion necessary to produce crack propagation. As soon as water or oxygen molecules are adsorbed on the metal surface, surface mobility will be inhibited.

If on the other hand, repassivation follows a dissolution and precipitation mechanism[55] we could expect a reaction like:

$$MeX_{ad} = X^- + Me^{2+} + e^-$$

$$Me^{2+} + H_2O = MeO_s + 2H^+$$

or similar, where X is an anion adsorbed to the metal surface. This would be a slower repassivation process that will allow for surface mobility, provided MX is a low melting point compound. According to the surface mobility mechanism, slow repassivation is a necessary but not a sufficient condition for SCC, a point confirmed by recent repassivation rate measurements.[125]

The application of the present mechanism to aqueous environments is not as straightforward as it is to LME or to gaseous environments. The competitive adsorption of MeX and water molecules leads to D_s values much lower than those found when only MeX is present. In this case only a qualitative evaluation of the degree of aggressiveness of the various compounds can be made, as shown in Table 1. The frequently reported observation of specificity in SCC can be explained in this way. In order to make a quantitative prediction of the V_p values, the degree of surface coverage by MeX, and its effect on D_s value, should be known.

It is concluded that the crack velocity, V_p, in SCC, LME and HE of non-hydride forming metals, could be predicted by the following equation:

$$V_p = \frac{D_s}{L}\left[\exp\left(\frac{\sigma a^3 + \alpha E_b}{kT}\right) - 1\right]$$

where D_s is the surface self-diffusion of the metal; L is a diffusion path, typically of 10^{-8} m; a is the atomic diameter; σ the maximum stress at the tip of the crack; E_b the hydrogen–vacancy binding energy; α the relative degree of saturation with hydrogen of a vacancy at the tip of a crack; k the Boltzmann constant; and T the absolute temperature. D_s is strongly affected by the composition of the environment, and an empirical relation is used for its calculation.

Acknowledgements—This research has been supported by the Proyecto Multinacional de Tecnología de Materiales OEA-CNEA. The author is grateful to Dr Eduardo Savino for many stimulating discussions that have helped in developing the SCC mechanism reported here. The support and stimulation of the author's students and Research Associates is also gratefully acknowledged.

REFERENCES

1. J. R. Galvele, *Proceedings of the 7th International Congress on Metallic Corrosion*, Vol. 1, p. 65. ABRACO-Rio de Janeiro (1978).
2. J. R. Galvele, *Bol. Acad. Nac. Ciencias, Córdoba, Argentina* **54**, 79 (1980).
3. F. S. Spiers (ed.), *The Failure of Metals Under Internal and Prolonged Stress—A General Discussion*. The Faraday Society, London (1921).
4. H. L. Logan, *The Stress Corrosion of Metals*. Wiley, New York (1967).
5. R. W. Staehle, A. J. Forty and D. van Rooyen (eds), *Fundamental Aspects of Stress Corrosion Cracking*. National Association of Corrosion Engineers, Houston (1969).
6. J. C. Scully (ed.), *The Theory of Stress Corrosion Cracking in Alloys*. NATO Scientific Affairs Division, Brussels (1971).
7. Z. A. Foroulis (ed.), *Environment-Sensitive Fracture of Engineering Materials*. The Metallurgical Society of AIME, New York (1979).
8. F. P. Ford, in *Corrosion Processes* (ed. R. N. Parkins), p. 271. Applied Science Publishers, London (1982).
9. J. C. Scully, in *Treatise on Materials Science and Technology. Vol. 23, Corrosion: Aqueous Processes and Passive Films* (ed. J. C. Scully), p. 103 (1983).
10. R. M. Latanision and J. R. Pickens (eds), *Atomistics of Fracture*. Plenum Press, New York (1983).
11. R. Rungta (ed.), *Predictive Capabilities in Environmentally Assisted Cracking*. The American Society of Mechanical Engineers, New York (1985).
12. N. S. Stoloff, in *Atomistics of Fracture* (eds R. M. Latanision and J. R. Pickens), p. 921. Plenum Press, New York (1983).
13. R. M. Latanision, in *Atomistics of Fracture* (eds R. M. Latanision and J. R. Pickens), p. 3. Plenum Press, New York (1983).
14. S. P. Lynch, *Scripta Metall.* **13**, 1051 (1979).
15. J. R. Galvele, International Society of Electrochemistry, 36th Meeting, Salamanca, Spain 1985. *Extended Abstracts*, p. 1.3.
16. J. R. Galvele, *J. electrochem. Soc.* **133**, 953 (1986).
17. M. F. Ashby, *Acta Metall.* **20**, 887 (1972).
18. G. E. Rhead, *Surf. Sci.* **47**, 207 (1975).
19. H. G. Van Bueren, *Imperfections in Crystals*, p. 236. North-Holland, Amsterdam (1960).
20. C. Herring, *J. appl. Phys.* **21**, 437 (1950).
21. T. Chuang and J. R. Rice, *Acta Metall.* **21**, 1625 (1973).
22. T. Chuang, K. I. Kagawa, J. R. Rice and L. B. Sills, *Acta Metall.* **27**, 265 (1979).
23. A. C. F. Cocks and M. F. Ashby, *Prog. Mat. Sci.* **27**, 189 (1982).
24. B. de Celis, A. S. Argon and S. Yip, *J. appl. Phys.* **54**, 4864 (1983).
25. A. Paskin, B. Massoumzadeh, K. Shukla, K. Sieradzki and G. J. Dienes, *Acta Metall.* **33**, 1987 (1985).

26. Y. Quéré, *Défauts Ponctuels Dans les Métaux*, p. 97. Masson et Cie, Paris (1967).
27. R. M. Thompson, in *Physical Metallurgy* (eds R. W. Cahn and P. Haasen), 3rd edn, p. 1490. North-Holland Physics Publishing, Amsterdam (1983).
28. J. R. Galvele, in *Predictive Cababilities in Environmentally Assisted Cracking* (ed. R. Rungta), p. 273. The American Society of Mechanical Engineers, New York (1985).
29. M. G. Alvarez, C. Manfredi, M. Giordano and J. R. Galvele, *Corros. Sci.* **24**, 769 (1984).
30. I. A. Maier, C. Manfredi and J. R. Galvele, *Corros. Sci.* **25**, 15 (1985).
31. R. N. Parkins, *Br. Corros. J.* **14**, 5 (1979).
32. A. Seeger, *J. Less-Common Metals* **28**, 387 (1972); A. H. Cottrell, *An Introduction to Metallurgy*, p. 356. St. Martin's Press, New York (1967).
33. L. Pauling, *The Nature of the Chemical Bond*, p. 410. Cornell University Press (1960).
34. P. Wynblatt and N. A. Gjostein, *Surf. Sci.* **12**, 109 (1968).
35. K. Vetter, *Electrochemical Kinetics*, p. 315. Academic Press, New York (1967).
36. E. B. Budevski, in *Comprehensive Treatise of Electrochemistry* (eds B. E. Conway, J. O'M. Bockris, E. Yeager, S. U. M. Khan and R. E. White), Vol. 7, p. 416. Plenum Press, New York (1985).
37. N. A. Gjostein, in *Surfaces and Interfaces*—I (eds J. J. Burke, N. L. Reed and V. Weiss), p. 271. Syracuse University Press (1967).
38. G. Neumann and G. M. Neumann, *Surface Self-Diffusion of Metals*, DMS-1, Diffusion Information Center, Switzerland (1972).
39. G. Ehrlich and K. Stolt, *Ann. Rev. Phys. Chem.* **31**, 603 (1980).
40. G. Ehrlich, *J. Vac. Sci. Technol.* **17**, 9 (1980).
41. G. E. Rhead, *Surf. Sci.* **15**, 353 (1969).
42. G. E. Rhead, *Surf. Sci.* **22**, 223 (1970).
43. F. Delamare and G. E. Rhead, *Surf. Sci.* **28**, 267 (1971).
44. O. Oda and G. E. Rhead, *Scripta Metall.* **13**, 985 (1979).
45. J. Henrion and G. E. Rhead, *Surf. Sci.* **29**, 20 (1972).
46. F. Delamare and G. E. Rhead, *Surf. Sci.* **35**, 172, 185 (1973).
47. M. Pichaud and M. Drechsler, *Surf. Sci.* **36**, 813 (1973).
48. K. Vetter, *Electrochemical Kinetics*, p. 283. Academic Press, New York (1967).
49. E. B. Budevski and A. R. Despić, in *Comprehensive Treatise of Electrochemistry* (eds B. E. Conway, J. O'M. Bockris, E. Yeager, S. U. M. Khan and R. E. White). Vol. 7, pp. 399, 451. Plenum Press, New York (1985).
50. A. R. Despić, private communication, I.S.E. Meeting, Salamanca (1985).
51. G. Grimvall and S. Sjödin, *Physica Scripta (Sweden)* **10**, 340 (1974).
52. M. O. Speidel, in *The Theory of Stress Corrosion Cracking in Alloys* (ed. J. C. Scully), p. 289. NATO Scientific Affairs Division, Brussels (1971).
53. R. N. Parkins, C. M. Rangel and J. Yu, *Metall. Trans.* **16A**, 1671 (1985).
54. M. O. Speidel and J. E. Bertilsson, *Corrosion in Power Generating Equipment* (eds M. O. Speidel and A. Atrens), p. 331. Plenum Press, New York (1984).
55. T. E. Evans, in *Passivity of Metals* (eds R. P. Frankenthal and J. Kruger), p. 410. The Electrochemical Society, New Jersey (1978).
56. R. W. Staehle, in *The Theory of Stress Corrosion Cracking in Alloys* (ed. J. C. Scully), p. 223. NATO Scientific Affairs Division, Brussels (1971).
57. R. C. Weast (ed.), *Handbook of Chemistry and Physics*, 54th edn. CRC Press, The Chemical Rubber Co., Cleveland, Ohio (1973–1974).
58. P. L. Daniel and R. A. Rapp, in *Advances in Corrosion Science and Technology* (eds M. G. Fontana and R. W. Staehle), Vol. 5, p. 55. Plenum Press, New York (1976).
59. C. J. Smithells and E. A. Brandes (eds), *Metals Reference Book*, 5th edn. Butterworths, London (1978).
60. Y. S. Park, J. R. Galvele, A. K. Agrawal and R. W. Staehle, *Corrosion* **34**, 413 (1978).
61. A. Kawashima, A. K. Agrawal and R. W. Staehle, *Stress Corrosion Cracking—The Slow Strain Rate Technique* (eds G. M. Ugiansky and J. H. Payer), p. 266. American Society for Testing Materials, Philadelphia (1979).
62. M. Saenz de Santa Maria and J. C. Scully, *Corros. Sci.* **23**, 753 (1983).
63. L. Graf, in *Fundamental Aspects of Stress Corrosion Cracking* (eds R. W. Staehle, A. J. Forty and D. van Rooyen), p. 187. National Association of Corrosion Engineering, Houston (1969).
64. R. N. Parkins and R. Usher, *First International Congress on Metallic Corrosion*, p. 289. Butterworths, London (1961).

65. T. P. Hoar and J. R. Galvele, *Corros. Sci.* **10**, 211 (1970).
66. M. J. Humphries and R. N. Parkins, *Corros. Sci.* **7**, 747 (1967).
67. T. P. Hoar and R. W. Jones, *Corros. Sci.* **13**, 725 (1973).
68. P. Pascal, *Nouveau Traité de Chimie Minérale, Vol. XVII, Deuxieme Fascicule*, p. 804. Masson et Cie, Paris (1963).
69. L. L. Shreir, *Corrosion*, p. 5:62. Newnes-Butterworths, London (1978).
70. M. F. Abd Rabboh and P. J. Boden, in *Localized Corrosion* (eds R. W. Staehle, B. F. Brown, J. Kruger and A. Agrawal), p. 653. National Association of Corrosion Engineers, Houston (1974).
71. T. R. Beck, in *Theory of Stress Corrosion Cracking in Alloys*, (ed. J. C. Scully), p. 67. NATO Scientific Affairs Division, Brussels (1971).
72. A. R. Ubbelohde, *Melting and Crystal Structure*. Claredon Press, Oxford (1965).
73. H. K. Birnbaum, in *Environment-Sensitive Fracture of Engineering Materials* (ed. Z. A. Foroulis), p. 326. The Metallurgical Society of AIME, New York (1979).
74. S. P. Lynch, *Acta Metall.* **32**, 79 (1984).
75. A. W. Thompson and I. M. Bernstein, in *Advances in Corrosion Science and Technology* (eds M. G. Fontana and R. W. Staehle), Vol. 7, p. 53. Plenum Press, New York (1980).
76. R. M. Latanision, O. H. Gastine and C. R. Compeau, in *Environment-Sensitive Fracture of Engineering Materials* (ed. Z. A. Foroulis), p. 48. The Metallurgical Society of AIME, New York (1979).
77. J. K. Nørskov, F. Besenbacher, J. Bøttiger, B. B. Nielsen and A. A. Pisarev, *Phys. Rev. Lett.* **49**, 1420 (1982).
78. K. B. Kim and S. I. Pyun, *Archiv für Eisenhüttenwesen* **53**, 397 (1982).
79. R. Gibala, in *Stress Corrosion Cracking and Hydrogen Embrittlement of Iron Base Alloys* (eds R. W. Staehle, J. Hochmann, R. D. McCright and J. E. Slater), p. 244. National Association of Corrosion Engineers, Houston (1977).
80. R. A. Oriani and P. H. Josephic, *Acta Metall.* **22**, 1065 (1974).
81. R. A. Oriani, in *Stress Corrosion Cracking and Hydrogen Embrittlement of Iron Base Alloys* (eds R. W. Staehle, J. Hochmann, R. D. McCright and J. E. Slater), p. 351. National Association of Corrosion Engineers, Houston (1977).
82. R. A. Oriani, *Ann. Rev. Mat. Sci.* **8**, 327 (1978).
83. H. K. Birnbaum, in *Atomistics of Fracture* (eds R. M. Latanision and J. R. Pickens), p. 733. Plenum Press, New York (1983).
84. R. H. Jones, S. M. Bruemmer, M. T. Thomas and D. R. Baer, *Metall. Trans.* **14A**, 1729 (1983).
85. R. A. Oriani and P. H. Josephic, *Acta Metall.* **25**, 979 (1977).
86. R. F. Hehemann, *Metall. Trans.* **16A**, 1909 (1985).
87. M. O. Speidel, *Metall. Trans.* **12A**, 779 (1981).
88. M. J. Blackburn, J. A. Feeney and T. R. Beck, in *Advances in Corrosion Science and Technology* (eds M. G. Fontana and R. W. Staehle), Vol. 3. p. 67. Plenum Press, New York (1973).
89. N. J. Magnani, in *Advances in Corrosion Science and Technology* (eds M. G. Fontana and R. W. Staehle), Vol. 6, p. 89. Plenum Press, New York (1976).
90. M. O. Speidel, unpublished data (1978); in *ARPA-Handbook on SCC* (eds R. W. Staehle and M. O. Speidel), in press.
91. N. S. Stoloff, in *Environment-Sensitive Fracture of Engineering Materials* (ed. Z. A. Foroulis), p. 486. The Metallurgical Society of AIME, New York (1979).
92. C. F. Old, *Metal Sci.* **14**, 433 (1980).
93. G. A. Whitlow, C. G. Beck, R. Viswanathan and E. A. Crombie, *Metall. Trans.* **15A**, 23 (1984).
94. L. Graf and W. Wittich, *Werkst. Korros.* **17**, 385 (1966).
95. H. R. Smith and D. E. Piper, in *Stress-Corrosion Cracking in High Strength Steels and in Titanium and Aluminium Alloys* (ed. B. F. Brown), p. 17. Naval Research Laboratory, Washington (1972).
96. P. Pascal, *Nouveau Traité de Chimie Minérale*, Vol. XX, 2eme Fascicule, p. 1762. Masson et Cie, Paris (1963).
97. M. O. Speidel, in *Corrosion in Power Generating Equipment* (eds M. O. Speidel and A. Atrens), p. 85. Plenum Press, New York (1984).
98. M. O. Speidel, presentation to ASTM Committee E-24-Sub IV, Los Angeles, 1971, and in *ARPA-Handbook on SCC* (eds R. W. Staehle and M. O. Speidel), in press.
99. T. R. Beck, M. J. Blackburn, W. H. Smyrl and M. O. Speidel, in *Advances in Corrosion Science and Technology* (eds M. G. Fontana and R. W. Staehle), Vol. 3, p. 184. Plenum Press, New York (1973).

100. M. O. Speidel, in *Proceedings of Conference: Hydrogen in Metals*, p. 249, ASM (1974), and in *ARPA-Handbook on SCC* (eds R. W. Staehle and M. O. SPeidel), in press.
101. R. N. Parkins, in *Corrosion in Power Generating Equipment* (eds M. O. Speidel and A. Atrens), p. 53. Plenum Press, New York (1984).
102. N. A. Nielsen, *Corrosion* **27**, 173 (1971).
103. A. J. Bursle and E. N. Pugh, in *Environment-Sensitive Fracture of Engineering Materials* (ed. Z. A. Foroulis), p. 18. The Metallurgical Society of AIME, New York (1979).
104. R. Liu, N. Narita, C. Altstetter, H. Birnbaum and E. N. Pugh, *Metall. Trans.* **11A**, 1563 (1980).
105. E. I. Meletis and R. F. Hochman, *Corros. Sci.* **24**, 843 (1984).
106. B. D. Lichter, T. B. Cassagne, W. F. Flanagan and E. N. Pugh, *Microstruct. Sci.* **13**, 361 (1985).
107. J. R. Galvele, S. M. de De Micheli, I. L. Muller, S. B. de Wexler and I. L. Alanis, in *Localized Corrosion* (eds R. W. Staehle, B. F. Brown, J. Kruger and A. Agrawal), p. 580. National Association of Corrosion Engineers, Houston (1974).
108. J. M. Silcock, *Br. Corros. J.* **16**, 78 (1981).
109. K. Sieradzki, R. L. Sabatini and R. C. Newman, *Metall. Trans.* **15A**, 1941 (1984).
110. E. I. Meletis and R. F. Hochman, *Corros. Sci.* **26**, 63 (1986).
111. B. Mills and P. Douglas, *Colloq. Intl. Cent. Nat. Rech. Sci.* No. 187, 207 (1970); *D.D.D.* **5**, (1) A13 (1971).
112. Do Van Hai, Kaganovskii, S. Yu, *Fiz. Metal. Metalloved.* **35**, 649 (1973); *D.D.D.* **8**, A36 (1974).
113. G. E. Kerns and R. W. Staehle, *Scripta Metall.* **6**, 1189 (1972).
114. K. Sieradzki and P. Ficalora, *Scripta Metall.* **13**, 535 (1979).
115. K. Sieradzki, *Acta Metall.* **30**, 973 (1983).
116. J. C. Carver, G. K. Schweitzer and T. A. Carlson, *J. Chem. Phys.* **57**, 973 (1972).
117. G. A. Vernon, G. Stucky and T. A. Carlson, *Inorg. Chem.* **15**, 278 (1976).
118. J. C. Scully, *Corros. Sci.* **7**, 197 (1967).
119. D. A. Vermilyea, *J. electrochem. Soc.* **119**, 405 (1972).
120. W. R. Wearmouth, G. P. Dean and R. N. Parkins, *Corrosion* **29**, 251 (1973).
121. H. J. Engell, in *The Theory of Stress Corrosion Cracking in Alloys* (ed. J. C. Scully), p. 68. NATO Scientific Affairs Division, Brussels (1971).
122. T. R. Beck, *J. electrochem. Soc.* **115**, 890 (1968).
123. J. R. Ambrose and J. Kruger, *J. electrochem. Soc.* **121**, 599 (1974).
124. N. Sato, in *Passivity of Metals* (eds R. P. Frankenthal and J. Kruger), p. 29. The Electrochemical Society, New Jersey (1978).
125. R. M. Carranza, Thesis, University of Buenos Aires (1986).

THE SUSCEPTIBILITY OF TYPE AISI 304 STAINLESS STEEL TO TRANSGRANULAR AND INTERGRANULAR SCC IN 40% $MgCl_2$ SOLUTION AT 100°C

C. MANFREDI,* I. A. MAIER and J. R. GALVELE

Departamento Materiales, Comisión Nacional de Energía Atómica, Avda. Libertador 8250, 1429 Buenos Aires, Argentina

Abstract—Stress corrosion cracking (SCC) of Type 304 austenitic stainless steel in 40% $MgCl_2$ solution at 100°C was studied with constant potential intermediate strain rate techniques and slow strain rate techniques. Loss of HCl from the solution, during SCC tests was found to have a strong effect on crack morphology. In fresh solutions potential regions with transgranular cracks and with intergranular cracks were observed. No critical potential for SCC could be found in those solutions. In preboiled solutions only the high potential cracking, predominantly transgranular, was found. In these solutions a critical potential for SCC could be defined. Contrary to what was reported in the literature, no evidence of anodic dissolution was found during the intergranular cracking. The results are discussed from the point of view of the surface mobility SCC mechanism.

INTRODUCTION

IN A previous paper[1] the intermediate strain rate test (ISRT) technique was applied to obtain the predicted crack velocity–potential diagrams for Type 304 stainless steel in $MgCl_2$, $CaCl_2$ and LiCl solutions at room temperature and at 90 and 100°C. This technique allowed the prediction of potential ranges of stress corrosion cracking (SCC) susceptibility and to estimate crack propagation rates.[1–9] These SCC diagrams indicated that at 90 and 100°C SCC susceptibility should be expected in a wide potential range below the pitting potential (E_p) and that crack propagation rates would increase by three orders of magnitude when the applied potential was shifted from the corrosion potential (E_c) to the pitting potential. It was also found, in agreement with results reported by Silcock and Swann,[10] that the morphology of the attack and crack propagation rates were a function of the solution pH. In potentiostatic SCC tests with Type AISI 304 stainless steel in $MgCl_2$[11–14] and $CaCl_2$[15] solutions, several authors found a critical potential above, but never below which, cracks propagate, in agreement with the predictions of the SCC diagrams.

Okada *et al.*[16] observed transgranular cracking in AISI 304 stainless steel smooth specimens tested in boiling $MgCl_2$ solution at 143°C, at constant applied load, without potential control. They found both trans- and intergranular fractures in samples exposed to solutions boiling at 125 and 115°C and they reported that the intergranular fracture region increased with decreasing temperature. Takano[17] and Nakayama and Takano[18] used notched specimens stressed at different strain rates. In a boiling 42% $MgCl_2$ solution at 143°C they observed that cracking was predominantly transgranular at low strain rates ($<9 \times 10^{-6}\ s^{-1}$) whereas intergranular cracking predominated at high strain rates. In a boiling 36% $MgCl_2$ solution at 128°C

* Present address: INTEMA, Juan B. Justo 4302, 7600 Mar del Plata, Pcia. Buenos Aires, Argentina.

Manuscript received 27 November 1986.

smooth samples at 1.67×10^{-5} s^{-1} strain rate and observed intergranular fractures using a boiling $MgCl_2$ solution at 135°C, whereas transgranular fractures were obtained in a boiling $MgCl_2$ solution at 154°C. Kuwano[20] found an interesting relation between the fracture mode and the applied load, working in a 42% $MgCl_2$ solution at 143°C. Under an applied stress of 15 kg mm^{-2} the fracture surface was mainly transgranular, with some intergranular fractures only in regions close to the center of the specimen cross section, while under a stress of 30 kg mm^{-2} the opposite result was obtained. In a later work, Kuwano *et al.*[21] studied the effect of stress on polarization curves of Type AISI 304 stainless steel in the same solution. They found that an increase of the applied stress caused a decrease in the corrosion and the pitting potentials of the specimens and also a decrease in the difference between E_c and E_p. They also observed that transgranular cracking predominated in anodically polarized samples, while intergranular cracking increased with cathodic polarization, thus explaining the influence of stress on the cracking mode.

Kessler and Kaesche[14] studied the fracture mode of Type 304 stainless steel as a function of potential, by constant load and slow strain rate tests (SSRT) in 35 and 38% $MgCl_2$ solutions at 120 and 135°C. They observed an increase in failure time and in fracture strength at potentials below −0.13 V(NHE). No intergranular cracking was found in the 35% $MgCl_2$ solution at 120°C, while in the 38% $MgCl_2$ solution at 135°C transgranular cracking predominated at potentials above −0.13 V(NHE), and both transgranular and intergranular cracking were obtained in the −0.13 to −0.17 V(NHE) potential range. Intergranular cracking increased with decreasing potential and finally became the predominant type of crack.

The purpose of the present work was to get more information about SCC attack in $MgCl_2$ solutions at high temperatures, especially in the range where a steep increase of crack propagation rate with potential is observed. Using the ISRT technique the corresponding SCC diagrams were plotted, extending the strain rate range used in our previous work. Predictions of the SCC diagrams were compared with the results of constant-potential SSRT (Parkins' technique) and the influence of the solution pH was determined as a possible explanation of some contradictory results reported in the references.

EXPERIMENTAL METHOD

The material used was a 0.075 cm diameter wire of Type AISI 304 stainless steel. The typical composition of the steel was: Cr, 18.7; Ni, 8.8; Si, 0.75; Mo, 0.3; C, 0.08; S, 0.05; Fe, balance, wt%. The wires were annealed at 1100°C for 30 minutes under 200 mmHg argon atmosphere and quenched in ice-containing water. Specimens used in the intermediate strain rate tests (ISRT) were slightly abraded with 600 grade SiC paper, because in a previous work[9] mechanically polished samples proved to give better predictions of crack propagation rates. Wires for the slow strain rate tests (SSRT) were electropolished to facilitate their observation under the scanning electron microscope. Electropolishing treatment was applied in a refrigerated 90% butylcellosolve +10% perchloric acid solution, at 36 V, in four one-minute periods. Before testing, the samples were cleaned with acetone and dried in hot air.

The cell used was described in a previous paper.[22] The 40% $MgCl_2$ solution was prepared with analytical grade reagents and double distilled water, immediately before testing. As the solution is oversaturated at room temperature, it had to be warmed at 80°C to complete salt dissolution. The cell was heated by an electric resistance system. Potentials were measured through a Luggin capillary with a saturated calomel electrode at room temperature, and are reported in the normal hydrogen electrode scale (NHE). A LYP Electronica potentiostat and millivoltimeter and a Tacussel EPL 2-20G recorder were used in the present work. The SSRT were performed in a straining machine made in our laboratory. The

cell was coupled to the moving grip of the machine through a pulley to ensure that no new metal surface would enter the cell during the stretching of the wires.[4]

ISRT were performed at initial strain rates of 4×10^{-3}, 8.3×10^{-3} and 1.7×10^{-2} s^{-1}. The 40% $MgCl_2$ solution was kept in the cell at 80°C for 30 min while it was de-aerated with nitrogen, purified according to the Gilroy and Mayne method.[23] Afterwards, the cell temperature was increased to 100°C, and the specimen was allowed to reach a steady potential for 15 min. The chosen potential was then applied for a 30 min-period while the current was recorded, and afterwards the wire was strained to fracture. For potentials close to the pitting potential the static period was less than 5 min, to prevent crevice corrosion under the stoppers of the cell and pitting of the sample.

For the SSRT at constant potential, strain rates of 1.5×10^{-5} and 1.5×10^{-6} s^{-1} were used. In these tests the solution was not de-aerated as the current was not recorded. Three types of solutions were used: (a) 'fresh' solution: the solution was prepared immediately before testing, as described above; (b) 'boiled' solution, like (a), but kept at slow ebullition (at approximately 140°C) for 55 min, and then brought to initial volume by adding distilled water; (c) 're-acidified' solution, prepared as in (b), and then brought to initial pH by HCl addition. The pH was measured by taking a sample of the oversaturated solution and diluting it in an equal volume of water.[24] The pH values here reported correspond to these diluted solutions. After fracture, the specimens of the SSRT were observed under a scanning electron microscope (Philips SEM 500) and then metallographically mounted and sectioned to measure the crack depth. From the length of the longest crack and the exposure time a mean crack penetration rate was calculated.

EXPERIMENTAL RESULTS

Intermediate strain rate tests (ISRT)

The intermediate strain rate technique, as used in the present work, has been described in previous publications.[2] By this technique, the following parameters are measured: the initial current density, i_s; the current density on the bare metal, i_b; the crack aspect ratio, i_b/i_s; and the predicted crack velocity, V_p.

As discussed before,[1,2,4-9] SCC susceptibility is expected for those potential ranges in which V_p and i_b/i_s are above a minimum value. The aspect ratio should be 10 and a minimum crack propagation rate of 1×10^{-10} ms^{-1} for Type AISI 304 stainless steel was empirically assumed.[9]

In Fig. 1, i_s and i_b for AISI 304 stainless steel in 40% $MgCl_2$ solution at 100°C are shown as a function of potential. From these values, anodic and cathodic polarization

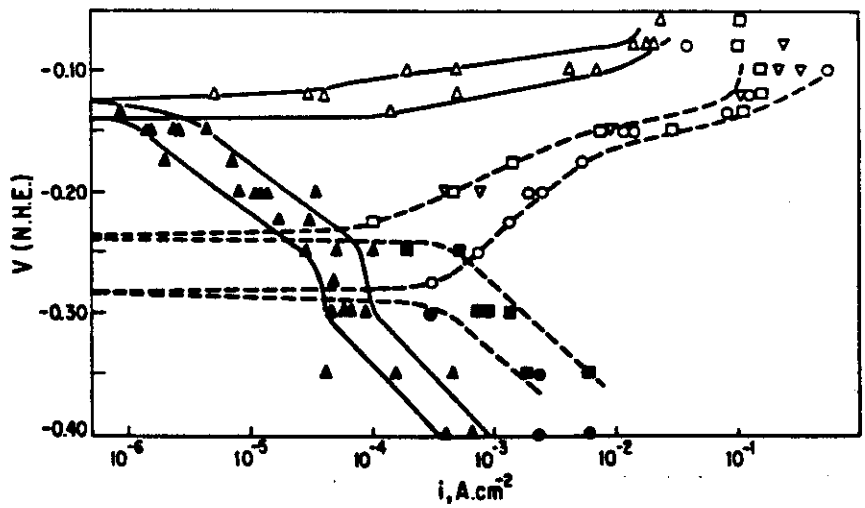

FIG. 1. Anodic and cathodic polarization curves for Type AISI 304 stainless steel in 40% $MgCl_2$ solution at 100°C. △ i_s anodic; ▲ i_s cathodic; ○ i_b anodic, $v = 1.7 \times 10^{-2}$ s^{-1}; ● i_b cathodic, $v = 1.7 \times 10^{-2}$ s^{-1}; ▽ i_b anodic, $v = 8.3 \times 10^{-3}$ s^{-1}; □ i_b anodic, $v = 4 \times 10^{-3}$ s^{-1}; ■ i_b cathodic, $v = 4 \times 10^{-3}$ s^{-1}.

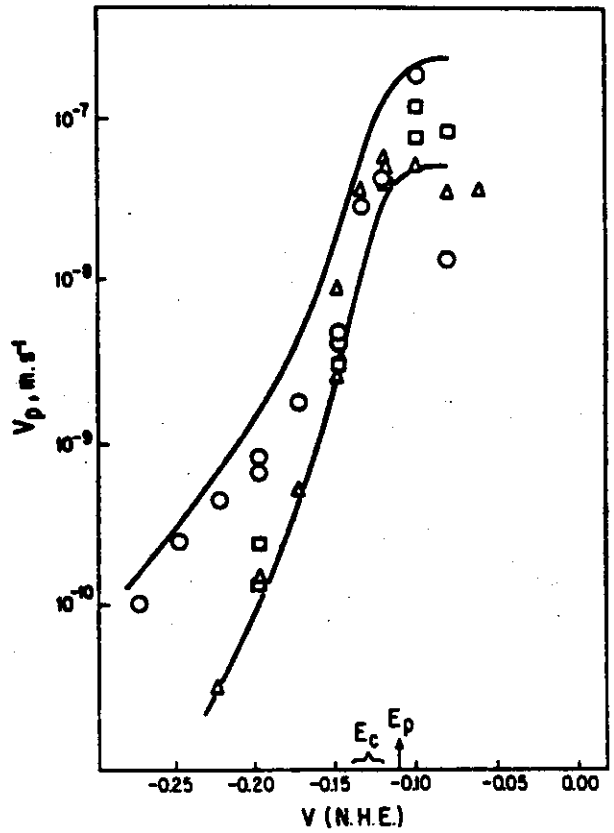

FIG. 2. Predicted crack velocities V_p as a function of potential for Type AISI 304 stainless steel stressed in 40% $MgCl_2$ solution at 100°C. △ $v = 4 \times 10^{-3}$ s^{-1}; □ $v = 8.3 \times 10^{-4}$ s^{-1}; ○ $v = 1.7 \times 10^{-5}$ s^{-1}.

curves for the static metal and the fresh metal are drawn. Results show some dispersion at potentials close to the corrosion potential. For the static metal, E_c lay between −0.125 and −0.14 V(NHE), and pitting was observed at potentials above −0.11 V(NHE). The cathodic polarization curve showed an inflection between −0.25 and −0.30 V(NHE), which would correspond to the anodic dissolution peak studied by Rockel and Staehle[25] and by Hoar and Slater.[26] The anodic polarization curve for the fresh metal was shifted about 100 mV below that of the static metal. The corresponding corrosion potential lay between −0.23 and −0.28 V(NHE). Therefore, anodically induced cracking could be expected in freshly exposed areas produced by straining, at potentials above −0.25 V(NHE).

Figure 2 shows crack penetration rates, V_p, predicted from ISRT as a function of potential. It can be observed that V_p increased with potential, up to the pitting potential E_p, where it reached a limit value in the 1×10^{-7} ms^{-1} range. The higher values generally correspond to results of the faster strain rate tests and tend to decrease with strain rate, but results showed some dispersion, especially at potentials above E_p. For each strain rate, there exists a minimum potential below which the initial cathodic current increased due to straining, and which were assumed to be the corrosion potential of the freshly exposed metal. Above this potential the initial cathodic current decreased or even turned anodic during straining, so this critical potential would be the lower limit of anodic dissolution of freshly exposed metal areas. This minimum potential value decreases when the strain rate increases.

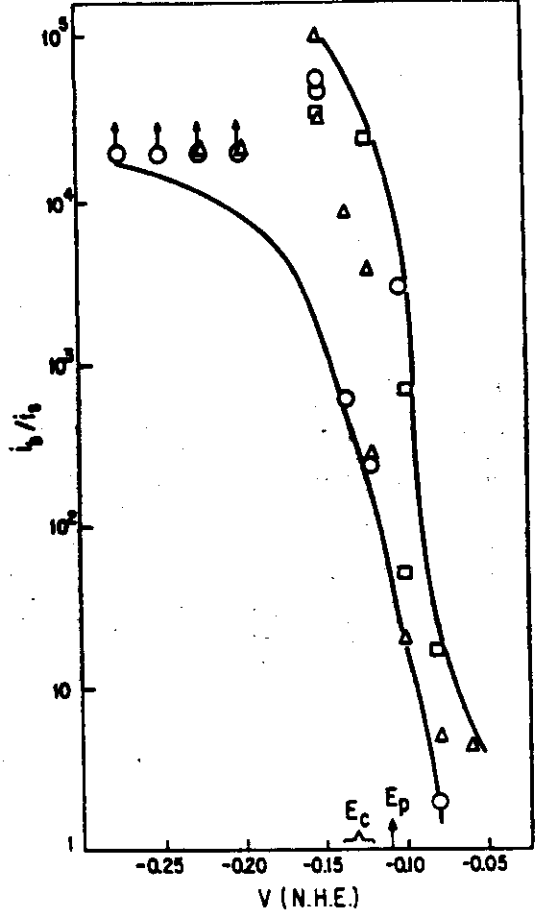

FIG. 3. Aspect ratio i_h/i_c, as a function of potential, for Type AISI 304 stainless steel stressed in 40% $MgCl_2$ solution at 100°C. △ $v = 4 \times 10^{-3}\ s^{-1}$; □ $v = 8.3 \times 10^{-3}\ s^{-1}$; ○ $v = 1.7 \times 10^{-2} s^{-1}$.

In Fig. 3 the aspect ratio is observed to be very high at potentials below E_c, decreasing steeply in the potential range between E_c and E_p and becoming lower than 10 at potentials above E_p. Based on the SCC diagrams represented in Figs 2 and 3 SCC susceptibility would be expected for AISI 304 stainless steel in 40% $MgCl_2$ at 100°C, in the potential range that begins 100 to 120 mV below E_c up to some 50 mV above E_p [i.e. approximately between −0.25 and −0.06 V(NHE)].

In the previous work[1] the predicted V_p values in 'fresh' solutions were compared with those obtained in an 'aged' solution, in which the pH value increased in two units (measured without dilution). It was observed that, at −0.10 V(NHE), V_p in the 'aged' solution was two orders of magnitude lower than the value determined in the 'fresh' solution. Using the scanning electron microscope the initial attack on the surface of wires strained at this potential at $2 \times 10^{-3}\ s^{-1}$ strain rate in both solutions was compared. Specimens strained in the 'fresh' solution exhibited heavy attack on slip lines, twin boundaries and grain boundaries, while a thick film formed on the surface of wires strained in the more alkaline solution, and cracks and pits nucleated in zones where the film was broken. These results were similar to those reported by Silcock and Swann,[10] who compared the morphology of samples strained in 42% $MgCl_2$ solution at 150°C, when strained in freshly prepared solutions or preboiled solutions. Attack in the preboiled solutions (in which the pH value had increased) was almost identical to that observed in the present 'aged' solution.

In the present work the pH of diluted samples of the 40% $MgCl_2$ solution taken before and after running the ISRT was measured. The initial pH was 4.0; after the tests a pH increase, of the order of 0.2–0.7 units was detected. Therefore, in an attempt to determine how V_p values were affected by this decrease in pH, some ISR tests at $1.2 \times 10^{-2}\ s^{-1}$ strain rate in a 40% $MgCl_2$ solution acidified by HCl addition were run. After testing, the pH of the diluted sample was 1.2, this showing that the acidity of the solution remained unchanged all through the experiment below the initial pH value of regular 40% $MgCl_2$ solutions. The applied potentials were −0.20 and −0.25 V(NHE). At −0.20 V(NHE) calculated V_p values lay between the limits of the values obtained in 'fresh' solutions (Fig. 2). At −0.25 V(NHE) V_p was increased by a factor two by acidification. This point is discussed at a later stage with the results of slow strain rate tests.

Slow strain rate tests (SSRT)

'Fresh' solution tests. Slow strain rate tests were run between −0.45 and +0.10 V(NHE). When straining at $1.5 \times 10^{-5}\ s^{-1}$ strain rate, no cracking was observed below −0.20 V(NHE), whereas straining at $1.5 \times 10^{-6}\ s^{-1}$ cracks were obtained all through the studied potential range. Figure 4 shows the measured crack penetration rates as a function of potential.. Good correlation was found between the predicted values and those measured with SSRT, at potentials above −0.14 V(NHE). Below −0.10 V(NHE) the wires showed slight surface corrosion plus cracking, and the

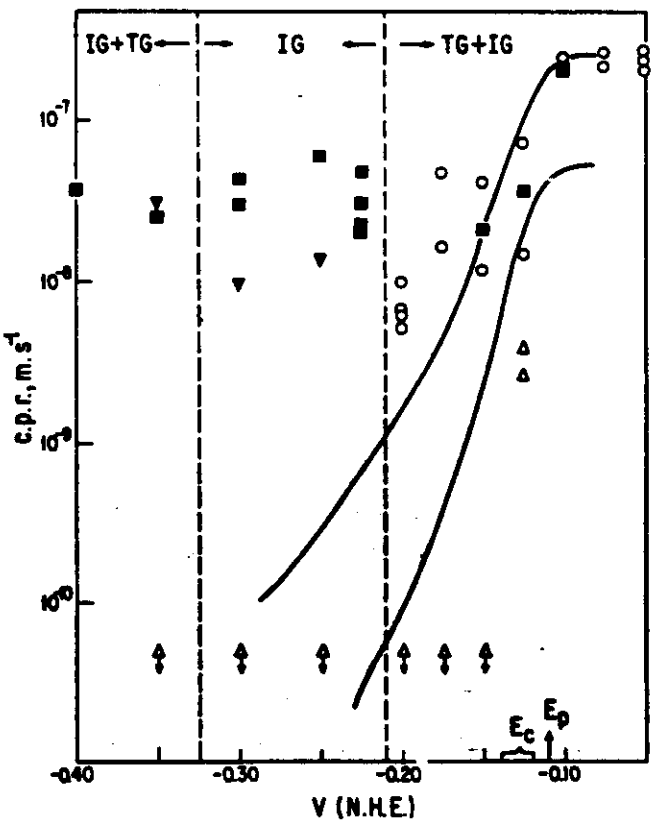

FIG. 4. Crack propagation rates for Type AISI 304 stainless steel measured in potentiostatic slow straining tests in 40% $MgCl_2$ solution at 100°C. ○ Fresh solution, $\nu = 1.5 \times 10^{-5}\ s^{-1}$; ■ fresh solution, $\nu = 1.5 \times 10^{-6}\ s^{-1}$; △ boiled solution, $\nu = 1.5 \times 10^{-6}\ s^{-1}$; ▼ reacidified solution, $\nu = 1.5 \times 10^{-6}\ s^{-1}$.

predominant (Fig. 7), whereas at higher potentials most of the brittle fracture was transgranular (Fig. 8). These results are similar to those reported by Kessler and Kaesche.[14] Above −0.10 V(NHE) strong surface attack was found and cracking density increased (Fig. 9). Fracture surface was predominantly transgranular. It was also observed that when straining at potentials above E_p cracking replaced pitting, as shown by West.[27]

In order to determine if the intergranular attack was due to improper heat treatment, the specimens were submitted to a standard test for sensitization.[28] A 1 A cm^{-2} anodic current density was applied for 120 s to the samples, in a 10 g oxalic acid in 100 ml distilled water solution. The wires showed no intergranular attack, thus confirming that they were not sensitized.

Below −0.14 V(NHE) the V_p values predicted by ISRT, Fig. 2, are from one to two orders of magnitude lower than those found after SSRT, Fig. 4. To make sure that this difference was not caused by an increase in pH during the ISRT, some tests were done in acidified solutions, as reported above, at −0.20 and −0.25 V(NHE). The low V_p values were found not to be due to a loss of HCl from the solution. The conclusion was that, below −0.14 V(NHE), ISRT consistently predicted much lower crack velocity values than those found in slow strain rate tests.

As the fractography of the samples below −0.14 V(NHE) showed a high proportion of intergranular cracks, the relative relation between intergranular and transgranular cracks was measured. The measurements were restricted to the SCC surface, ignoring the dimple region. Figure 10 shows the fraction of area of transgranular cracks found at various potentials. In the region where ISRT and SSRT coincided, above −0.14 V(NHE), more than 70% of the fracture surface was transgranular. At lower potentials the proportion of transgranular cracks dropped quickly, and at −0.20 V(NHE) practically all the crack surface was intergranular.

Assuming that transgranular and intergranular cracks propagated independently, the fraction of area of each type of crack should be proportional to its relative velocity. Then the product of the total crack velocity, measured by SSRT, times the fraction of area of transgranular cracks, Fig. 10, should give a rough estimate of the

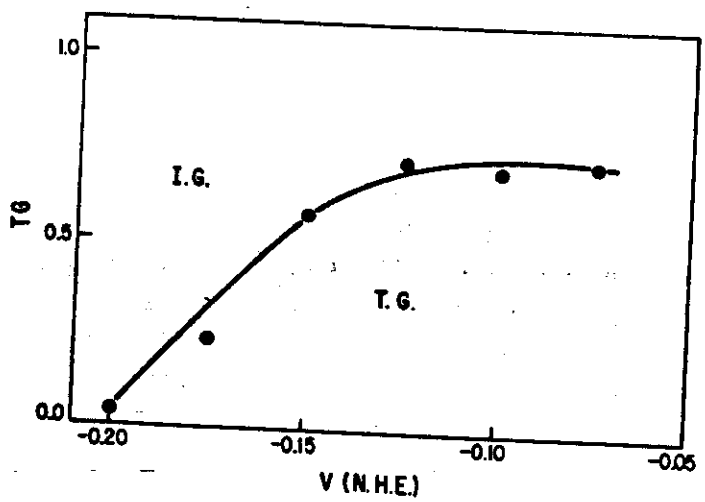

FIG. 10. Transgranular cracks fraction area percentage, as a function of potential, for Type AISI 304 stainless steel, stressed in fresh 40% $MgCl_2$ solution at 100°C; strain rate, $1.5 \times 10^{-5}\ s^{-1}$.

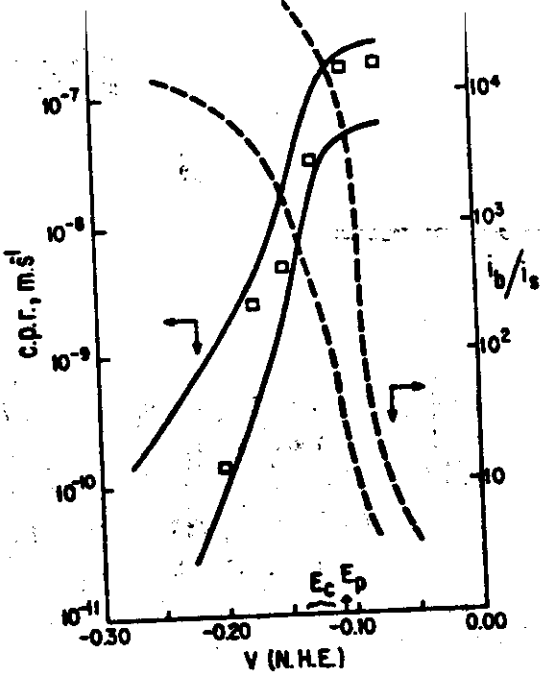

FIG. 11. Transgranular crack velocity values, measured in slow strain rate tests, for Type AISI 304 stainless steel in fresh 40% $MgCl_2$ solution at 100°C: strain rate, 1.5×10^{-5} s^{-1}. The continuous lines show the crack velocity values predicted by the intermediate strain rate tests (see Fig. 2).

transgranular crack velocity. Figure 11 shows that the transgranular crack velocity values fit very well with the predictions of ISRT. Since the ISRT is based on anodic dissolution measurements, the results in Fig. 11 indicate that in the present system, if there is any relation between SCC and anodic dissolution, it should involve only transgranular cracks. This observation contradicts the assumption made by the supporters of the cleavage SCC mechanism [29] who suggested that only intergranular cracks could be related to anodic dissolution processes.

Some SSRT were performed at very low potentials, below −0.30 V(NHE), where, as shown in Fig. 1, high cathodic currents were observed both on the filmed metal and on the freshly exposed surface. In this region transgranular cracks were again observed, as shown in Fig. 12.

'Boiled' solution tests. 'Boiled' $MgCl_2$ solutions were prepared as described above. The pH of samples diluted to half the concentration was measured and the main value obtained was 8.1, thus indicating that alkalinization of the solution by loss of HCl took place. SSR tests at 1.5×10^{-6} s^{-1} were run in this solution and the corresponding results are shown in Fig. 4. At potentials equal to or lower than −0.15 V(NHE) no cracks were observed. At higher potentials the measured crack penetration rates were one order of magnitude lower than those obtained in the 'fresh' solution and the cracks were predominantly transgranular.

'Re-acidified' solution tests. SSRT were run in the boiled and re-acidified solution at a 1.5×10^{-6} s^{-1} strain rate and at −0.25, −0.30 and −0.35 V(NHE). The results obtained are also shown in Fig. 4. At −0.25 and −0.30 V(NHE), cracking was

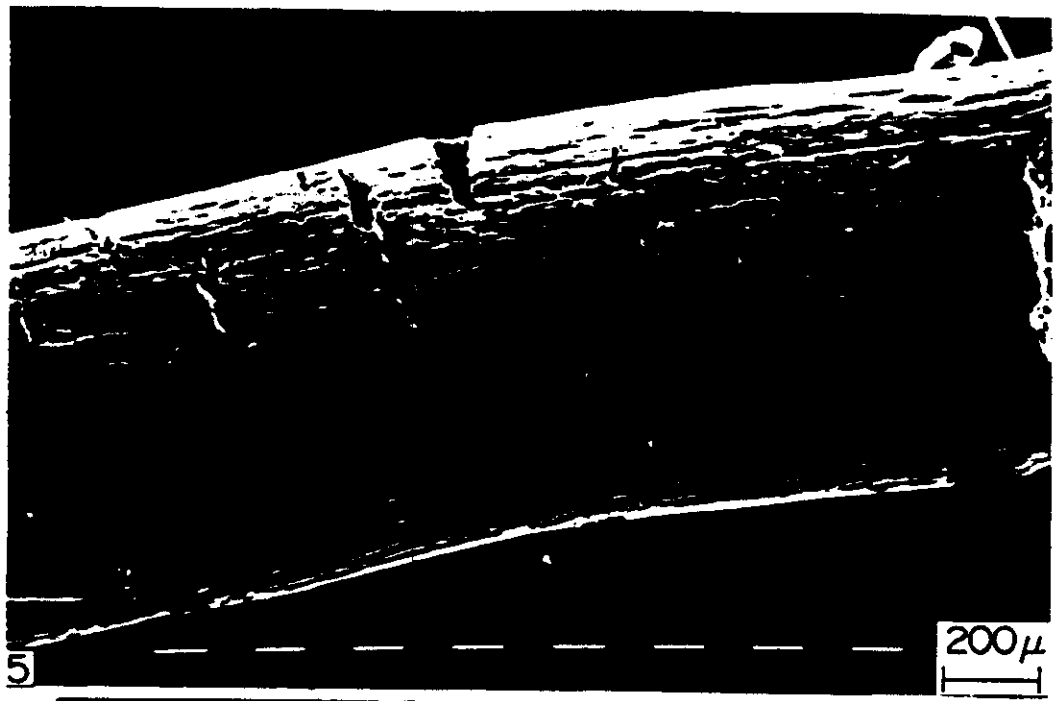

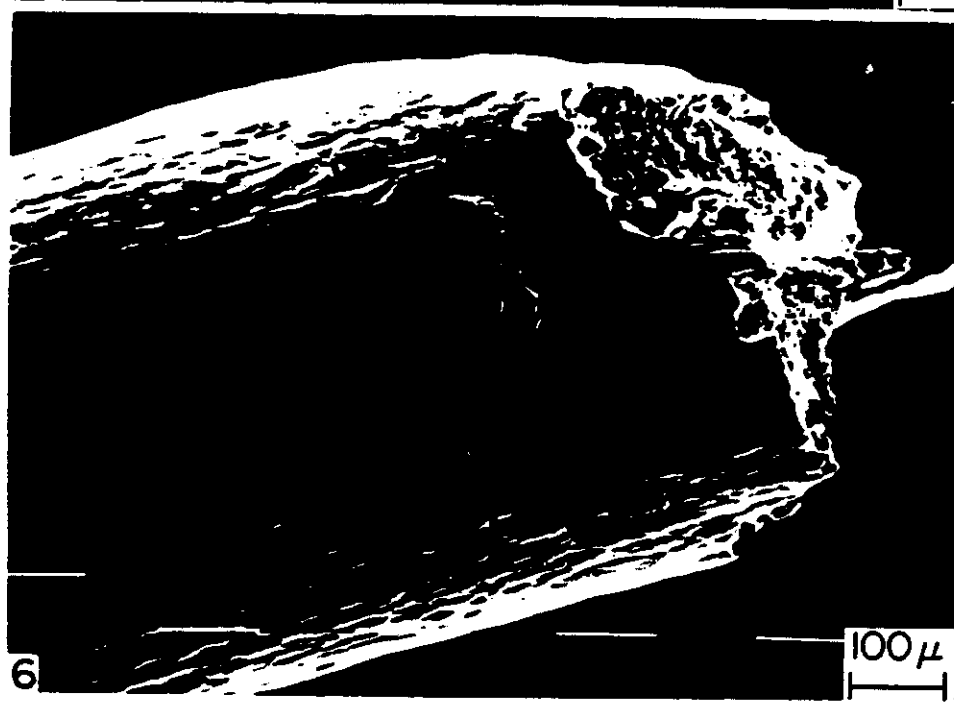

FIG. 5. Corroded surface of a Type AISI 304 stainless steel wire, stressed in fresh 40% $MgCl_2$ solution at 100°C. Potential: −0.10 V(NHE); strain rate, $1.5 \times 10^{-5} s^{-1}$; failure time, 19 min.

FIG. 6. Corroded surface of a Type AISI 304 stainless steel wire stressed in fresh 40% $MgCl_2$ solution at 100°C. Potential −0.175 V(NHE); strain rate, 1.5×10^{-5} s^{-1}; failure time, 94 min.

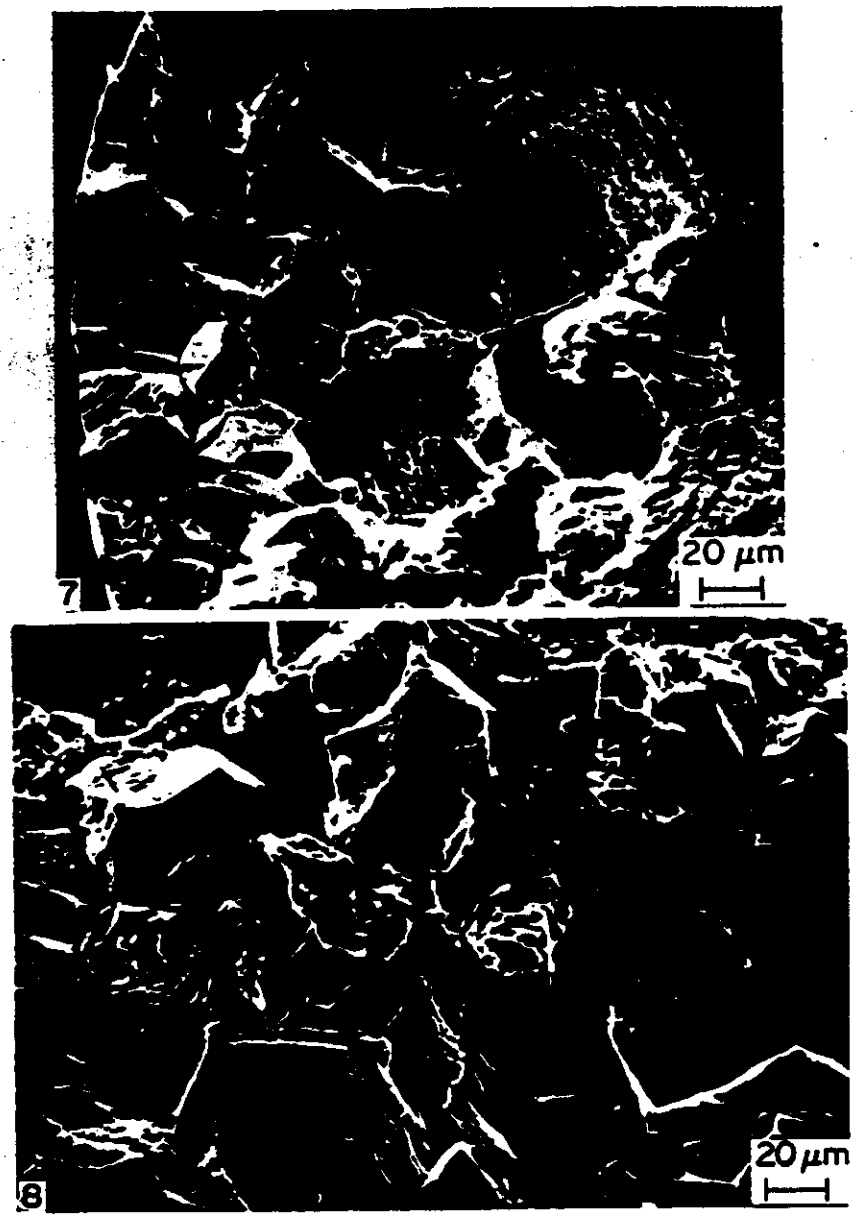

FIG. 7. Fracture surface of a Type AISI 304 stainless steel wire stressed in fresh 40% $MgCl_2$ solution at 100°C. Potential, −0.175 V(NHE); strain rate, 1.5×10^{-5} s^{-1}; failure time, 94 min.

FIG. 8. Fracture surface of a Type AISI 304 stainless steel wire stressed in fresh 40% $MgCl_2$ solution at 100°C. Potential, −0.10 V(NHE); strain rate, 1.5×10^{-5} s^{-1}; failure time, 19 min.

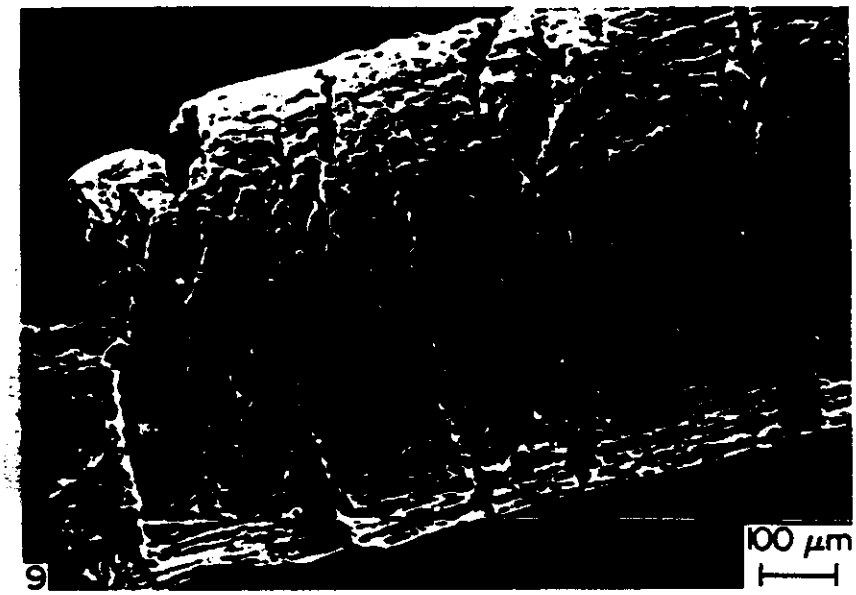

FIG. 9. Corroded surface of a Type AISI 304 stainless steel wire stressed in fresh 40% $MgCl_2$ solution at 100°C. Potential −0.075 V(NHE); strain rate, 1.5×10^{-5} s^{-1}; failure time, 12 min.

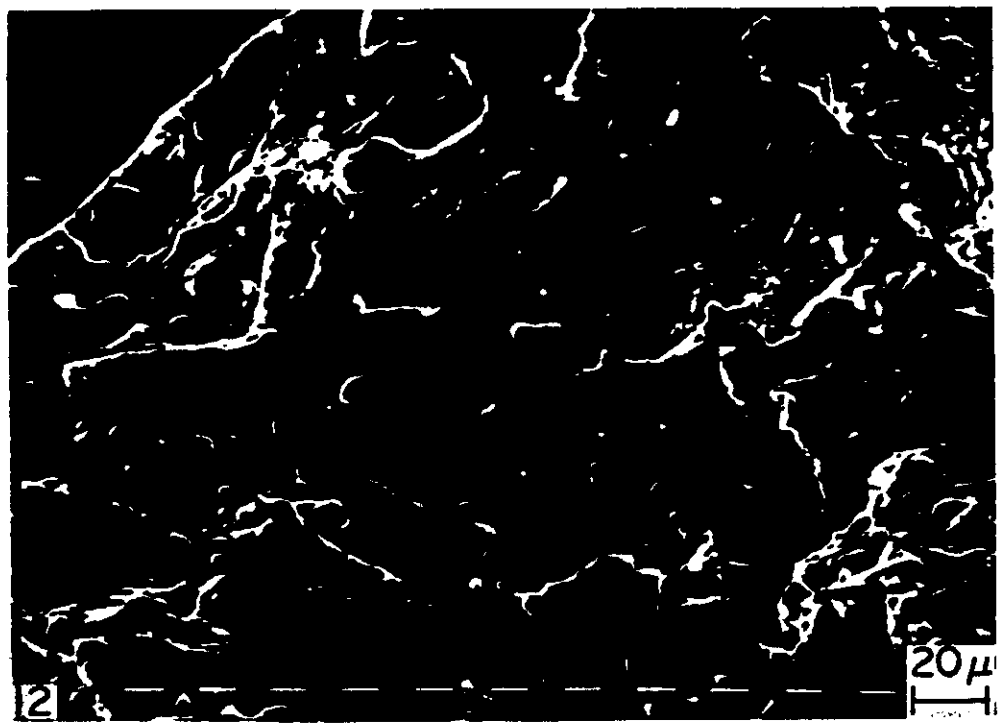

FIG. 12. Fracture surface of a Type AISI 304 stainless steel wire stressed in fresh 40% $MgCl_2$ solution at 100°C. Potential, −0.40 V(NHE); strain rate, $1.5 \times 10^{-6} s^{-1}$; failure time, 148 min.

FIG. 13. Type AISI 304 stainless steel wire strained in reacidified 40% $MgCl_2$ solution at 100°C. Potential, −0.30 V(NHE); strain rate, 1.5×10^{-6} s^{-1}; failure time, 187 min. Metallographic section of the corroded wire, diamond polished and etched, showing predominantly intergranular fracture.

FIG. 14. Type AISI 304 stainless steel wire strained in reacidified 40% $MgCl_2$ solution at 100°C; potential, −0.35 V(NHE); strain rate, 1.5×10^{-6} s^{-1}; failure time, 180 min. Metallographic section of the corroded wire, diamond polished and etched, showing predominantly transgranular fracture.

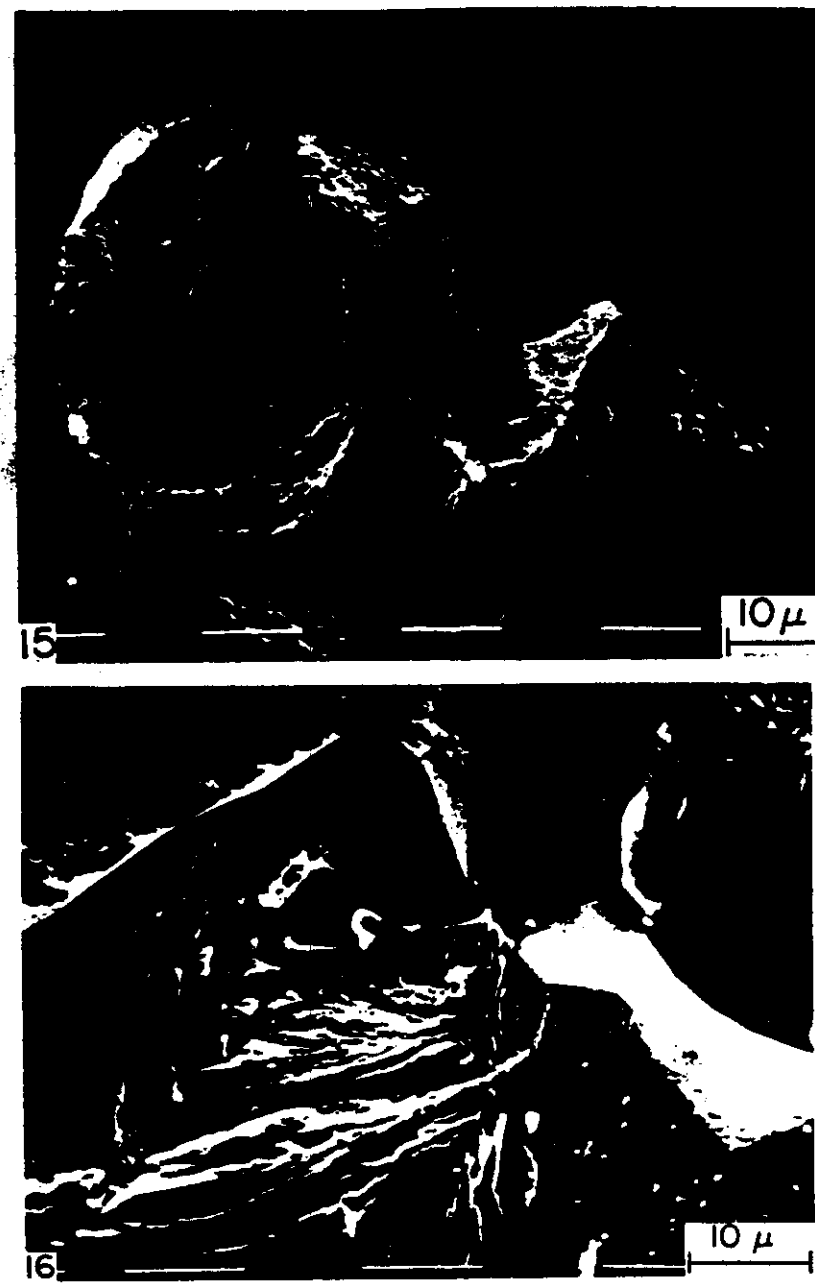

FIG. 15. Fracture surface of a Type AISI 304 stainless steel wire stressed in fresh 40% $MgCl_2$ solution at 100°C. Potential, −0.20 V(NHE); strain rate, $1.5 \times 10^{-5} s^{-1}$, failure time, 160 min.

FIG. 16. Detail of the fracture surface of a Type AISI 304 stainless steel wire stressed in fresh 40% $MgCl_2$ solution at 100°C. Potential, −0.15 V(NHE); strain rate, $1.5 \times 10^{-6} s^{-1}$; failure time, 125 min.

FIG. 17. Detail of the fracture surface of a Type AISI 304 stainless steel wire stressed in fresh 40% $MgCl_2$ solution at 100°C. Potential, −0.125 V(NHE); strain rate, $1.5 \times 10^{-5} s^{-1}$; failure time, 29 min.

FIG. 18. Detail of the fracture surface of a Type AISI 304 stainless steel wire stressed in fresh 40% $MgCl_2$ solution at 100°C. Potential, −0.10 V(NHE); strain rate, $1.5 \times 10^{-5} s^{-1}$; failure time, 19 min.

417

predominantly intergranular (Fig. 13), as found in the tests performed in 'fresh' solutions, even though crack penetration rates were somewhat lower for the 're-acidified' solutions. At −0.35 V(NHE) the crack penetration rate was similar to the value measured in the 'fresh' solution and the attack morphology was also similar, showing mainly transgranular cracks, Fig. 14.

The results obtained indicate that, when the $MgCl_2$ solution is kept at temperatures close to the boiling point for long periods, HCl is lost and the pH of the solution increases. This alkalinization makes the transgranular crack propagation rate decrease, shifts the SCC susceptibility to higher potentials, and eliminates the intergranular cracking region. If we compare Figs 5 and 6, we see that intergranular crack density is smaller than transgranular crack density and also that the former propagate in a more occluded type of cracks, as shown in Fig. 15. Apparently intergranular cracks are more difficult to nucleate than transgranular cracks, as shown by the difference in density. On the other hand, the occluded type of cracks suggests that the composition changes inside the cracks favour intergranular crack propagation.

The present results show the strong influence of the pH of the $MgCl_2$ solution both on crack penetration rates and on crack morphologies. This could explain discrepancies in the results reported by different authors, and what is more important, HCl evaporation during long tests, could lead to erroneous interpretations. For example, the results of Nakayama and Takano,[18] who found intergranular SCC at high strain rates and transgranular SCC at low strain rates, could be explained as differences in the loss of HCl, due to differences in the exposure time.

Surface mobility as the cause of SCC

Recent publications[30,31] postulate that SCC is related to an enhanced surface mobility process. The present work was not intended to check the validity of the surface mobility mechanism. Nevertheless, it is important to see if the present results are in agreement with that theory, which predicts, for aqueous environments, three types of SCC processes: (I) *Specific SCC susceptibility*: when by anodic reaction with the environment, a low melting point compound is formed on the metal surface. (II) *Intrinsic SCC susceptibility*: when either the metal itself, or impurities segregated to grain boundaries, have a low melting point value. In this case SCC will be observed under those chemical or electrochemical conditions that hinder the formation of high melting point oxide films on the metal surface (e.g. acidified or strongly alkaline solutions for amphoteric oxide films). (III) *Hydrogen embrittlement*: if case II is reached under conditions of hydrogen evolution, the interaction of hydrogen with vacancies will cause a substantial increase in the crack velocity.[31]

As shown in Fig. 4, three different SCC regions were detected for AISI 304 austenitic stainless steel in $MgCl_2$ solutions. At potentials close to the pitting potential, cracking is mainly transgranular, and it is observed in both fresh and boiled $MgCl_2$ solutions. It is believed to be type I SCC. Pitting of stainless steels in acid chloride solutions has been described as a special case of pitting.[32] It can be seen as the result of the formation of chloride-rich salt films on the metal–solution interface. As reported earlier,[31] the specificity of halide ions in producing SCC in austenitic stainless steels is due to the low melting point of iron halide compounds. On a stressed metal, the surface oxide film will be ruptured at the slip steps. Near the pitting potential, the metal halide compounds will be preferentially formed on those

slip steps, which are the initiation sites for transgranular SCC. Figures [illegible] how the attack on the slip steps is increased by increasing the electrode potential. This type of cracking fits in the definition of specific SCC, type I.

Below the corrosion potential, if the potential is lowered, the rate of transgranular crack propagation decreases to very low values, and eventually it goes down to zero. In the boiled $MgCl_2$ solutions no cracking is observed in this region of potentials. Both in the fresh and in the re-acidified solutions, however, there is a region of potentials where only intergranular cracks are observed. According to the measurements reported by Rockel and Staehle[25] and by Hoar and Slater,[26] this is the region where active dissolution of the alloy is taking place. If there is any intrinsic susceptibility, it should be shown in this region of potentials. Intergranular cracking is believed to be due to segregation of impurities to grain boundaries. High purity alloys should not show this type of cracking. Since these cracks are observed below the corrosion potential, i.e. under hydrogen evolution, it is not possible in the present case to determine if the cracking is of either type II or type III.

Below −0.30 V(NHE) strong cathodic currents are observed even on freshly exposed metal, Fig. 1. Under these conditions a high fugacity of hydrogen should be expected in the metal surface layers. It has been reported[33] that this high fugacity hydrogen induces phase transformations in the austenitic stainless steels as well as transgranular cracking. This type of cracking falls outside the scope of the surface mobility SCC mechanism.

The SCC observations made in the present work are consistent with the predictions of the surface mobility SCC mechanism.

CONCLUSIONS

Three different regions for SCC were found for AISI 304 austenitic stainless steel in a 40% $MgCl_2$ solution at 100°C. The occurrence of these regions was a function of the potential and of the degree of acidity of the solution.

Above −0.20 V(NHE) intergranular and transgranular cracks were observed. The proportion of transgranular cracks increased with increase in the potential. Above the corrosion potential cracking was observed in all the solutions tested. Below this potential no cracking was found in previously boiled $MgCl_2$ solutions. Transgranular cracking was predictable by the intermediate strain rate technique (ISRT). Intergranular cracking was not predicted by this technique.

Between −0.20 and −0.30 V(NHE) only intergranular cracks were observed, and only if fresh or HCl acidified $MgCl_2$ solutions were used.

Below −0.30 V(NHE) transgranular cracks were found again. These transgranular cracks were attributed to the presence of high fugacity hydrogen in the metal. Again this cracking was found only in fresh or in HCl acidified $MgCl_2$ solutions.

All the above observations were consistent with the surface mobility SCC mechanism.

Acknowledgements—This research has been supported by the Proyecto Multinacional de Investigación y Desarrollo en Materiales OEA-CNEA, by the Comisión de Investigaciones Científicas, Prov. Buenos Aires and by the Consejo Nacional de Investigaciones Científicas y Técnicas from Argentina. We are most grateful for the experimental assistance with S. E. M. by N. J. Marcone, I. S. Losada and F. E. Bottini.

REFERENCES

1. I. A. Maier, E. López Pérez and J. R. Galvele. *Corros. Sci.* **22**, 537 (1982).

PVP-Vol. 99, p. 273. The American Society of Mechanical Engineers, New York (1985).
3. T. P. Hoar and J. R. Galvele, *Corros. Sci.* **10**, 211 (1970).
4. J. R. Galvele, S. B. de Wexler and I. Gardiazábal, *Corrosion* **31**, 352 (1975).
5. J. R. Galvele and I. A. Maier, *Passivity and its Breakdown on Iron and Iron Base Alloys* (eds R. W. Staehle and H. Okada), p. 178. NACE, Houston (1976).
6. J. S. Park, J. R. Galvele, A. K. Agrawal and R. W. Staehle, *Corrosion* **34**, 413 (1978).
7. I. A. Maier and J. R. Galvele, *Corrosion* **36**, 60 (1980).
8. M. G. Alvarez, C. Manfredi, M. Giordano and J. R. Galvele, *Corros. Sci.* **24**, 769 (1984).
9. I. A. Maier, C. Manfredi and J. R. Galvele, *Corros. Sci.* **25**, 15 (1985).
10. J. M. Silcock and P. R. Swann, *Environment-Sensitive Fracture of Engineering Materials* (ed. Z. A. Foroulis), p. 133. The Metallurgical Society of AIME, Warrendale, Pa. (1979).
11. H. H. Uhlig and E. W. Cook Jr, *J. electrochem. Soc.* **116**, 173 (1969).
12. K. Sugimoto, K. Takahashi and J. Sawada, *Trans. Japan Inst. Metals* **19**, 422 (1978).
13. A. Goretski and M. Smyalovski, *Prot. Metals* **9**, 223 (1974).
14. K. J. Kessler and H. Kaesche, *Werkst. Korros.* **35**, 171 (1984).
15. S. Brennert, *TVF* **32**, 139 (1961).
16. H. Okada, Y. Hosoi and S. Abe, *Corrosion* **27**, 424 (1971).
17. M. Takano, *Corrosion* **30**, 441 (1974).
18. T. Nakayama and M. Takano, *Corrosion* **42**, 10 (1986).
19. F. Stalder and D. J. Duquette, *Corrosion* **33**, 67 (1977).
20. S. Kuwano, *J. Soc. Material Sci. J.*, **27**, 539 (1978).
21. S. Kuwano, M. Anma and T. Oki, *J. Inst. Metals* **44**, 815 (1980).
22. J. R. Galvele, S. M. de De Micheli, I. L. Muller, S. B. de Wexler and I. L. Alanis, *Localized Corrosion* (ed. R. W. Staehle), p. 580. NACE, Houston (1974).
23. D. Gilroy and J. E. O. Mayne, *J. Appl. Chem.* **12**, 382 (1962).
24. J. M. Silcock, *Br. Corros. J.* **14**, 206 (1979).
25. M. Rockel and R. W. Staehle, quoted by R. W. Staehle, in *The Theory of Stress Corrosion Cracking in Alloys* (ed. J. C. Scully), p. 265. NATO, Brussels (1971).
26. T. P. Hoar and J. E. Slater, *Corros. Sci.* **14**, 415 (1974).
27. J. M. West, *Electrodeposition and Corrosion Processes*, p. 155. D. Van Nostrand, London (1965).
28. Norm ASTM A-262 Practice A—Electrolytic Oxalic Acid Etching Test—American Society for Testing and Materials, Philadelphia, Part 10, p. 2 (1981).
29. E. N. Pugh, *Corrosion* **41**, 517 (1985).
30. J. R. Galvele, *J. electrochem. Soc.* **133**, 953 (1986).
31. J. R. Galvele, *Corros. Sci.*, **27**, 1 (1987).
32. J. R. Galvele, J. B. Lumsden and R. W. Staehle, *J. electrochem. Soc.* **125**, 1204 (1978).
33. J. P. Bricout, R. Missiaen, J. C. Bavay and C. Moriamez, *Mém. Et Sci. Rev. Mét.* **81**, 259 (1984).

REPASSIVATION KINETICS IN STRESS CORROSION CRACKING—I. TYPE AISI 304 STAINLESS STEEL IN CHLORIDE SOLUTIONS

R. M. CARRANZA and J. R. GALVELE

Departamento Materiales. Comisión Nacional de Energía Atómica. Avda. Libertador 8250, Buenos Aires (1429). Argentina

Abstract—The repassivation kinetics of AISI 304 austenitic stainless steel was studied in 0.5 M Na_2SO_4 solution, 1 M HCl solution and 1 M NaCl solution, at room temperature and at various electrode potentials. Under the experimental conditions used in the present work, stress corrosion cracking (SCC) of the steel was known to occur only in the HCl solutions. The repassivation kinetic results were described by relations of the type $i = A \cdot t^b$. In Na_2SO_4 solutions $b = -1$ was found. In NaCl solutions and in HCl solutions $b = -1$ was found only in the first 100 ms after straining. In the next 10 s a value of $b = -0.5$ was recorded, and for longer exposures values of $b = 0.5$ and $b = 1$ were observed. There is strong evidence that a dissolution–precipitation film formation mechanism is involved in the region where $b = -0.5$. By comparing the results in HCl solutions with those in NaCl solutions, slow repassivation, of the type $b = -0.5$, is concluded to be a necessary but not sufficient electrochemical condition for SCC susceptibility.

INTRODUCTION

NUMEROUS theoretical[1–8] and experimental[9–17] papers indicate that repassivation rate is an essential factor in the stress corrosion cracking (SCC) of metals and alloys. Repassivation describes the process by which a damaged surface film is reformed. All these papers are based on the assumption that the presence of a surface film is a necessary condition for SCC in aqueous environments. The various models assume that if the localization of corrosion is due to the rupture of the passive film and the reaction of the bare metal to the environment, the repassivation rate should determine the susceptibility to SCC as well as the crack velocity. An inadequate repassivation rate should be the key point for SCC susceptibility.[18] A fast repassivation rate will not allow enough localized corrosion to lead to crack formation, while, on the other hand, a slow repassivation rate should lead to extensive metal waste, giving rise to pitting instead of SCC. A non-quantified intermediate repassivation rate would be the essential condition for SCC.

In the present work the repassivation rate of type AISI 304 austenitic stainless steel was studied in sodium sulphate solution and in various chloride-containing solutions, at room temperature. Austenitic stainless steels are susceptible to transgranular SCC in acidic chloride solutions, at room temperature.[19] No SCC was reported for these steels in neutral NaCl or Na_2SO_4 solutions.[19–23] In the above[19] as well as in other environments[12–14,17,24,25] cracking susceptibility of these steels is believed to be a function of the repassivation rate. To damage the surface films a fast straining rate technique[8,13] was chosen. The reason for this choice is the assumption that the metallurgical changes introduced by straining are closer to those found at the bottom of the crack[26] than to those produced by other techniques such as scratching

Manuscript received 27 April 1987.

or abrasion. From the results of the present work the rate of repassivation is concluded to be a necessary but not a sufficient electrochemical condition for SCC in aqueous environments.

EXPERIMENTAL METHOD

The measurements were performed with commercial type 304 austenitic stainless steel wire, 0.8 mm in diameter. The composition of the steel was, in weight, Cr: 18.2%; Ni: 9.9%; Mo: 0.30%; C: 0.07%; balance Fe. Samples 25 cm long were prepared. The samples were degreased with acetone, annealed for 1 h at 1100°C in argon atmosphere, and water-quenched. Before the measurements the samples were electropolished for 4 min in a cooled 90% butyl cellosolve plus 10% perchloric acid solution, washed with distilled water and alcohol, and dried with hot air. The solutions were prepared with analytical grade reagents and distilled water, and were degassed with prepurified nitrogen, according to the Gilroy and Mayne techaique.[27] All the measurements were performed at room temperature. For straining the wires a fast strain rate technique ($10\ s^{-1}$) was used. For this purpose a device by which the release of a spring produced a 10% elongation of the wires was used, Fig. 1. The elongation was completed in less than 10^{-2} s. The cell used was described in a previous publication.[28]

The potential was kept constant with a potentiostat PARC Model 173 with a fast response module (Model 176). It was measured through a Luggin capillary, with saturated calomel reference electrodes for the chloride-containing solutions, and with a saturated mercurous sulphate electrode for the sulphate-containing solutions. All the potentials are reported on the normal hydrogen electrode scale.

The cell was flushed with pre-purified nitrogen prior to the introduction of the solution in the cell, which was degassed with the same gas during 90 min. After allowing the solution into the cell, the degassing was continued, while the specimen was allowed to reach a constant open circuit potential, which usually took from 1 to 2 hours. Once the steady open circuit potential was reached, the working potential was applied and the specimen was allowed to reach a stationary current (2–30 min). Only then the spring was released and the current transient was measured.

The current–time data was recorded with the equipment schematically described in Fig. 2. Due to the wide change in i–t values, three systems were simultaneously used. A Hewlett–Packard 3052A data acquisition system, with readings every 60 μs, was used for the readings between 0 and 0.06 s. A Tektronix 5115 oscilloscope was used for the readings between 0 and 1 s, and a mechanical Houston X–Y recorder for the values between 0 and 400 s. Good overlapping was found between the three sets of measurements. The measured values were fed to a Hewlett–Packard 9825B microcomputer for processing.

EXPERIMENTAL RESULTS

The first approach to the study of repassivation kinetics of AISI 304 was the study of the metal behaviour only during the few milliseconds after the rupture of the surface film. For this purpose, using a Hewlett–Packard HP 6942A multiprogrammer, the current was recorded every 60 μs during the first 60 ms.

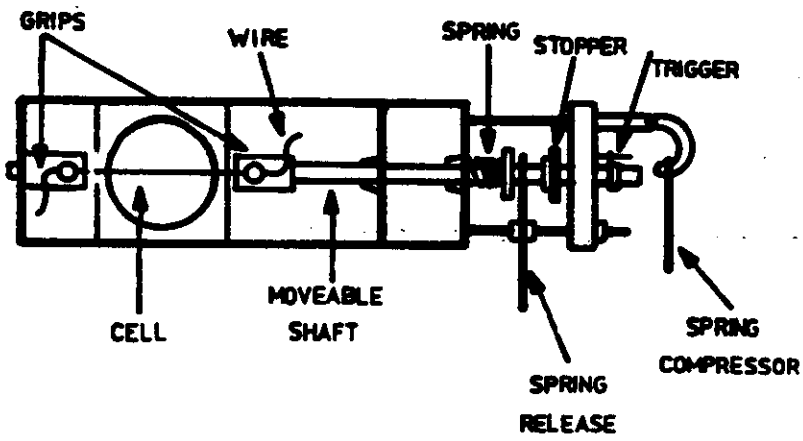

FIG. 1. Schematic view of the device used for the fast straining rate experiments.

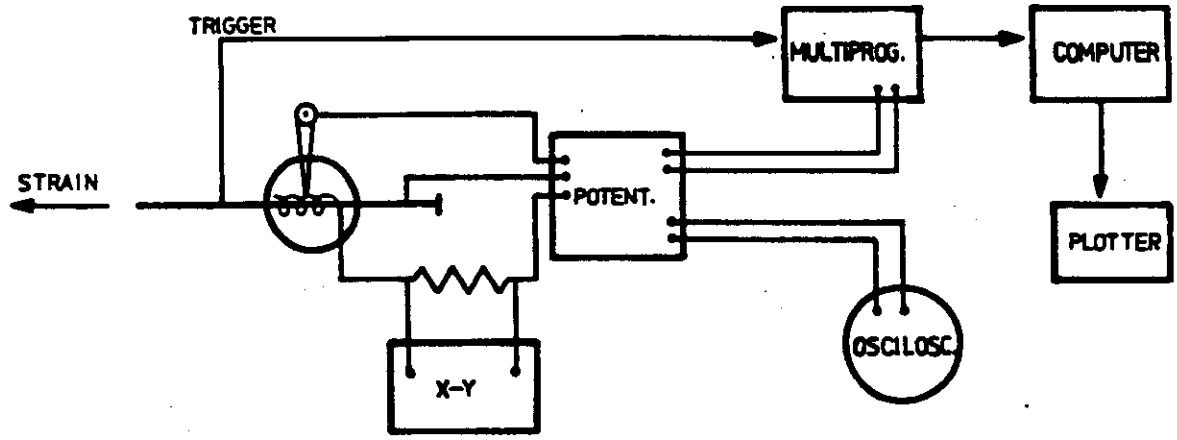

FIG. 2. Schematic description of the equipment used in the measurement of the current–time transients after straining the samples.

Measurements were made in the following environments, and at the following electrode potentials:

(a) environments producing SCC in AISI 304:
- 1 M HCl solution, at −0.09 V(NHE)
- 1 M HCl + 1 M NaCl solution, at −0.090 V(NHE)
- 1 M HCl + 2 M NaCl solution, at −0.090 V(NHE)

(b) environments where no SCC of AISI has been reported:
- 1 M NaCl solution, at 0.200 V(NHE)
- 2 M NaCl solution, at 0.200 V(NHE)
- 3 M NaCl solution, at 0.200 V(NHE)
- 0.5 M Na_2SO_4 solution, at −0.140 V(NHE)
- 1 M Na_2SO_4 solution, at −0.140 V(NHE)
- 1.5 M Na_2SO_4 solution, at −0.140 V(NHE).

To calculate the current density on the freshly exposed metal it is necessary to know the area of bare metal exposed by straining. For this purpose the model developed by Gravano,[29] Fig. 3, was used. According to this model, the area exposed

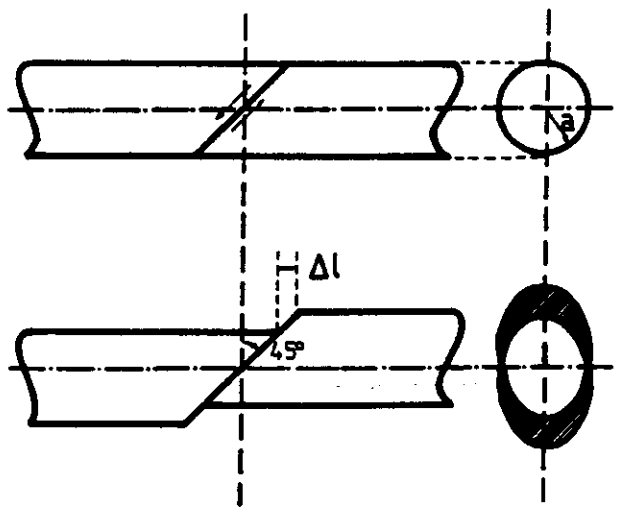

FIG. 3. Calculation of the area of bare metal exposed by straining, after an elongation Δl, according to the model developed by Gravano.[29] The shaded area is the area of the bare metal and a is the radius of the wire sample.

by straining, S_b, is given by

$$S_b = \frac{\pi a \Delta l}{\sin 45°}, \tag{1}$$

a being the radius of the wire sample and $\Delta l = l_0 \varepsilon$, where l_0 is the initial length of the wire inside the cell, and ε is the strain. Since after straining part of the wire sample leaves the cell, the following correction was introduced:

$$S_b = \frac{\pi a \Delta l}{\sin 45°} \frac{l_0}{l_0 + \Delta l}. \tag{2}$$

S_b being the area of bare metal exposed by straining. If the current measured at any time is I, the current density on the bare metal (i_b) will be found in the following way:

$$I = i_b \cdot S_b + i_s \cdot S_s \tag{3}$$

where S_s is the sample area covered by passive film, after straining, and i_s is the current density on the passive metal, which is taken as equal to the current density before straining. If S_0 is the initial area of sample exposed in the cell

$$S_s = \frac{S_0 l_0}{l_0 + \Delta l} = \frac{S_0}{1 + \varepsilon} \tag{4}$$

and

$$i_b = \frac{[\, I(1 + \varepsilon) - i_s S_0 \,] \sin 45°}{\pi a l_0 \varepsilon}. \tag{5}$$

For small strain values ($\varepsilon < 0.20$) the values of i_b given by equation (5) are very close to those calculated by using the model of Bubar and Vermilyea.[30]

Figure 4 shows a typical current transient measured in these experiments. Two

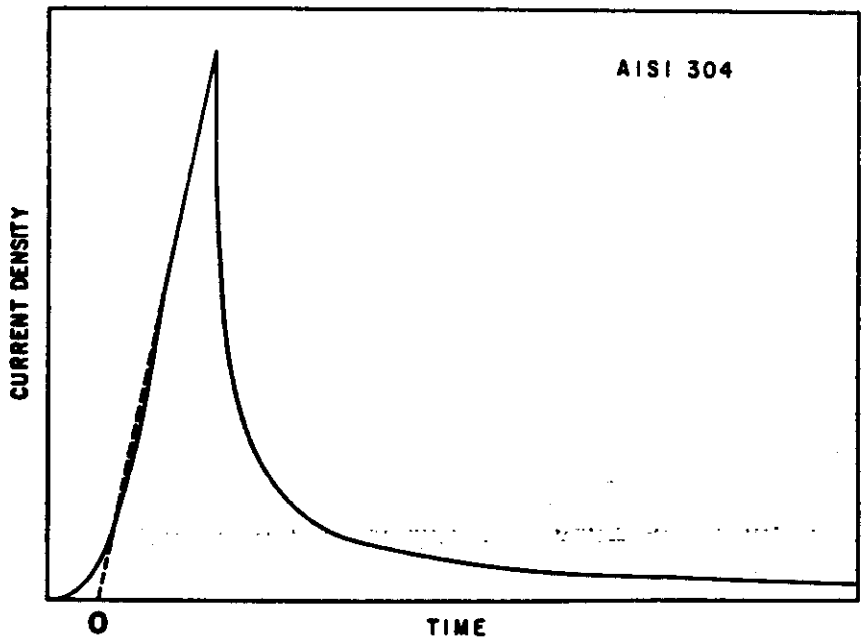

FIG. 4. Typical current–time transient, measured during the fast straining experiments. The current increase takes place during the straining of the wire and its maximum is reached when straining is interrupted. The dotted line shows the method used to define the initial time, t_0.

parts are to be distinguished in these curves. The first one is the large, nearly linear, current increase during straining. The second one is the current change after straining. The object of the present work is the analysis of this second part. The current density in this second part is given by:[31]

$$i_h = i_c + i_a = i_c + i_p + i_{O_2} + i_d + i_x \tag{6}$$

where i_c is the cathodic current density on the bare metal, i_p is the current density due to the passive film formation, i_{O_2} is the current density due to oxygen evolution, i_d is the current density due to dissolution, and i_x is that due to the oxidation of species present in the solution. In the present work the contributions of i_c, i_{O_2} and i_x have been ignored. At the potentials used there is no evolution of oxygen, and the only cathodic reaction possible, in the de-aerated solutions used, is evolution of hydrogen, which, again, at the potentials used, can be ignored. On the other hand, no contribution of i_x should be expected under the present experimental conditions. When passive films are formed, the dissolution current is usually very small, unless passivity breakdown due to pitting is present; otherwise it is assumed that $i_h = i_p$.

During the constant potential straining process, the charge of the double layer on the newly exposed metal surface will appear as a contribution to the measured current. It will be shown that this contribution is very small and can be ignored. The value of the capacitance of the double layer on platinum, mercury and other metallic surfaces ranges between 10 and 40 μF cm^{-2},[32] the value of the capacitance being a function of the concentration of the electrolyte, its composition and the applied potential. To make a conservative estimate, the maximum capacitance value will be assumed for the samples used in the present work. The fresh metal, exposed during straining, is subjected to a potential change:

$$\Delta E = E - E_h \tag{7}$$

where E is the applied potential and E_h is the open circuit potential of the bare metal. In the case of AISI 304 in 1 M HCl solution[33] the value of E_h is less than 0.1 V lower than the corrosion potential of the alloy in the same solution. Under the present experimental conditions ΔE is lower than 0.2 V. Using again a conservative approach, the change in potential of the double layer will be assumed to be ΔE = 1 V. Then, a grossly overestimated value for the charge of the double layer during straining would be:

$$Q = C \cdot \Delta E = 40\,\mu\text{C cm}^{-2}. \tag{8}$$

As shown below the values found by integration of the i–t curves are much higher than that involved in the double layer charge process and this can be safely ignored.

For good characterization of the current–time curve in part two, Fig. 4, a logarithmic scale was used. For this purpose it was necessary to establish the time zero, or the initiation time for straining. Small changes in this value introduce significant changes in the shape of the initial part of the log i–log t curves. Some authors[8–10] have chosen as time zero the instant when the current starts to increase. It is difficult to measure this point with adequate precision. Other authors[11,12] prefer to start counting t at the time the current ceases to increase. The drawback of this criterion is that it ignores the charge circulated during straining. Another criterion used[34] was to choose a value of t_0 in the middle of the above-mentioned values. No satisfactory reason was given for this approach. In the present work the current

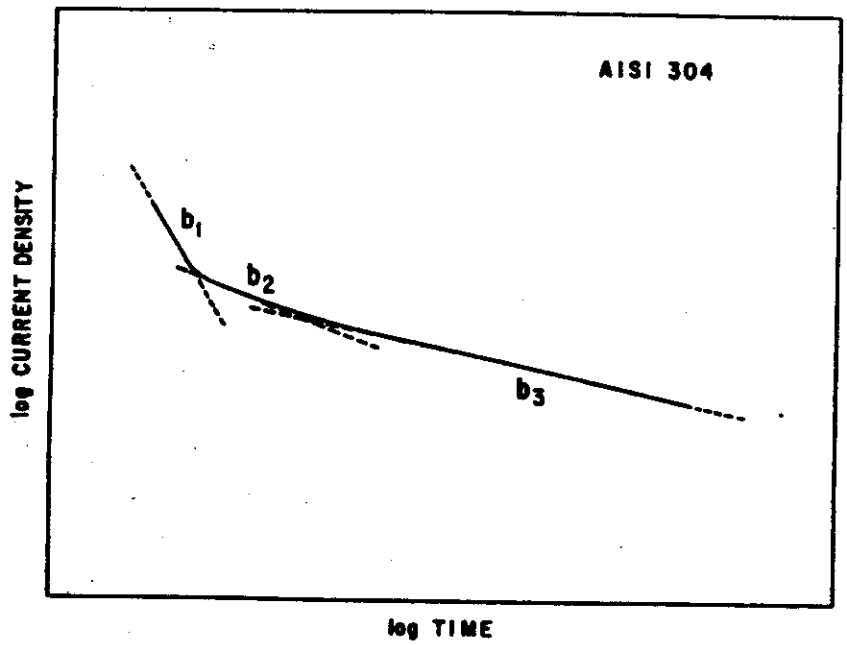

FIG. 5. Typical repassivation curve, plotted in logarithmic scale. The experimental results can be described by three curves of the type $i = A \cdot t^b$, with different values for b. Exposure time: 60 ms.

increase during straining was assumed to be linear. A straight line was drawn from the maximum current (Fig. 4), making sure that the area covered (charge) by the straight line was equal to the experimental one. The intercept with the origin of the current was taken as time zero. Figure 5 shows a typical log–log curve of the repassivation measurements. The experimental results could be interpreted as three straight lines, following a relation of the type:

$$i = A \cdot t^b. \tag{9}$$

Then the full repassivation curve, for the first 60 ms, is described by the following relation:

$$i = \sum_{1}^{n} A_n \cdot t^{b_n} \quad (n = 1\text{–}3). \tag{10}$$

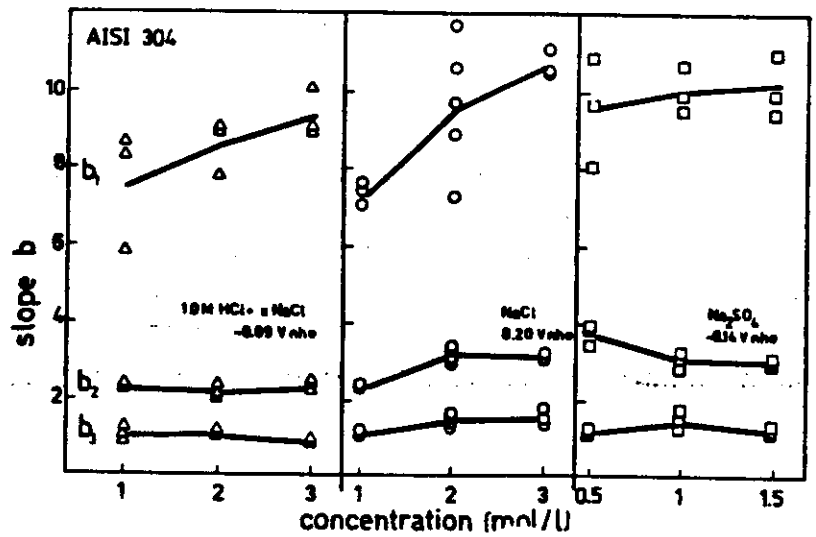

FIG. 6. Slopes of the log i–log t curves for the repassivation of AISI 304 austenitic stainless steel in various electrolytes and during the first 60 ms of repassivation time.

TABLE 1. MEAN VALUES AND STANDARD DEVIATIONS FOR THE MAXIMUM CURRENT (i_m) AND THE SLOPES b_1, b_2 AND b_3 IN THE LOG i–LOG t CURVES FOR REPASSIVATION OF AISI 304 AUSTENITIC STAINLESS STEEL IN VARIOUS ENVIRONMENTS, MEASURED DURING THE FIRST 60 ms OF THE REPASSIVATION PROCESS

Environment	Parameter	Mean	Standard deviation	%
HCl 1 M	b_1	7.5	1.6	20.7
−90 mV(NHE)	b_2	2.25	0.03	1.3
	b_3	1.1	0.2	16.8
	i_m(A cm^{-2})	0.11	0.06	5.5
HCl 1 M + NaCl 1 M	b_1	8.5	0.7	8.7
−90 mV(NHE)	b_2	2.2	0.2	8.5
	b_3	1.05	0.03	3.0
	i_m(A cm^{-2})	0.12	0.01	9.8
HCl 1 M + NaCl 2 M	b_1	9.3	0.6	0.8
−90 mV(NHE)	b_2	2.3	0.1	5.4
	b_3	0.87	0.05	5.3
	i_m(A cm^{-2})	0.28	0.09	3.2
NaCl 1 M	b_1	7.3	0.3	4.2
200 mV(NHE)	b_2	2.29	0.07	2.9
	b_3	1.12	0.04	3.6
	i_m(A cm^{-2})	0.31	0.04	11.6
NaCl 2 M	b_1	9.9	1.7	16.9
200 mV(NHE)	b_2	3.0	0.4	14.9
	b_3	1.3	0.3	20.4
	i_m(A cm^{-2})	0.33	0.03	9.1
NaCl 3 M	b_1	10.8	2.0	18.7
200 mV(NHE)	b_2	2.8	0.4	15.5
	b_3	1.5	0.1	8.9
	i_m(A cm^{-2})	0.32	0.02	6.8
Na_2SO_4 0.5 M	b_1	9.5	1.4	14.6
−140 mV(NHE)	b_2	3.7	0.3	7.6
	b_3	1.21	0.04	3.3
	i_m(A cm^{-2})	0.13	0.02	13.0
Na_2SO_4 1 M	b_1	10.0	0.6	6.1
−140 mV(NHE)	b_2	3.1	0.2	6.4
	b_3	1.5	0.2	14.0
	i_m(A cm^{-2})	0.14	0.02	14.3
Na_2SO_4 1.5 M	b_1	10.1	0.8	8.3
−140 mV(NHE)	b_2	3.2	0.3	7.9
	b_3	1.29	0.02	1.9
	i_m(A cm^{-2})	0.13	0.01	10.6

The values of b_n were calculated by the least squares technique and each experiment was repeated at least in triplicate. The mean values and standard deviations are shown in Table 1. A comparison of the b_1, b_2 and b_3 mean values is shown in Fig. 6. The values of b_1 show the widest dispersion. This is due to the experimental difficulty in obtaining reproducible results in this very short initial transient. No significant differences were found in the values of b in the various electrolytes and concentrations tested. Taking into account that environments producing SCC (HCl solutions) are compared with other environments where no such corrosion is found (NaCl

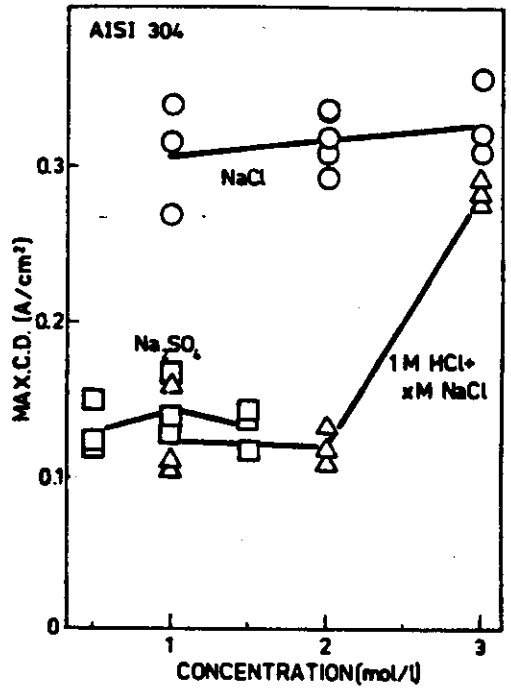

FIG. 7. Maximum current density values recorded in the repassivation measurements for AISI 304 austenitic stainless steel in the following environments: △: 1 M HCl + x M NaCl solution; □: Na_2SO_4 solutions; ○: NaCl solutions.

solutions and Na_2SO_4 solutions) the slopes b, as shown in Fig. 6, are concluded to be irrelevant with regard to SCC.

Another important parameter in defining the repassivation curves is the maximum current value reached at the end of straining. Figure 7 shows the maximum current density values found in the repassivation measurements. As the values for HCl solutions are equal to those for Na_2SO_4 solutions, it must be concluded again that the present repassivation measurements show no distinction between susceptibility and non-susceptibility to SCC.

In view of the above results, it was decided to run a second set of experiments, with longer exposure times. The intention was to see if the differences in SCC susceptibility were noticeable over longer exposures. It was decided to extend the repassivation measurements up to 400 s. It was known from intermediate strain rate techniques[19,33,35] that from straining experiments lasting less than 400 s it was possible to detect SCC susceptibility by electrochemical techniques. Incidentally, this exposure time was also used by Ford[26] in the study of repassivation of stainless steels in high temperature aqueous solutions.

In this second set of experiments it was decided to increase the range of electrode potentials tested. The experiments were performed in the following systems:

1.0 M HCl solution, at 0.0, −0.09, −0.10 and −0.11 V(NHE)

1.0 M NaCl solution, at −0.16, 0.20 and 0.30 V(NHE)

0.5 M Na_2SO_4 solution, at 0.04 and 0.65 V(NHE).

Typical log i–log t curves are shown in Figs 8–10. For the sake of comparison, a selection of those curves was collected in Fig. 11. In a 0.5 M Na_2SO_4 solution (Fig. 10) after some 30 ms the repassivation rate follows a straight line with a slope of $b = -1$. In HCl solutions and in NaCl solutions, on the other hand, no straight lines are observed. In both solutions, for long exposure times, the current starts to increase and eventually a change in the sign of b is found. In view of the clear difference

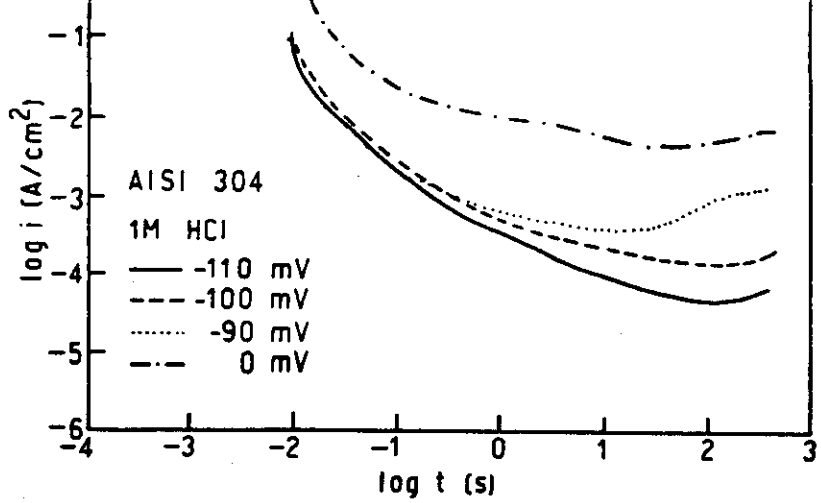

FIG. 8. Typical current–time repassivation curves for AISI 304 in a 1 M HCl solution at various potential values. Exposure time: 400 s.

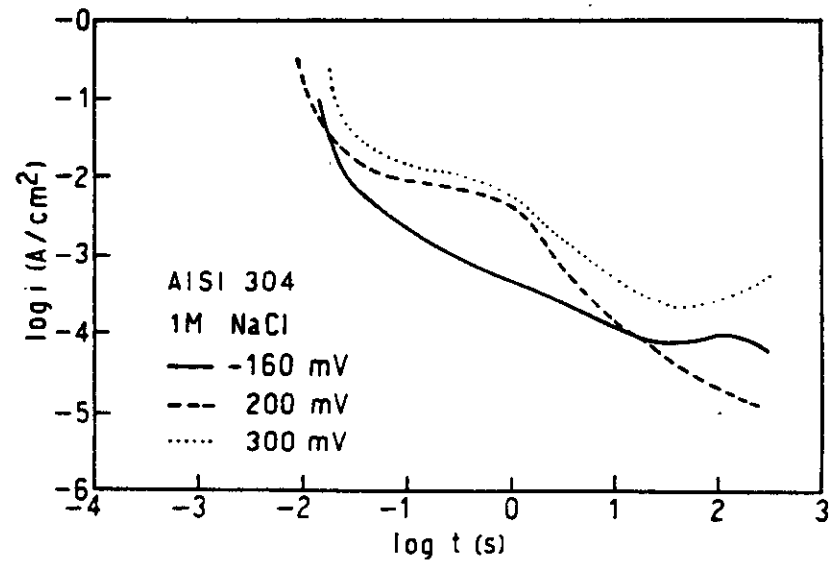

FIG. 9. Typical current–time repassivation curves for AISI 304 in a 1 M NaCl solution at various electrode potentials. Exposure time: 400 s.

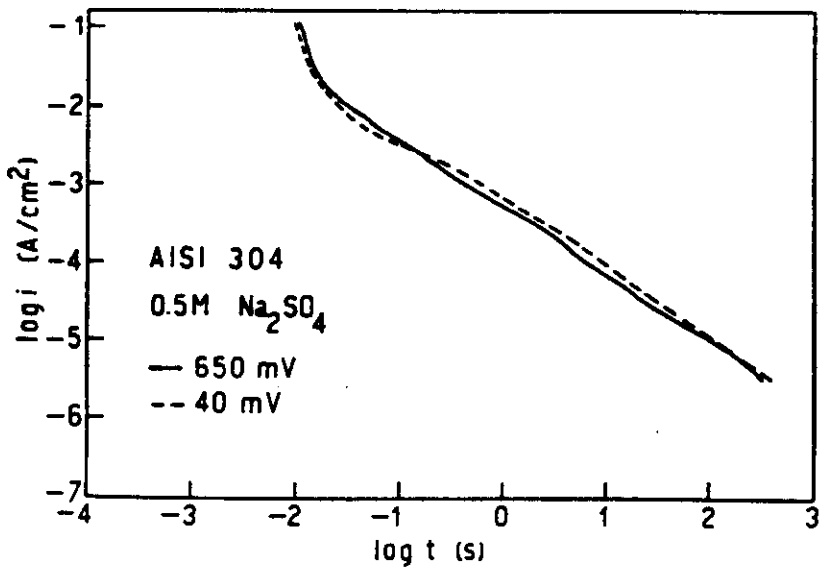

FIG. 10. Typical current–time repassivation curves for AISI 304 in a 0.5 M Na_2SO_4 solution at two different electrode potentials. Exposure time: 400 s.

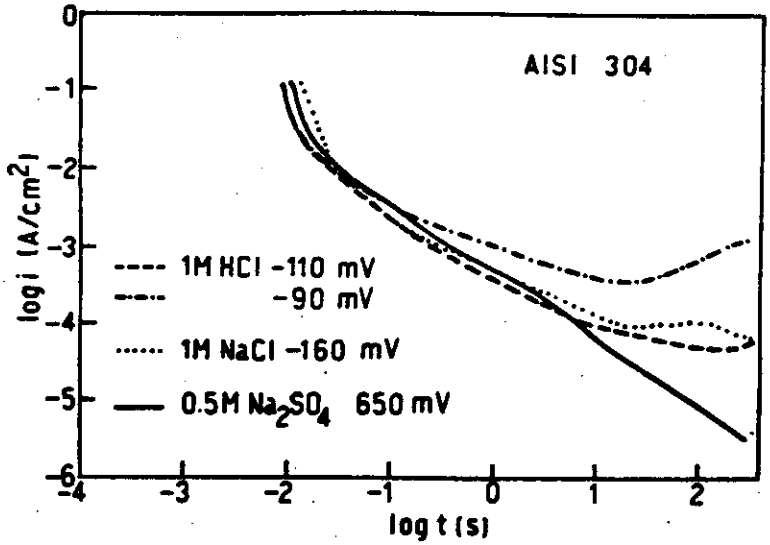

Fig. 11. Comparison of selected current–time repassivation curves for AISI 304 austenitic stainless steel in various environments. The steel, under the present experimental conditions, is susceptible to SCC in the 1 M HCl solution, but is immune to SCC in the other two solutions. No clear indication of susceptibility to SCC can be given from the shape of these repassivation curves.

between the curves in Na_2SO_4 solutions and those in HCl solutions, Fig. 11, it could be argued that there is a relationship between repassivation rates and SCC susceptibility. The fastest repassivation rate is found in Na_2SO_4 solutions, under experimental conditions where no SCC of AISI 304 is observed. This conclusion loses ground when comparing the curves in HCl solutions with those in NaCl solutions. It has been reported that no SCC is observed in NaCl solutions under the present experimental conditions,[22] but there is almost no difference between the repassivation curves in a 1 M HCl solution at −0.11 V(NHE) and those in a 1 M NaCl solution at −0.16 V(NHE). It is impossible to predict in which solution AISI 304 will be susceptible to SCC just from the shape of the repassivation curves.

DISCUSSION

According to Ford,[26] from the log i–log t transients it should be possible to predict the SCC crack velocity. The analysis is based on SCC mechanisms dominated by anodic dissolution, based mainly on the constant charge criterion introduced by Scully[1] and the constant time approach used by Vermilyea.[3] From the current–time transients the charge density vs time is calculated (Fig. 12). If the frequency of film rupture under slow strain rate conditions, t_f, is known, the crack propagation rate (CPR) is given by:

$$\text{CPR} = (M/\varrho Fz)(Q_f/t_f) \tag{11}$$

M being the atomic weight and ϱ the density of the metal reacting at the tip of the crack, z the valence of the reacted metal, F the Faraday constant and Q_f the density of charge consumed during t_f. The value of t_f is given by:

$$t_f = \varepsilon_f/\nu \tag{12}$$

where ε_f is the strain at which the passive film cracks and ν is the strain rate used during the SCC test. A typical value for ε_f[26] is $\varepsilon_f = 0.001$, and since the calculations for the transient reported in the present work are going to be compared with SCC

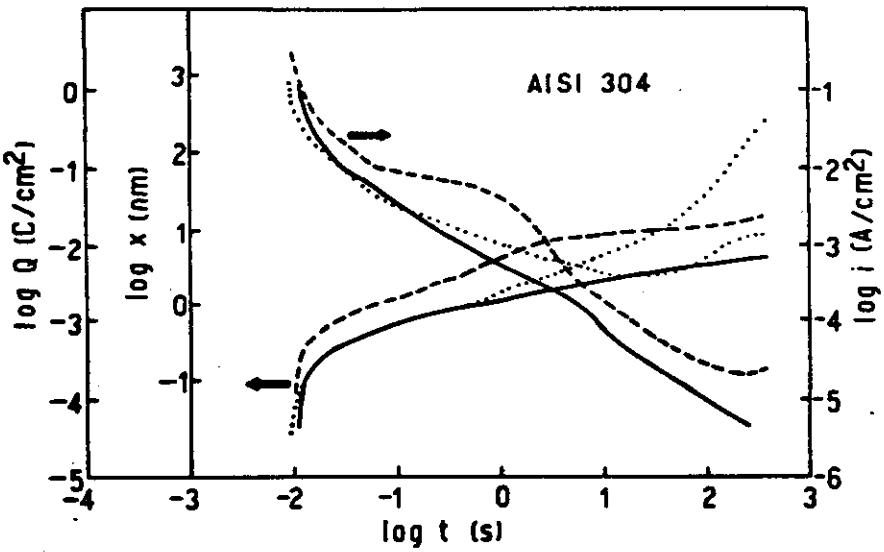

FIG. 12. Changes in charge density, Q, and film thickness, X calculated from the repassivation current–time curves, for AISI 304 austenitic stainless steel in the following environments: ———: 0.5 M Na_2SO_4 solution, at 0.65 V(NHE); -----: 1 M NaCl solution, at 0.20 V(NHE): and .....: 1 M HCl solution, at −0.09 V(NHE).

tests[19] where $v = 4 \times 10^{-6}\ s^{-1}$ was used, it is concluded that $t_f = 250$ s. The other values used were: $M = 55.20$, $\varrho = 7.8\ g\ cm^{-3}$, $z = 3$, and $F = 96500$ C.

Figure 13 shows the crack propagation rates predicted for AISI 304 in a 1 M HCl solution, using the treatment suggested by Ford. The same figure also shows the experimentally measured crack velocities. It is observed that the values predicted are

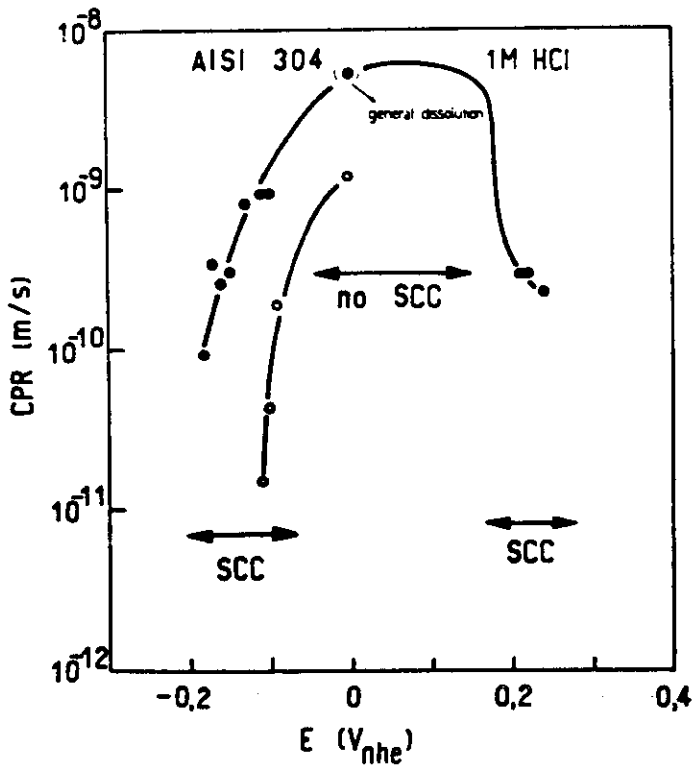

FIG. 13. Crack velocities for AISI 304 austenitic stainless steel in a 1 M HCl solution, at various electrode potentials, at room temperature. ○: Values predicted by the repassivation rate measurements, following the treatment introduced by Ford;[26] ●: experimental values reported by Maier *et al.*[19] The predicted values are lower than the experimental results. Better predictions were reported by the intermediate strain rate technique.[19,35]

TABLE 2. COMPARISON BETWEEN THE CRACK VELOCITIES PREDICTED FROM THE REPASSIVATION RATE MEASUREMENTS, ACCORDING TO FORD,[26] AND THE EXPERIMENTAL VALUES REPORTED BY MAIER *et al.*,[19] FOR AISI 304 AUSTENITIC STAINLESS STEEL IN VARIOUS ENVIRONMENTS

Solution	Potential [V(NHE)]	Experimental crack velocity ($m s^{-1}$)	Predicted crack velocity ($m s^{-1}$)	Charge density Q ($C cm^{-2}$)
HCl 1 M	−0.110	9.2×10^{-10}	1.50×10^{-11}	2.55×10^{-2}
HCl 1 M	−0.100	1.3×10^{-9}	4.20×10^{-11}	4.30×10^{-2}
HCl 1 M	−0.090	1.7×10^{-9}	1.89×10^{-10}	1.93×10^{-1}
HCl 1 M	0.0	5.5×10^{-9}*	1.21×10^{-9}	1.24
NaCl 1 M	−0.160	No SCC	2.46×10^{-11}	2.52×10^{-2}
NaCl 1 M	0.200	No SCC	2.13×10^{-11}	2.18×10^{-2}
NaCl 1 M	0.300	No SCC	1.01×10^{-10}	1.04×10^{-1}
Na_2SO_4 0.5 M	0.650	No SCC	0.90×10^{-11}	9.25×10^{-3}

* Generalized dissolution.

consistently lower than those experimentally measured. The difference is higher at lower potentials and it is almost two orders of magnitude lower than the measured value at −0.11 V(NHE). It should be pointed out that, from a predictive point of view, considerably better coincidence between prediction and experiment is found when using the intermediate strain rate technique.[19,35]

Table 2 shows the crack velocity values predicted for all the environments tested. As expected from the repassivation rate curves, this approach does not make a distinction between HCl solutions and NaCl solutions. SCC should be found in both solutions and with similar crack velocities. The analysis of Ford predicts SCC even in a 0.5 M Na_2SO_4 solution, at 0.65 V(NHE), and with a crack velocity close to that predicted for a 1 M NCl solution at −0.11 V(NHE).

Matsuda *et al.* measured, by ellipsometry, the passive film thickness on 18-8 austenitic stainless steel in a 1 M Na_2SO_4 solution[36] and in a 0.1 M Na_2SO_4 solution.[37] They found similar results in both solutions, reporting that the film thickness changed from 1.2 to 4.2 nm when the potential changed from 0.1 to 1.0 V(NHE). By integration of the current transients, in the present work, in a 0.5 M Na_2SO_4 solution at 0.65 V(NHE), Fig. 12, the film thickness after 400 s was found to be 4.0 nm. A very good coincidence is observed between the ellipsometric measurements reported by Matsuda *et al.* and those in Fig. 12, indicating that all the current measured during the repassivation transient was used in the film formation process. This gives support to the assumption made in the present work that the contribution of i_c in equation (6) could be ignored.

Smialowska and Lukomski[38] measured, by ellipsometry, the film growth rate on AISI 304 austenitic stainless steel in a 1 M HCl solution. They reported, for exposures between 2.5 and 12 min, a film growth from 3 to 10 nm. Figure 12 shows that a film thickness of 10 nm is observed on AISI 304 in a 1 M HCl solution, at −0.09 V(NHE), after some 30 s exposure. As described below, the high apparent film thickness values, found at longer exposures, could be due to a pitting process. Again this observation gives support to the assumption that i_c in equation (6) is very small, and could be ignored.

The various film formation mechanisms are related to well-defined b values in equation (9).[31] The experimental results of the present work were analysed taking

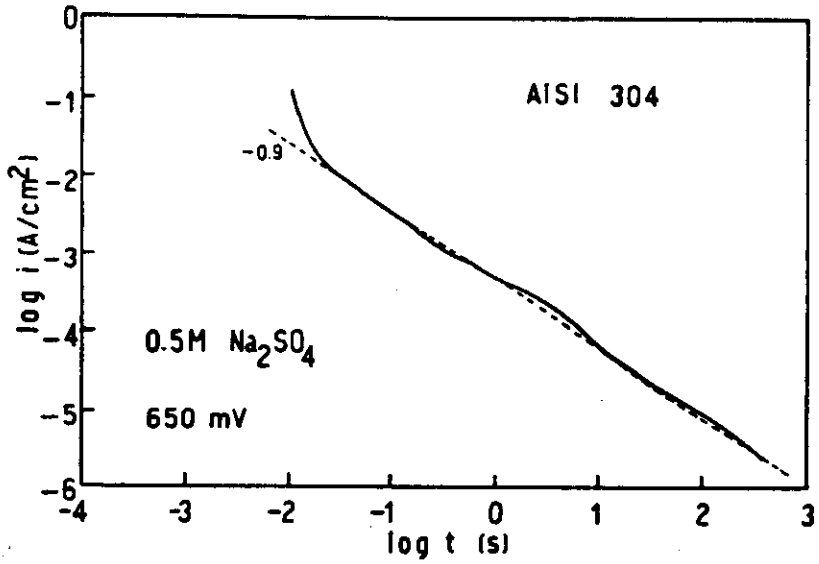

FIG. 14. Analysis of the log i–log t repassivation curves. AISI 304 in a 0.5 M Na_2SO_4 solution, at 0.65 V(NHE). The results follow a law of the type $i = A \cdot t^{-1}$, indicating that most probably a high field film growth mechanism is operative.

into account those b values. Figures 14–18 show some of the experimental log i–log t curves broken into straight lines of well-established b values. The simplest case is that of AISI 304 strained in a 0.5 M Na_2SO_4 solution (Fig. 14). In this case, after the first 20 ms, a slope of -1 is found. The charge involved in the first 20 ms involves the formation of a film monolayer (Fig. 12). The slope of -1, that involves the main part of the repassivation process, is typical of the high field film formation reaction on valve metals.[39,40] A mechanism of film formation with a slope of -1 was also described by Sato and Cohen[41] for iron in borate solutions. This mechanism involves a place exchange process. This type of slope $b = -1$ is usually related to the formation of a compact highly protective passive film.

The behaviour of AISI 304 in 1 M HCl solutions, Figs 15–17, is not as simple as

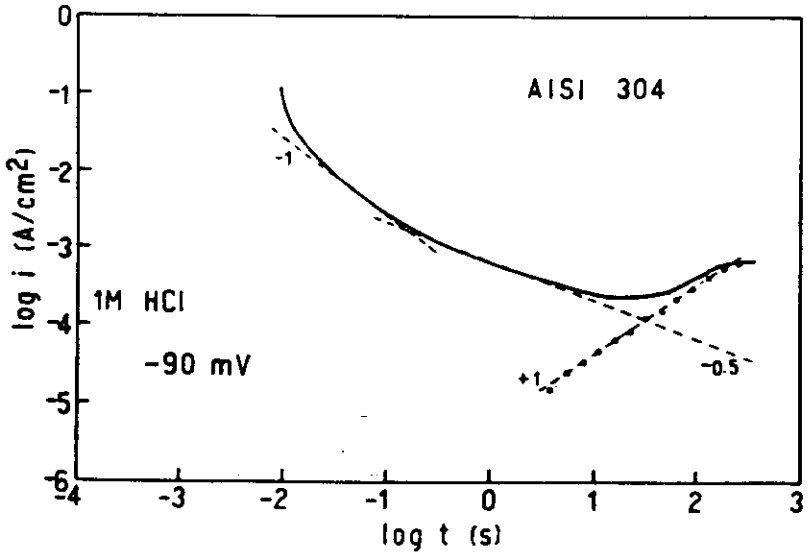

FIG. 15. Analysis of the log i–log t repassivation curves. AISI 304 in a 1 M HCl solution, at −0.11 V(NHE). An initial part of high field film growth mechanism is followed by a mechanism of the type $i = A \cdot t^{-0.5}$, most probably due to a dissolution and precipitation film formation process. At longer exposures a process of the type $i = A \cdot t^{-1}$, attributed to pitting, is observed.

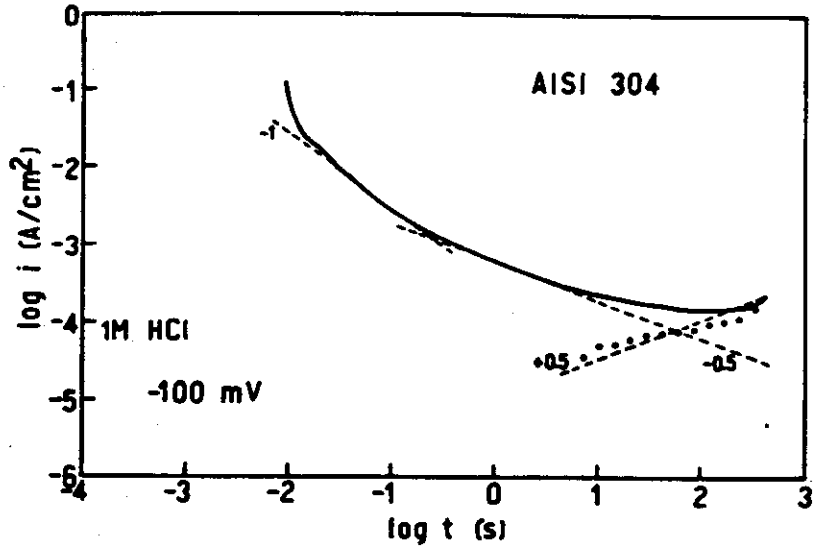

FIG. 16. Analysis of the log i–log t repassivation curves. AISI 304 in a 1 M HCl solution, at −0.10 V(NHE). As in Fig. 15, a sequence of high field film growth mechanism is followed by a dissolution and precipitation film growth mechanism, and finally a pitting process is observed. In this case, the pitting/growth process seems to follow a law of the type $i = A \cdot t^{n}$.

that in Na_2SO_4 solutions. A region with a slope of −1 is observed in all the measurements, in the initial portion of the log i–log t curves. This behavior lasts <100 ms. Afterwards a change from slope −1 to slope −0.5 is observed. A slope of $b = -0.5$ is usually attributed to diffusion processes, either in the solid or in the liquid phase.[42,43] In such cases a relation of the type:

$$i = (\varrho D C_0 / M)^{1/2} \cdot zFt^{1/2} \tag{13}$$

should be expected, D being the diffusion coefficient, C_0 the concentration of the diffusing species at the metal/oxide interphase, M the molecular weight of the film and ϱ its density, z is the valence and F the Faraday constant. From equation (13) a rough estimate of the value of D can be made. The film is assumed to be composed

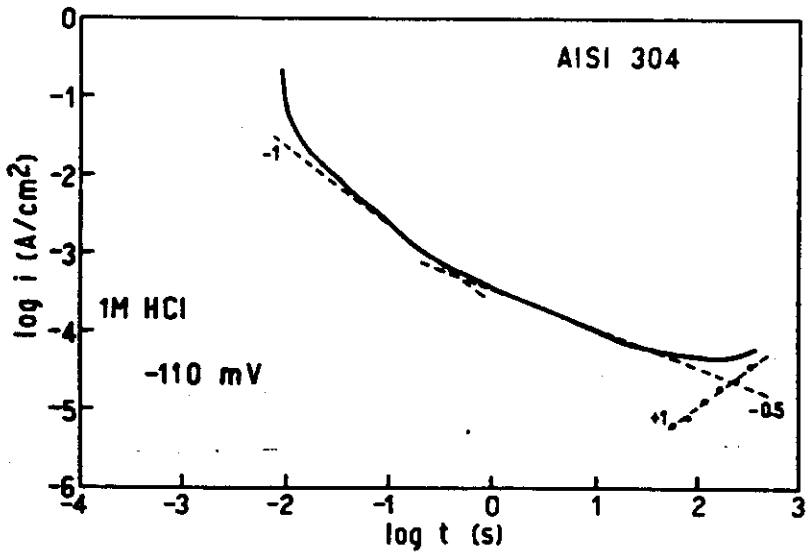

FIG. 17. Analysis of the log i–log t repassivation curves. AISI 304 in a 1 M HCl solution, at −0.09 V(NHE). As in Fig. 15, a sequence of high field film growth followed by a dissolution–precipitation film growth and by pitting, is observed.

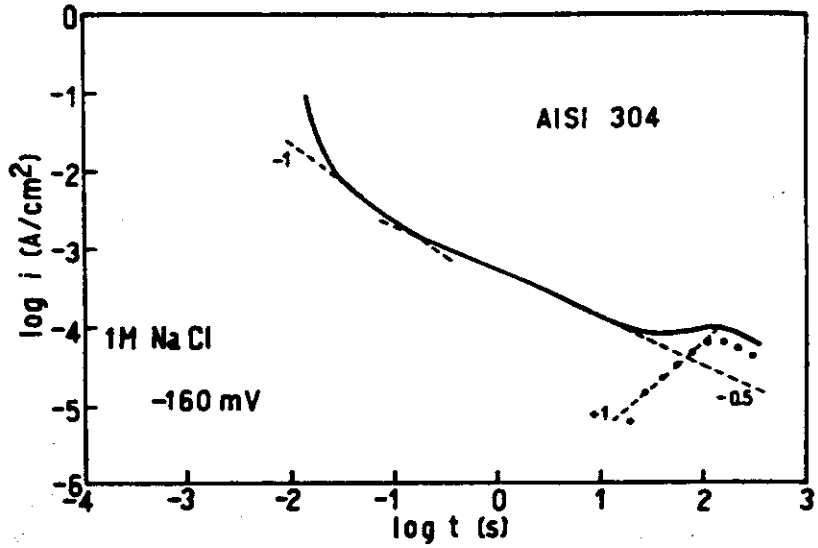

FIG. 18. Analysis of the log i–log t repassivation curves. AISI 304 in a 1 M NaCl solution, at −0.16 V(NHE). As in Fig. 15, a sequence of high field film growth, dissolution–precipitation film growth and pitting, is observed.

by Fe_2O_3 plus Cr_2O_3, and the values $M = 158$ and $\varrho = 5.23\ g\ cm^{-3}$ will be used. The value for C_0 is unknown and a very conservative approach would be to use the atomic concentration of the metal in the alloy, $C_0 = 0.14$ mol cm^{-3}. Table 3 shows the diffusion coefficients thus calculated. Since the value of C_0 is probably much lower than that assumed here, the real diffusion coefficients should be higher than those given in Table 3. No diffusion coefficients for Fe_2O_3 and Cr_2O_3 at room temperature have been found in the literature, and extrapolated values will have to be used. By extrapolation from high temperature[44,45] an oxide like Fe_2O_3 should have a value of $D = 1.5 \times 10^{-62}\ m^2\ s^{-1}$ at 20°C. Although this extrapolation certainly involves gross errors, the comparison with Table 3 suggests that the diffusion through a solid film is very improbable in the case of Figs 15–17. Current–time curves with a slope of $b = -0.5$ and high diffusion coefficients, as found in the present work, are more compatible with a porous film that grows by a dissolution and precipitation process.[43] Tarnish films formed by this process have been reported in various SCC systems, like mild steel in caustic solutions or brass in ammoniacal solutions.[43] Most probably a similar process was present in Figs 15–17.

Figures 15–17 show that after some 10 s exposure a new process, with a slope of $b = 1$ or $b = 0.5$, is detected. Positive slopes like these are usually related to a process

TABLE 3. DIFFUSION COEFFICIENTS CALCULATED FOR THE FILM FORMATION PROCESS ON AISI 304 IN VARIOUS ENVIRONMENTS

Environment	Potential [V(NHE)]	Diffusion coefficient ($m^2 s^{-1}$)
HCl 1 M	−0.090	1.12×10^{-19}
HCl 1 M	−0.100	8.53×10^{-20}
HCl 1 M	−0.110	2.82×10^{-20}
NaCl 1 M	−0.160	7.09×10^{-20}

of nucleation and growth of a new phase[46] or to a process of nucleation and growth of pits.[47] Most probably the second alternative applies to the present work, since the presence of pits has been reported in those systems.[22]

A similar analysis of the log i–log t curves could not be extended to AISI 304 in a 1 M HCl solution at 0.0 V(NHE) because of the high generalized dissolution taking place at this potential. As for the measurements in NaCl solutions, Fig. 18 shows that at −0.16 V(NHE) regions with slopes of $b = -1$, $b = -0.5$ and $b = 1$ are observed, similar to those found in HCl solutions. At higher potentials, 0.2 and 0.3 V(NHE), a pitting process obscures the film formation process.

CONCLUSIONS

The results in the present work indicate that in the initial stages of repassivation, up to approx. 60 ms, the repassivation rate is the same in solutions producing SCC and in those where no SCC is found. If there are any relevant differences, they are observed only about 100 ms after straining.

For AISI 304 in a 0.5 M Na_2SO_4 solution the only process detected is the formation of a highly protective passive film. The log i–log t curve shows a slope $b = -1$, and the passive film is formed either by a high field Cabrera–Mott mechanism or by the place exchange Sato and Cohen mechanism.

Below the pitting potential there is no significant difference between the repassivation curves of AISI 304 in HCl solutions and those in NaCl solutions. Since SCC is found only in the HCl solutions, the conclusion is that the shape of the repassivation curves is not sufficient to predict SCC susceptibility.

A change in the repassivation rate, from $b = -1$ to $b = -0.5$, was found for AISI 304 in chloride-containing solutions. There is strong evidence that a dissolution–precipitation film formation mechanism is involved. Since similar mechanisms have been reported for other SCC systems, this could be a necessary, albeit not a sufficient, electrochemical condition for SCC susceptibility.

Acknowledgements—The present research has been supported by the Programa Latinoamericano de Lucha Contra la Corrosión OEA–CNEA, and by the Consejo Nacional de Investigaciones Científicas y Técnicas, Argentina.

REFERENCES

1. J. C. Scully, *Corros. Sci.* 7, 197 (1967).
2. J. Kruger, in Fall Meeting, *The Electrochem. Soc., Extended Abstracts*, Vol. 75-2, Abstract No. 69, p. 175. Dallas, Texas (1975).
3. D. A. Vermilyea, in *Stress Corrosion Cracking and Hydrogen Embrittlement of Iron-Base Alloys* (eds R. W. Staehle, J. E. Hochmann, R. R. McRight and J. R. Slater), p. 208. National Association of Corrosion Engineers, Houston (1977).
4. H. J. Engell, in *The Theory of Stress Corrosion Cracking in Alloys* (ed. J. C. Scully), p. 86. NATO Scientific Affairs Division, Brussels (1971).
5. R. W. Staehle, *ibid.*, p. 223.
6. W. R. Wearmouth, G. P. Dean and R. W. Parkins, *Corrosion* **29**, 251 (1973).
7. G. Bignold, *Corrosion* **28**, 307 (1972).
8. R. W. Staehle, in *Passivity and its Breakdown on Iron and Iron-Base Alloys* (eds R. W. Staehle and H. Okada), p. 155. National Association of Corrosion Engineers, Houston (1976).
9. R. B. Diegle and D. A. Vermilyea, *J. electrochem. Soc.* **122**, 180 (1975).
10. J. R. Ambrose and J. Kruger, *J. electrochem. Soc.* **121**, 599 (1974).
11. J. F. Rimbert and J. Pagetti, *Corros. Sci.* **20**, 189 (1980).

12. F. P. Ford and M. Silverman, *Corrosion* **36**, 558 (1980).
13. T. Shibata and R. W. Staehle, in *5th Int. Congress on Metallic Corrosion, Extended Abstracts*, p. 145. Tokyo (1972).
14. J. R. Ambrose and J. Kruger, *Corrosion* **28**, 30 (1972).
15. T. R. Beck, *J. electrochem. Soc.* **115**, 890 (1968).
16. T. R. Beck, *Corrosion* **30**, 408 (1974).
17. A. Frignani, F. Zucchi, M. Zuchini and G. Trabanelli, *Corros. Sci.* **20**, 791 (1980).
18. J. C. Scully, *Corros. Sci.* **20**, 997 (1980).
19. I. A. Maier, C. Manfredi and J. R. Galvele, *Corros. Sci.* **25**, 15 (1985).
20. G. Bianchi, F. Mazza and S. Torchio, *Corros. Sci.* **13**, 165 (1973).
21. B. F. Brown, *Stress Corrosion Cracking Control Measurements*, NBS monograph 156, Chap. 7, p. 55. Washington (1977).
22. J. E. Truman, *Corros. Sci.* **17**, 737 (1977).
23. R. N. Parkins, *Stress Corrosion Cracking—The Slow Strain Rate Technique* (eds G. M. Ugiansky and J. H. Payer), p. 5. American Society for Testing Materials, Philadelphia (1979).
24. P. Engseth and J. C. Scully, *Corros. Sci.* **15**, 505 (1975).
25. M. Barbosa and J. C. Scully, in *Environment-Sensitive Fracture of Engineering Materials* (ed. Z. A. Foroulis), p. 91. The Metallurgical Society of AIME, New York (1979).
26. F. P. Ford, *Mechanisms of Environmental Cracking in Systems Peculiar to Power Generation Industry*, EPRI NP-2589, RP1332-1, Final Report (1982).
27. D. Gilroy and J. E. Mayne, *J. appl. Chem.* **12**, 382 (1962).
28. J. R. Galvele, S. M. de De Micheli, I. L. Muller, S. B. de Wexler and I. L. Alanis, in *Localized Corrosion* (eds R. W. Staehle, B. F. Brown, J. Kruger and A. Agrawal), p. 580. National Association of Corrosion Engineers, Houston (1974).
29. S. M. Gravano, Thesis, Instituto Balseiro, Universidad Nacional de Cuyo, Argentina (1986).
30. S. F. Bubar and D. A. Vermilyea, *J. electrochem. Soc.* **113**, 892 (1966).
31. J. W. Schultze, M. M. Lohrengel and D. Ross, *Electrochim. Acta* **28**, 973 (1983).
32. K. J. Vetter, *Electrochemical Kinetics (Theoretical Aspects)*, p. 79. Academic Press, New York (1967).
33. J. R. Galvele, S. B. de Wexler and I. Gardiazabal, *Corrosion* **31**, 352 (1975).
34. G. T. Burstein and P. I. Marshall, *Corros. Sci.* **23**, 125 (1983).
35. J. R. Galvele, in *Predictive Capabilities in Environmentally Assisted Cracking* (ed. R. Rungta), p. 273. The American Society of Mechanical Engineers, New York (1985).
36. S. Matsuda, K. Sugimoto and Y. Sawada, *Trans. Japan Inst. Met.* **18**, 66 (1977).
37. S. Matsuda, K. Sugimoto and Y. Sawada, in *Passivity of Metals* (eds R. P. Frankenthal and J. Kruger), p. 699. The Electrochem. Soc. Inc., New Jersey (1978).
38. S. Szklarska-Smialowska and N. Lukomski, *Corrosion* **34**, 177 (1977).
39. N. Cabrera and N. F. Mott, *Rep. Progr. Phys.* **12**, 163, (1949).
40. T. R. Beck, *J. electrochem. Soc.* **129**, 2500 (1982).
41. N. Sato and M. Cohen, *J. electrochem. Soc.* **111**, 512, (1964).
42. A. T. Fromhold Jr, *Theory of Metal Oxidation, Vol. 1, Fundamental-Series Defects in Crystalline Solids, Vol. 9* (eds S. Amelinckx, R. Gerves and J. Nihoul). North-Holland Publishing Co., New York (1976).
43. T. E. Evans, in *Passivity of Metals* (eds R. P. Frankenthal and J. Kruger), p. 410. The Electrochem. Soc. Inc., New Jersey (1978).
44. A. M. Brown and M. F. Ashby, *Acta Met.* **28**, 1085 (1980).
45. O. Kubaschebski and B. R. Hopkins, *Oxidation of Metals and Alloys*, 2nd edn. Butterworth, London (1962).
46. M. Fleischman and H. R. Thirsk, *Adv. Electrochem. Eng.* (ed. P. Delahay), Chap. 3, p. 123. Wiley, New York (1963).
47. S. Szklarska-Smialowska, in *Localized Corrosion* (eds R. W. Staehle, B. F. Brown, J. Kruger and A. Agrawal), p. 312. National Association of Corrosion Engineers, Houston (1974).

REPASSIVATION KINETICS IN STRESS CORROSION CRACKING – II. α-BRASS IN NON-AMMONIACAL SOLUTIONS

R. M. CARRANZA and J. R. GALVELE

Departamento Materiales, Comisión Nacional de Energía Atómica, Avda. Libertador 8250, Buenos Aires 1429, Argentina

Abstract—The repassivation rate kinetics of α-brass in $NaNO_2$ solutions of various concentrations, in borate buffered Na_2SO_4 solutions, and in sulphide-containing Na_2SO_4 solutions was studied. Slow repassivation rates, with slopes of $b = -0.5$ in the current decay curves, were observed to be present in all the cases where SCC was found. This slow repassivation rate also proved to be a necessary, but not a sufficient condition for SCC, since the same slope was found in some cases where no SCC occurred. The use of repassivation rate techniques in the prediction of SCC susceptibility was evaluated, and the limitations of those techniques are discussed.

INTRODUCTION

THE SUSCEPTIBILITY of brasses to stress corrosion cracking (SCC) in a great variety of non-ammoniacal solutions has been broadly recognized,[1–4] nitrite solutions being of special interest for brass,[5,6] as well as for pure copper,[7] because of the very high crack propagation rate found in these solutions. Anodic dissolution is frequently referred to as the active mechanism in SCC,[5,6,8,9] both in ammoniacal and in non-ammoniacal solutions. As mentioned in the first part of this work,[10] the essential requirement for crack propagation, in anodic dissolution mechanisms, is an intermediate repassivation rate. It should be neither too high, because the film is rapidly repaired and no cracking is produced, nor too small because generalized corrosion or pitting is produced. In the first part of this study it was shown that this was not the case for type 304 stainless steel in chloride and in sulphate solutions at room temperature. Slow repassivation, in these cases, seemed to be a necessary, but not a sufficient, electrochemical condition for SCC.

In the present work the relation between the repassivation rate and SCC of 64/36 α-brass in a variety of solutions, is studied. The high strain rate technique[11] was used because it is considered as an analogy to the conditions at the tip of the crack. Here again, the repassivation rate is found to be a necessary but not sufficient electrochemical condition for SCC to occur.

EXPERIMENTAL METHOD

The material used was wire (0.08 mm diameter) of alpha brass cut in appropriate lengths. The composition of the brass was Cu 63.7; Sn < 0.1; Pb ~ 0.01; Zn balance, wt%. The wires were degreased with acetone and annealed at 450°C for 24 h under a 120 mmHg argon atmosphere and quenched in water at room temperature. Metallographic observations indicated that this time was sufficient to obtain a full alpha phase alloy. Before the tests the specimens were chemically polished for a few seconds at room temperature in a solution containing 25% acetic acid, 55% phosphoric acid and 20% nitric acid, cleaned with distilled water and alcohol and dried in hot air.

Manuscript received 17 June 1987; in amended form 22 October 1987.

Solutions were prepared with analytical grade chemicals and de-ionized-distilled water, and were de-aerated with purified nitrogen according to the Gilroy and Mayne method.[12] The following solutions and potentials were used:

Solution	*Potential* [mV(NHE)]
1 M $NaNO_2$; pH 10	70; 125; 150; 200; 250
0.1 M $NaNO_2$; pH 10	125; 150; 200; 250; 350
0.01 M $NaNO_2$; pH 10	70; 125; 150; 200; 250; 350; 500
1 M $NaNO_2$ + 0.5 M Na_2SO_4; pH 10	70; 125; 150; 200; 250; 325
0.1 M $NaNO_2$ + 0.5 M Na_2SO_4; pH 10	70; 125; 150; 200; 250
0.01 M $NaNO_2$ + 0.5 M Na_2SO_4; pH 10	70; 125; 150; 200; 250
0.5 M Na_2SO_4 + 0.2 M(H_3BO_3 + NaH_2BO_3); pH 9.2	200; 250; 300; 325; 335; 350
0.01 M Na_2S + 0.5 M Na_2SO_4	−200; 200; 300; 350; 400; 550
0.05 M Na_2S + 0.5 M Na_2SO_4	−200; 200; 300; 350; 400; 550; 650; 800

In some of these solutions the occurrence of SCC is a function of the applied potential. At sufficiently low potentials cracking can be stopped. The tests were run at room temperature and at least in triplicate. The cell used was described in a previous paper.[13] The same applies to the high strain rate machine and ancillary equipment.[10] Wire samples were strained 10% at a strain rate of 10 s^{-1}, and the current was recorded during and after the interruption of straining. Anodic potentiodynamic polarization curves, at 0.2 mV s^{-1}, were also run in a conventional three electrode electrolytic cell. In these last measurements, sample wires of 1 cm^2 were used, and these tests were run at least in duplicate. In all the tests, potentials were measured through a Luggin capillary with a $Hg-Hg_2SO_4$ reference electrode and they are reported in the normal hydrogen electrode scale (NHE). The counter electrode was a platinum spiral wire around the working electrode. The measurement technique was described in the first part of this work.[11]

EXPERIMENTAL RESULTS

Figure 1 shows the potentiodynamic polarization curves for brass in 1 M, 0.1 M and 0.01 M $NaNO_2$ solutions, at pH 10. A passive zone is observed, followed by a passivity rupture potential. The smaller the $NaNO_2$ concentration the higher the potential. In a 1 M $NaNO_2$ solution an anodic peak is found before passivity rupture. The potential of this peak is close to the Cu_2O/CuO thermodynamic equilibrium potential at pH 10.[14]

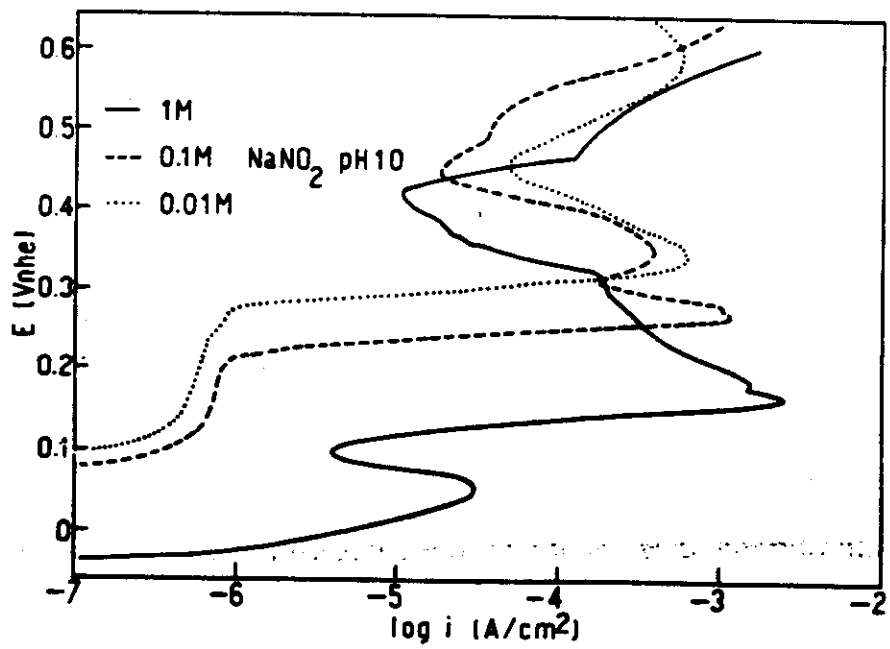

FIG. 1. Potentiodynamic polarization curves (0.2 mV s^{-1}) for brass in $NaNO_2$ solutions at different concentrations at pH 10. The passivity rupture potential is higher the smaller the $NaNO_2$ concentration.

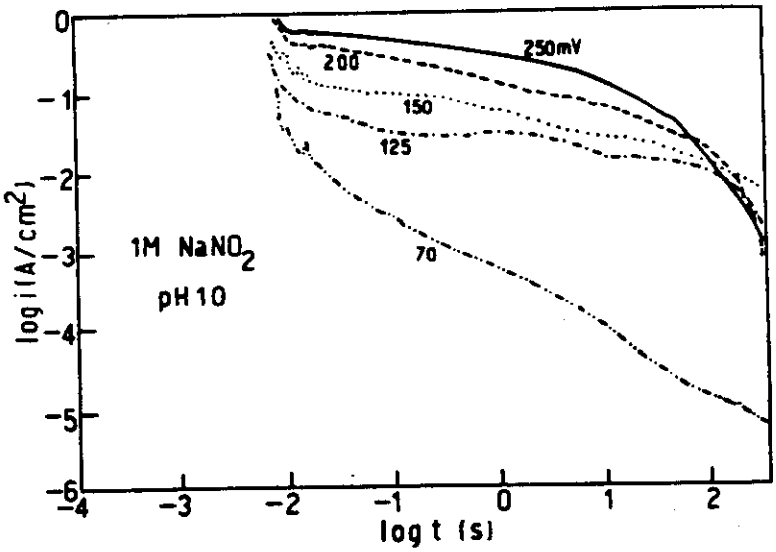

FIG. 2. Typical current–time repassivation curves for brass in a 1 M $NaNO_2$ solution at various potential values. Exposure time: 400 s.

In another set of measurements, 0.5 M Na_2SO_4 was added to the $NaNO_2$ solutions, keeping the pH of the solution at 10. Sulphate ion is aggressive and produces pitting on brass.[3] Another effect of the presence of sulphate in the solution could be an increase in its electrical conductivity. Little difference is observed between the polarization curves obtained with the sulphate containing solution, and those measured in the absence of sulphates. The main difference is found at high potentials, above the passivity breakdown potential, where the current density values reached in the sulphate containing solutions are much higher than those measured in its absence. Above the passivity breakdown potential a tarnish film is formed on the surface of the samples. By XPS (X-ray Photo-electron Spectroscopy) and by electron diffraction the tarnish film was found to be mainly Cu_2O. No CuO was detected through these techniques.

Figures 2–5 show the repassivation curves obtained after rapid straining of brass wires in the $NaNO_2$ and $NaNO_2$ + Na_2SO_4 solutions. The way in which the bare metal current density (i_b) was calculated was described in the first part of this work.[10] In a 1 M $NaNO_2$ solution (Fig. 2) at 0.070 V, log i decays almost linearly with log t, following a simple law $i = At^b$, with a b value of -0.84. At higher potentials, although the current density diminishes with time, its behaviour is not as simple as that at 0.070 V. There is an intermediate lapse of time where the current decay is very slow. For long periods of time the current remains at values as high as 0.1 Acm^{-2} or higher, and is a function of the applied potential.

Repassivation curves in 0.1 M and 0.01 M $NaNO_2$ solutions (Figs. 3 and 4) exhibit some differences with respect to those in a 1 M $NaNO_2$ solution. At low potentials the shape of the curve is similar to that in a 1 M $NaNO_2$ solution at 0.070 V, although its decay is not so linear. At higher potentials, after an exposure time of the order of 1 s the current starts to increase, reaching a maximum, and decreasing again. The value of this maximum is a function of both the applied potential and the solution concentration. Surface observation with the scanning electron microscope (SEM) shows the surfaces covered with thick brittle oxide films, particularly at high potentials and in the more concentrated $NaNO_2$ solutions. In a 0.01 M $NaNO_2$

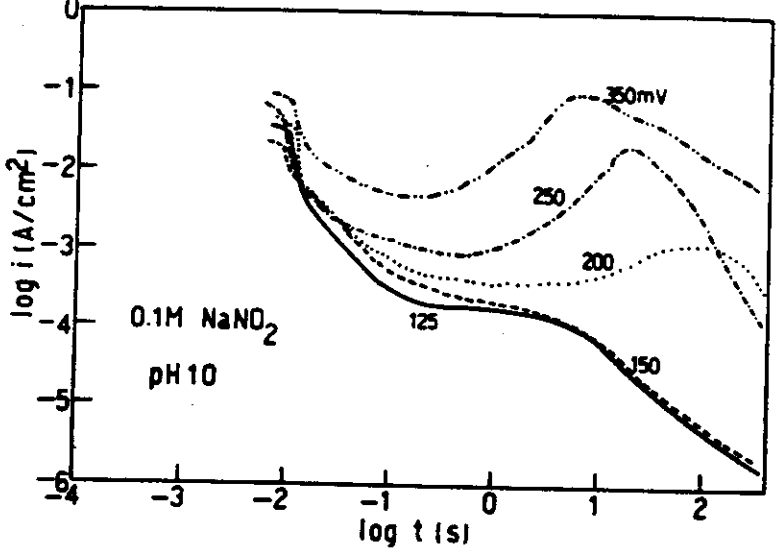

FIG. 3. Typical current–time repassivation curves for brass in a 0.1 M $NaNO_2$ solution at various potential values. Exposure time: 400 s.

solution, at potentials above 0.125 V, where the sample surface shows few corrosion products, crystallographic pits were observed. SCC has been reported[6-15] in all these $NaNO_2$ solutions at the potentials studied.

The addition of 0.5 M Na_2SO_4 to the nitrite solutions caused a change in the log i–log t curves only in 1M $NaNO_2$ solutions (Figs 2 and 5). The presence of sulphate in the 1 M $NaNO_2$ solution produced current maxima similar to those observed in pure 0.1 M and 0.01 M $NaNO_2$ solutions. The addition of Na_2SO_4 to 0.1 M and 0.01 M $NaNO_2$ solutions, on the other hand, had little effect on the repassivation curves. In all these solutions the surface of the strained specimens showed abundant corrosion products, the magnitude of which increased with the potential. Crystallographic pits were observed at all the concentrations tested.

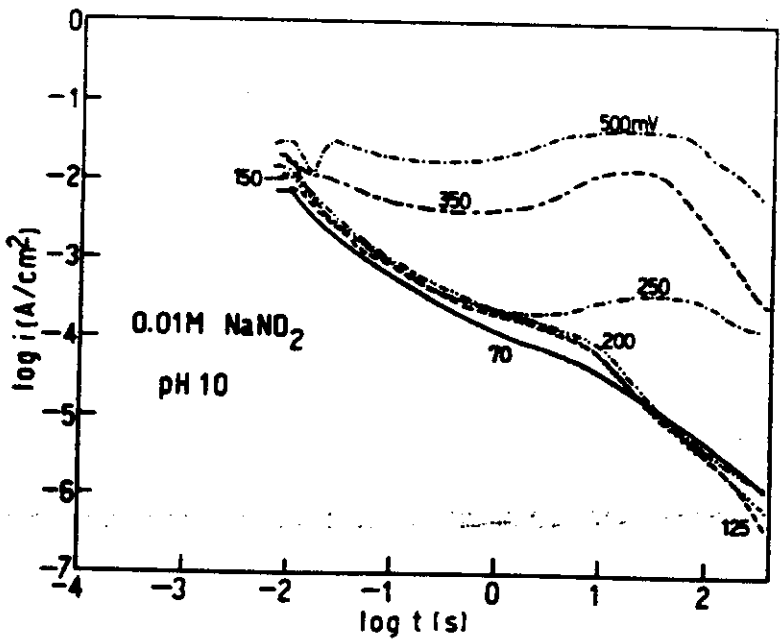

FIG. 4. Typical current–time repassivation curves for brass in a 0.01 M $NaNO_2$ solution at various potential values. Exposure time: 400 s.

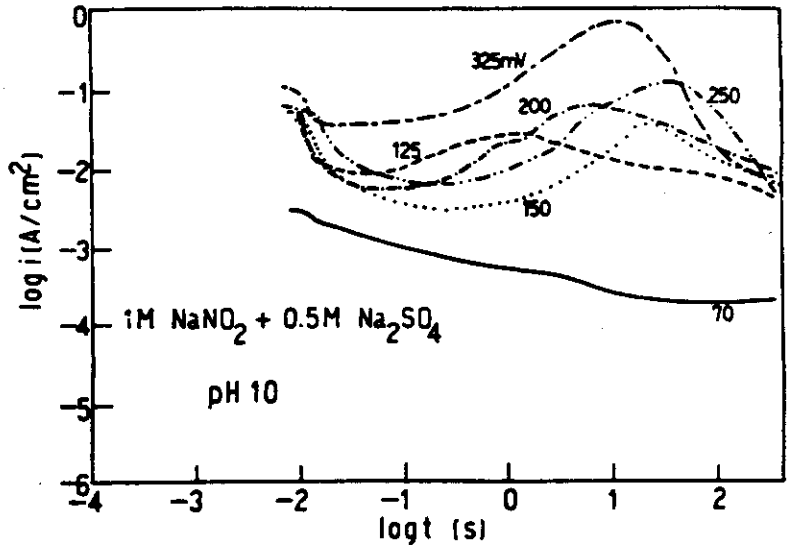

FIG. 5. Typical current–time repassivation curves for brass in a 1 M $NaNO_2$ + 0.5 M Na_2SO_4 solution at various potential values. Exposure time: 400 s.

Repassivation rates of brass were studied also in borate buffered Na_2SO_4 solutions. In Fig. 6 the anodic polarization curve of brass in a 0.5 M Na_2SO_4 + 0.2 M(H_3BO_3 + NaH_2BO_3) solution, pH 9.2, is shown. This curve shows a first anodic peak at a potential very close to that given in the Pourbaix diagrams[14] for the equilibrium Cu_2O/CuO at pH 9.2. At higher potentials a short passive zone is observed and passivity rupture is produced at potentials close to 0.400 V. Crystallographic pits were observed with the SEM. Straining tests in this solution were performed within the passive zone potentials (Fig. 7). At the lowest applied potential, 0.2 V, the current decreased following a simple logarithmic law with a slope of $b = -1$, until the stationary current value of the prestrained samples was reached. At higher potentials current increases and current maxima were observed.

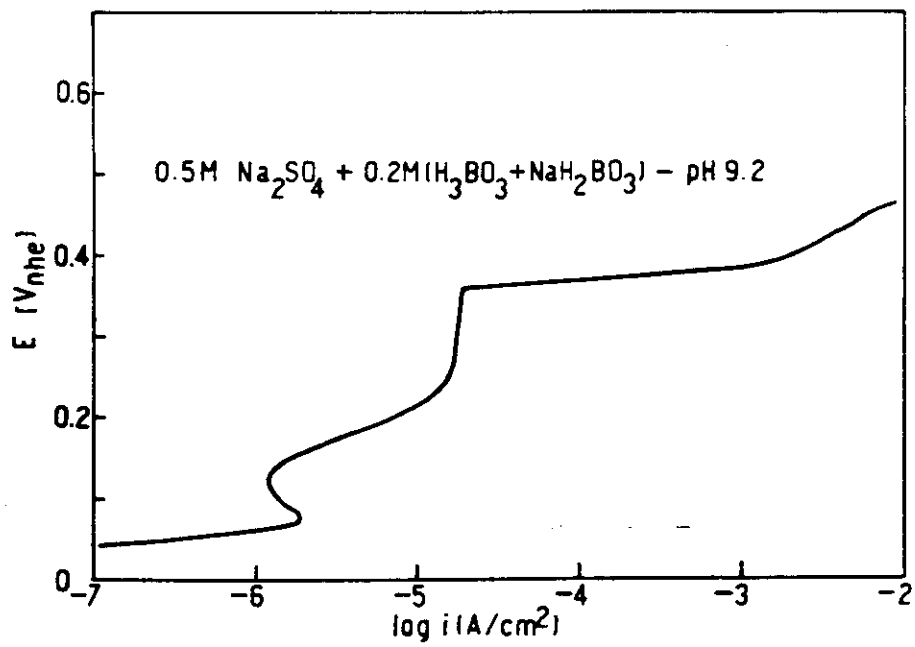

FIG. 6. Potentiodynamic polarization curve (0.2 mV s^{-1}) for brass in a 0.5 M Na_2SO_4 + 0.2 M (H_3BO_3 + NaH_2BO_3) solution at pH 9.2.

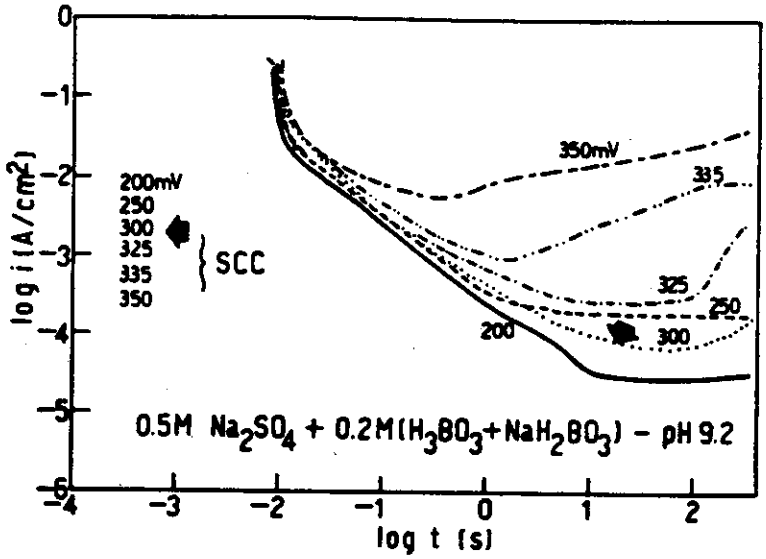

FIG. 7. Typical current–time repassivation curves for brass in a 0.5 M Na_2SO_4 + 0.2 M (H_3BO_3 + NaH_2BO_3) solution, pH 9.2, at various potential values. Exposure time: 400 s. The arrow shows the lowest potential at which SCC was found. No distinction can be made in the repassivation curves in potentials where SCC is found from those where no cracking was reported.

The curves at these potentials are similar in shape to those found for brass in diluted $NaNO_2$ solutions. Brass suffers transgranular SCC in a 0.5 M Na_2SO_4 + 0.2 M (H_3BO_3 + NaH_2BO_3), pH 9.2, solution at potentials equal to, or higher than, 0.300 V.[3]

Figure 8 shows the polarization curves for brass in Na_2S + Na_2SO_4 solutions. At potentials above the corrosion potential, a sharp current increase is observed, reaching a maximum of about 10^{-4} A cm^{-2}. The current density remains at this value, with small alterations, for a wide range of potentials. The pseudo-passive region was

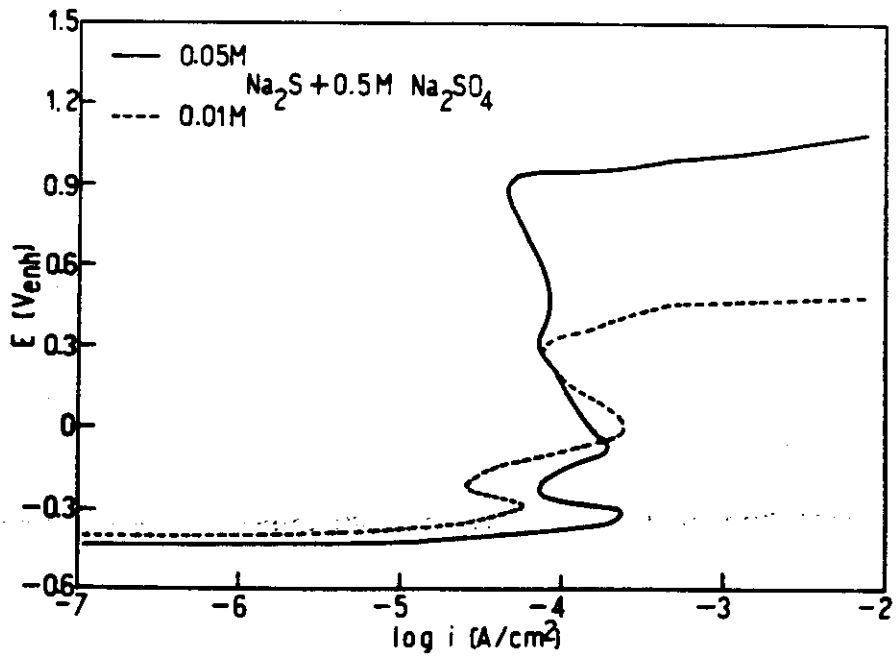

FIG. 8. Potentiodynamic polarization curves (0.2 mV s^{-1}) for brass in 0.05 M and 0.01 M Na_2S solutions with the addition of 0.5 M Na_2SO_4. The sulphide ions act as pitting inhibitors.

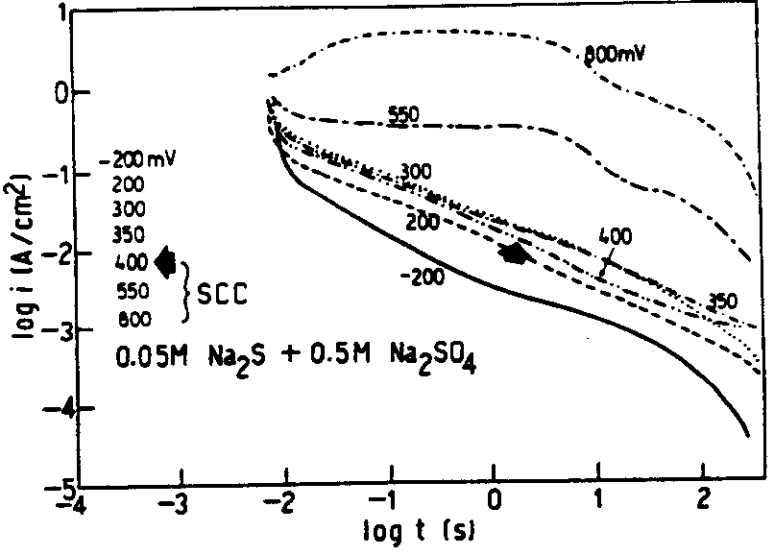

FIG. 9. Typical current–time repassivation curves for brass in a 0.05 M Na_2S + 0.5 M Na_2SO_4 solution at various potential values. Exposure time: 400 s. The arrow shows the lowest potential at which SCC was found. No distinction can be made in the repassivation curves in potentials where SCC is found from those where no cracking was reported.

wider in the solution with the higher Na_2S content. In a 0.05 M Na_2S + 0.5 M Na_2SO_4 solution the region of quasi-constant current density spanned over 1 V, while in the 0.01 M Na_2S + 0.5 M Na_2SO_4 solution it covered only 400 mV. At higher potentials a passivity breakdown process is found. Once passivity breakdown has taken place, the sample is covered by a thick layer of black corrosion products. This layer of corrosion products is loosely adherent and is easily removed by rinsing the samples with water. After removal of the corrosion products, the metal surface shows crystallographic pits. Most probably the passivity rupture is due to the sulphate ions and the sulphide ions are acting as pitting inhibitors, as expected from a weak acid salt.[16]

The repassivation transients measured in both sulphide-containing Na_2SO_4 solutions were similar. Figure 9 shows those for 0.05 M Na_2S + 0.5 M Na_2SO_4 solution. At low potentials a linear behaviour, with a slope of $b = -0.5$ is observed in both solutions. At higher potentials the current remains high during the first few seconds after straining, but shows a decreasing trend afterwards. In this case, the current decrease is most probably due not to a repassivation process, but to a mechanical shielding effect of the loose corrosion products accumulated on the metal surface. The potential at which the surface corrosion products start to accumulate is lower in the strained samples than that observed during the potentiokinetic polarization curves. As shown in Fig. 9, SCC of brass was found during slow strain rate experiments[3] only at potentials equal to or higher than 0.4 V. Figure 9 shows no difference between the repassivation rate of brass in this solution at 0.4 V, where SCC is found and the rate at lower potentials, where no SCC was observed.

DISCUSSION

As in Part I of this work,[10] the repassivation rate data were used to predict SCC velocities. These predictions are based on the assumption that the SCC mechanism is a film rupture process, where the repassivation rate plays a key role.[17–20]. In these

calculations the equations used by Ford[11] were applied. The crack propagation rate (CPR) is given by:

$$\text{CPR} = \frac{MQ_f}{\varrho F z t_f}; \quad t_f = \frac{\varepsilon_f}{v}. \tag{1}$$

M (64.20 g/mol) being the mean atomic weight of the alloy and ϱ(8.47 g cm^{-3}) its density. z (1.36) is the mean change in valence for the alloy leading to Cu_2O plus ZnO; F the Faraday constant; Q_f the charge density circulated during the time t_f; t_f being the periodicity of film rupture. This value is calculated from the strain at rupture ($\varepsilon = 0.001$) divided by the strain rate applied to the alloy (v). For the strain rates quoted in this discussion[3] (2×10^{-4} and 1.7×10^{-5} s^{-1}) the values for t_f were 5 s and 85.5 s respectively. The predicted crack velocity values, for brass in three different concentrations $NaNO_2$ solutions, and in a 0.5 M Na_2SO_4 + 0.2 M (H_3BO_3 + NaH_2BO_3), pH 9.2 solution, are shown in Figs 10–13. These values are compared with experimental crack velocities reported for the same solutions.[3,6,15] The crack velocities predicted by the charge integration technique are consistently lower than the experimentally measured values. It is worthwhile to note that, as a

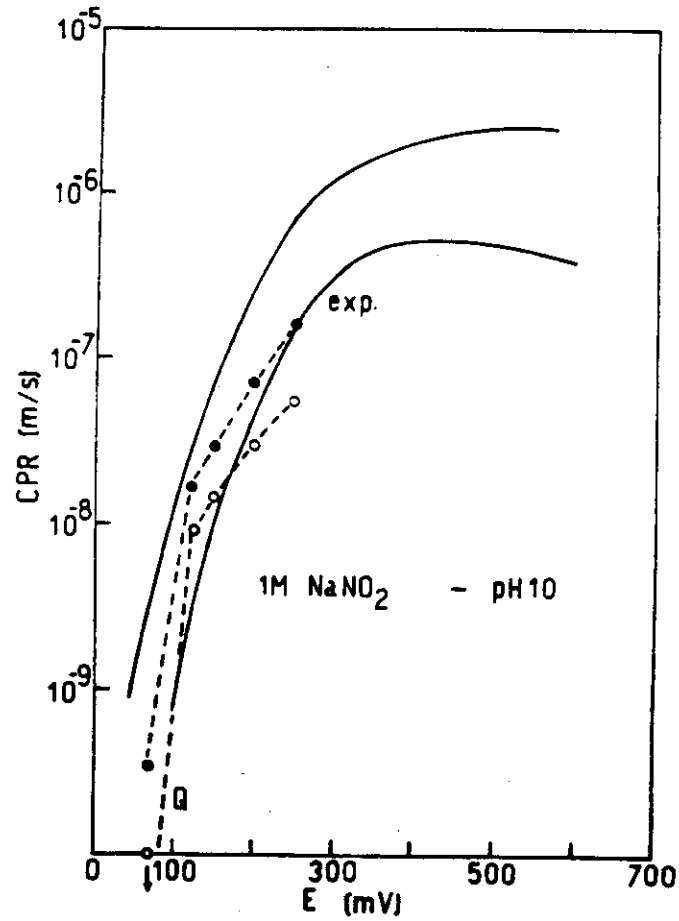

FIG. 10. Crack velocities (CPR) for brass in a 1 M $NaNO_2$ solution at various electrode potentials, at room temperature. - - - : Values predicted by the repassivation rate measurements, following the treatment introduced by Ford,[11] for different film rupture periodicities (t_f). ○: t_f = 58.8 s, ●: t_f = 5 s; ——: band of experimental values obtained for different strain rates by Alvarez *et al.*[6] In this case a reasonably good agreement is obtained at high potentials, while at low potentials the predictions give too low values.

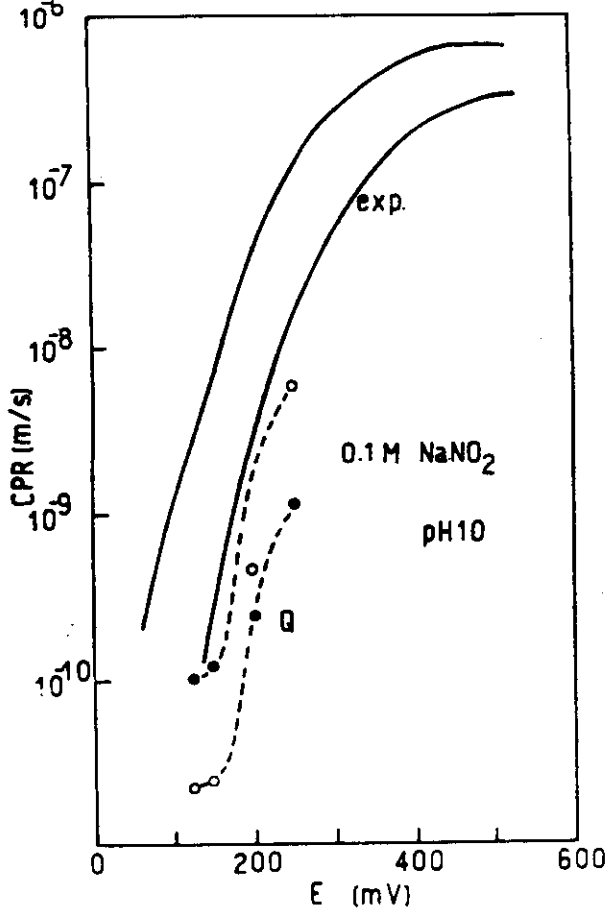

FIG. 11. Crack propagation rates (CPR) for brass in a 0.1 M $NaNO_2$ solution at various electrode potentials. - - -: Values predicted by the repassivation rate measurements following the treatment introduced by Ford,[11] for different film rupture periodicities (t_f). ○: t_f = 58.8 s, ●: t_f = 5 s; ——: band of experimental values obtained for different strain rates by Rebak *et al.*[15] The predicted values are lower than the experimental results.

predictive technique, the intermediate strain rate technique gives a better correlation between the predicted and the measured values.[6,15,21]

A detailed analysis of the repassivation curves for type 304 stainless steel in various solutions was reported in the first part of this work,[10] where, for the charge density values involved, the contribution of the charging of the double layer was shown to be negligible and the first monolayers of the passive film shown to be formed in the first ms after straining. As in the previous paper, it will be assumed that the current densities measured are due only to the anodic reaction of the alloy with the environment and that reactions like oxygen evolution or solution decomposition can be ignored.

Figures 14 to 17 show the decomposition of the repassivation curves, various anodic processes being taken into account. As reported in Part I, a slope $b = -1$ is expected when the film grows by a high field ion migration mechanism,[22-23] or by a place exchange mechanism.[24] Brass in 1 M $NaNO_2$ solutions at 0.070 V, Fig. 14, shows a slope of $b = -0.84$. This value could be misleading. The values of $b = -1$ found in the literature[23,25] show some scattering and $b = -0.84$ could fit inside this scattering. On the other hand, separate observations put some doubt on the existence of a very protective film on brass in a 1 M $NaNO_2$ solution, at 0.070 V, as

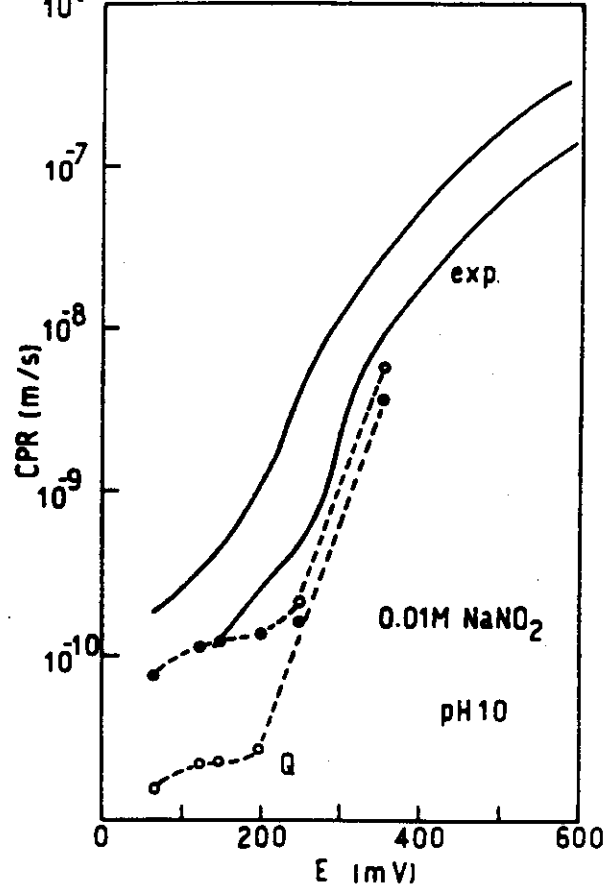

FIG. 12. Crack propagation rates for brass in a 0.01 M $NaNO_2$ solution at various electrode potentials. - - -: Values predicted by the repassivation rate measurements for different film rupture periodicities. ○: t_f = 58.8 s, ●: t_f = 5 s; ——: band of experimental values obtained for different strain rates by Rebak *et al.*[15] The predicted values are lower than the experimental results.

it should be expected from $b = -1$. If the samples are left for more than 24 h at 0.070 V, the surface of the metal shows incipient tarnishing, suggesting that a thick film has been formed. Most probably the repassivation curve observed at 0.070 V is an incipient stage of what is observed at higher potentials. Then it is believed that the curve at 0.070 V is not a scattered value of $b = -1$, but, due to an incipient process of passivity breakdown, it is a mixture of slopes $b = -1$ plus slopes $b = -0.5$.

At 0.125 V (Fig. 14), the repassivation curve has a shape found to be typical of all the measurements made in $NaNO_2$ containing solutions (Figs 14–16). A short region of $b = -1$ is followed by a diffusion controlled mechanism, $b = -0.5$,[26,27] probably due to a dissolution and precipitation film formation process.[10] Then a current increase is found, with $b = 1$, due either to the nucleation of a new phase[28] or to the nucleation of pits.[29] This last alternative seems to be the most probable, since pits are observed, under the scanning electron microscope, on the corroded samples. The soluble salts, produced inside the pits, are hydrolysed and the precipitation of oxides or hydroxides leads to the occlusion of the pits and to a reduction in the measured current. This current decrease, due to accumulation of corrosion products on the pits, was reported by Alvarez and Galvele[30] for repassivation after scratching of zinc above the pitting potential.

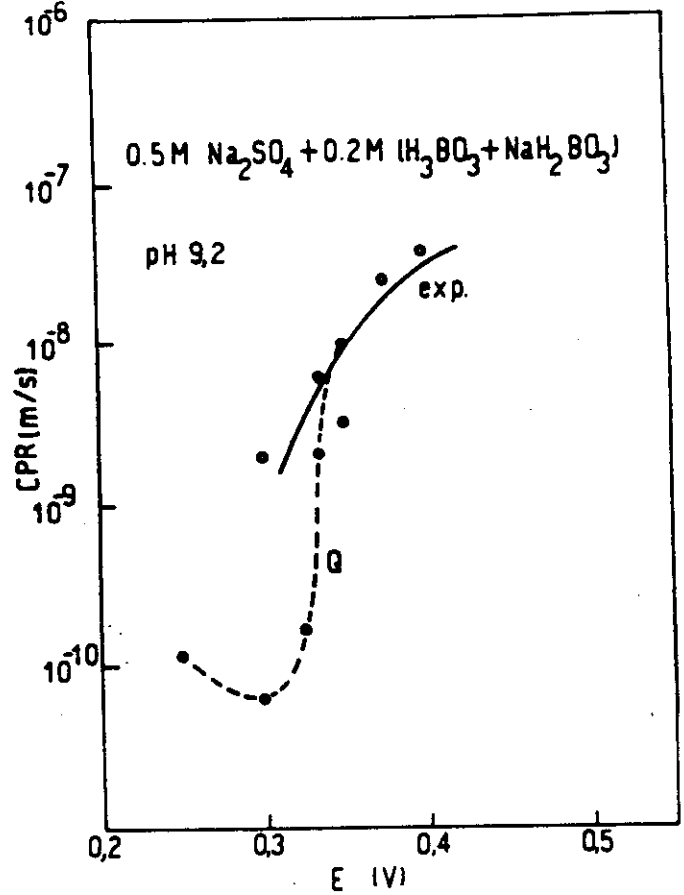

FIG. 13. Crack propagation rates for brass in a 0.5 M Na_2SO_4 + 0.2 M (H_3BO_3 + NaH_2BO_3) solution at various electrode potentials. - - -: Values predicted by the repassivation rate measurements. t_f = 58.8 s; ——: experimental values obtained at 1.7×10^{-5} s^{-1} by Alvarez *et al.*[3] The predicted values are lower than the experimental ones.

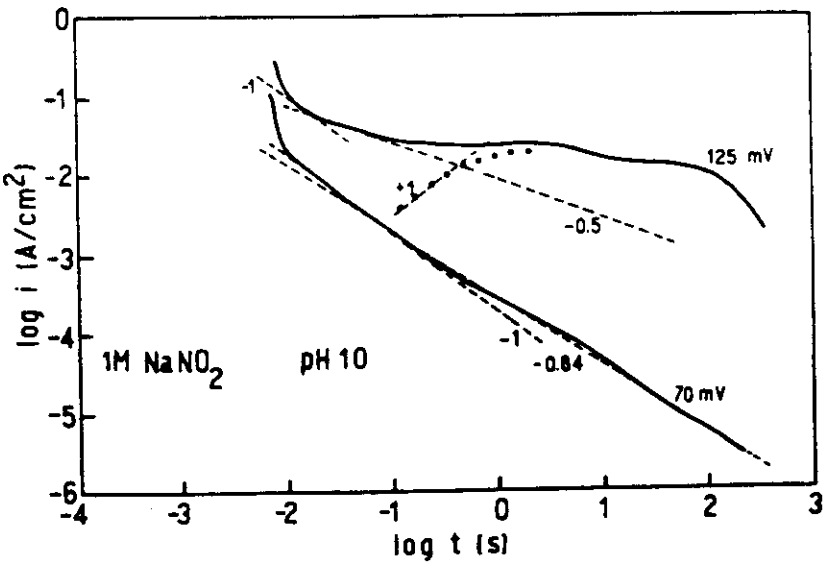

FIG. 14. Analysis of the log i–log t repassivation curves. Brass in a 1 M $NaNO_2$ solution at 70 and 125 mV(NHE). 70 mV: it is believed that the −0.84 slope is a mixture of slopes −1 plus slopes −0.5; 125 mV: an initial part of high field film growth mechanism ($b = -1$) followed by a mechanism of the type $i = At^{-1/2}$ most probably due to a dissolution and precipitation film formation process. At longer exposures a process of the type $i = At^{+1}$, attributed to pitting, is observed. The ulterior decrease in current is due to accumulation of corrosion products on pits.

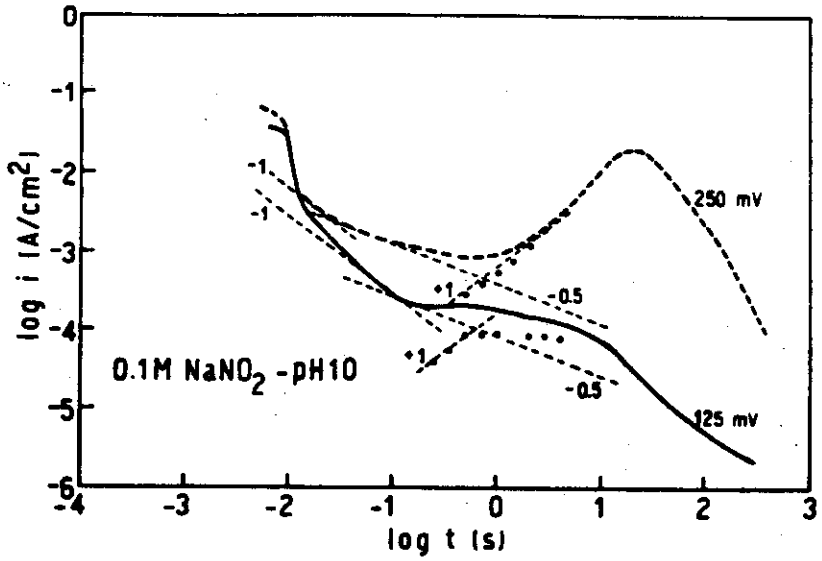

FIG. 15. Analysis of the log i–log t repassivation curves. Brass in a 0.1 M $NaNO_2$ solution at 125 and 250 mV(NHE). As in Fig. 14, a sequence of high field film growth mechanism is followed by a dissolution and precipitation film growth mechanism, and finally a pitting process is observed, with an appreciable accumulation of corrosion products on pits.

The same decomposition of the repassivation curves was done for 0.1 M $NaNO_2$ (Fig. 15); 0.01 M $NaNO_2$ (Fig. 16); 1 M $NaNO_2$ + 0.5 M Na_2SO_4; and 0.1 M $NaNO_2$ + 0.5 M Na_2SO_4 solutions. As with the 1 M $NaNO_2$ solution, an initial stage of $b = -1$ was observed (attributed to the growth of a thin, homogeneous and protective film). This stage was usually short and was replaced by a slope of $b = -0.5$ (diffusion controlled film growth). After an exposure of about 1 s, positive slopes with b values of 0.5, 1 or 2, due both to the nucleation and growth of pits, were observed. The pitting process was confirmed by the presence of pits under the

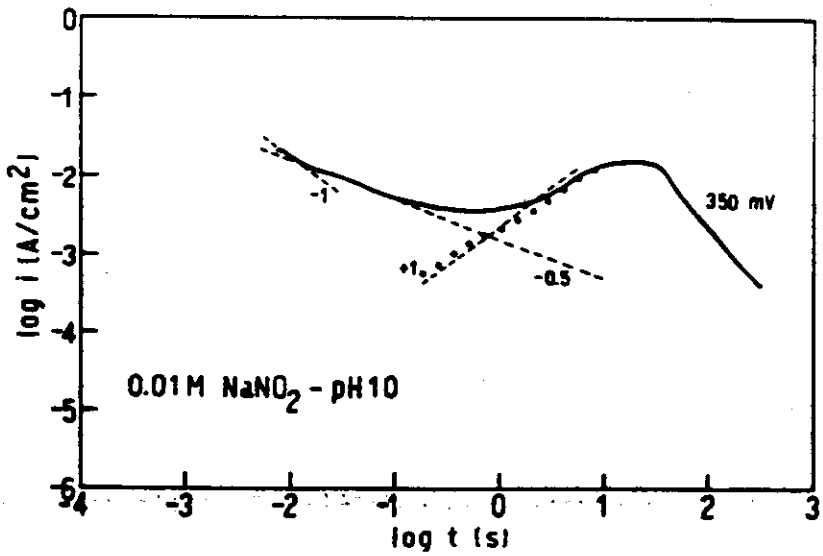

FIG. 16. Analysis of the log i–log t repassivation curves. Brass in a 0.01 M $NaNO_2$ solution at 350 mV(NHE). As in Fig. 14, a sequence of high field film growth followed by a dissolution–precipitation film growth and by pitting with accumulation of corrosion products on pits, is observed.

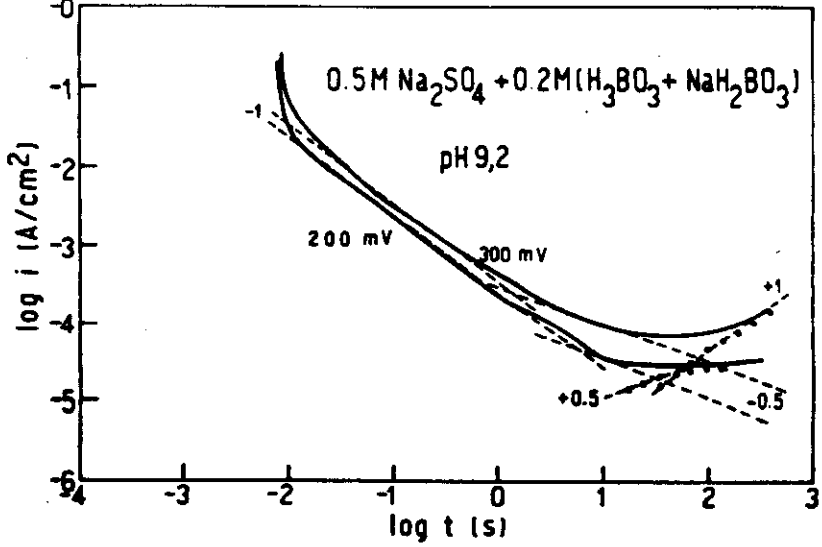

FIG. 17. Analysis of the log i–log t repassivation curves. Brass in a 0.5 M Na_2SO_4 + 0.2 M (H_3BO_3 + NaH_2BO_3) solution at 200 and 300 mV(NHE). An extended region of $b = -1$ is observed, followed by a dissolution precipitation mechanism and by pitting ($b = +1$ or $+0.5$). For 200 mV the inflection observed is probably not related with any passivity breakdown process because the final current density is close to the steady state value.

scanning electron microscope. For long exposures a current decrease due to the occlusion of pits was detectable.

The region with slope $b = -1$ for brass in 0.5 M Na_2SO_4 + 0.2 M (H_3BO_3 + NaH_2BO_3), pH 9.2 solution (Fig. 17) is more extended than that found in $NaNO_2$ containing solutions. With this solution, again regions with slopes $b = -0.5$ and positive values of 0.5, 1 or 2, are found. The decomposition of the curve for 0.200 V should be taken with caution. The current density value at which the transition from $b = -1$ to $b = -0.5$ takes place, is very low. The current density at this point, 10^{-5} Acm^{-2}, is very close to the steady state current density of brass before straining and most probably the inflection observed in the repassivation curve is not related to any passivity breakdown process. No cracking was found in brass at this potential.[3] In this solution cracking was reported only for potentials equal to, or higher than, 0.300 V. In the repassivation curves at potentials where SCC was detected, a transition from $b = -1$ to $b = -0.5$ was clearly detectable.

Slow strain rate experiments with brass in a 0.05 M Na_2S + 0.5 M Na_2SO_4 solution,[3] showed that stress corrosion cracking appears only at potentials equal to, or higher than, 0.400 V. No cracking was found at lower potentials. The repassivation curves show a slope very close to $b = -0.5$, indicating a diffusion-controlled process. No distinction can be made between the repassivation curves in potentials where SCC is found and those where no cracking is reported.

Most of the repassivation curves analysed in this paper had regions with a slope $b = -0.5$. This slope indicates a diffusion-controlled film growth process. As it was the case with stainless steel, in Part I of this work,[10] an approximate estimation of the diffusion coefficient was made. The diffusion coefficient values were again found to be too high to assume diffusion through a solid phase and the process was concluded to be controlled by diffusion in a liquid phase, in the film pores. As in the case of stainless steels, the film grows when $b = -0.5$, by a dissolution and precipitation

mechanism[27] by ions diffusing in the solution inside the pores of the film, at constant potential.

CONCLUSIONS

Repassivation rate measurements on austenitic stainless steels, as shown in the first part of this work,[10] or on brass, as shown in the present work, indicated that whenever SCC was found, regions of slow repassivation rate, $b = -0.5$, were detected. Fast repassivation rates, as indicated by $b = -1$, were usually associated with immunity to SCC. On the other hand, the presence of regions of slow repassivation did not prove to be sufficient condition for SCC, since it was observed in several cases where no SCC was detected by slow strain rate techniques. It is then concluded that a slow repassivation rate, as given by $b = -0.5$, seems to be a necessary, but not a sufficient electrochemical condition for stress corrosion cracking susceptibility. A SCC mechanism that takes into account this alternative has been recently published.[31] It is also concluded that the use of repassivation rate techniques for predicting SCC susceptibility is unsafe. the crack velocities predicted by those techniques, for both stainless steel and brass, where considerably lower than the measured crack velocities. On the other hand, the repassivation rate techniques predict crack velocities even under good passivity conditions, where no SCC is found, and arbitrary limits for minimum crack velocities have to be introduced. This limitation is shared with other electrochemical techniques that indirectly use the repassivation rate of the metal, such as the intermediate strain rate technique,[21] or the potential scanning technique.[32]

Acknowledgements—The present research has been supported by the Programa Latinoamericano de Lucha Contra la Corrosión, OEA-CNEA and by the Consejo Nacional de Investigaciones Científicas y Técnicas, Argentina.

REFERENCES

1. A. Kawashima, A. K. Agrawal and R. W. Staehle, in *Stress Corrosion Cracking—The Slow Strain Rate Technique* (eds G. M. Ugiansky and J. H. Payer), p. 266. American Society for Testing Materials, Philadelphia (1979).
2. S. Shiga and M. Hoshino, in *Conf. on Environmental Degradation of Engineering Materials in Aggressive Environments*, p. 201. Blacksburg, Va (1981).
3. M. G. Alvarez, C. Manfredi, M. Giordano and J. R. Galvele; to be published.
4. R. C. Newman and G. T. Burstein, *J. Electrochem. Soc.* **127**, 2527 (1980)
5. V. K. Gouda, S. M. Sayed and H. A. El-Sayed, in *Proc. 9th Cong. on Met. Corr.* Vol. I, p. 121. National Research Council, Toronto, Canada (1984).
6. M. G. Alvarez, C. Manfredi, M. Giordano and J. R. Galvele, *Corros. Sci.* **24**, 769 (1984).
7. S. P. Pednekar, A. K. Agrawal, H. E. Chaung and R. W. Staehle, *J. Electrochem. Soc.* **126**, 701 (1979).
8. R. C. Newman and G. T. Burstein, *Corros. Sci.* **21**, 119 (1981).
9. E. N. Pugh, in *The Theory of Stress Corrosion Cracking in Alloys* (ed. J. C. Scully), p. 418. NATO Scientific Affairs, Brussels (1971).
10. R. M. Carranza and J. R. Galvele, *Corros. Sci.* **28**, 233 (1988).
11. F. P. Ford, Mechanisms of environmental cracking in systems peculiar to power generation industry, EPRI NP-2589, RP1332-1, Final Report (1982).
12. D. Gilroy and J. E. Mayne, *J. appl. Chem.* **12**, 382 (1962).
13. J. R. Galvele, S. M. de De Micheli, I. L. Muller, S. B. de Wexler and I. L. Alanis, in *Localized Corrosion* (eds R. W. Staehle, B. F. Brown, J. Kruger and A. Agrawal), p. 580. National Association of Corrosion Engineers, Houston, TX (1974).

14. M. POURBAIX, Atlas of Electrochemical Equilibria in Aqueous Solutions, p. 86. Pergamon Press, London (1966).
15. R. B. REBAK, R. M. CARRANZA and J. R. GALVELE; to be published.
16. J. R. GALVELE, *J. Electrochem. Soc.* **123**, 464 (1976).
17. R. W. STAEHLE, in *The Theory of Stress Corrosion Cracking in Alloys* (ed. J. C. SCULLY), p. 223. NATO Scientific Affairs, Brussels (1971).
18. J. C. SCULLY, *Corros. Sci.* **7**, 197 (1967).
19. D. A. VERMILYEA, *J. Electrochem. Soc.* **149**, 405 (1972).
20. T. R. BECK, *Corrosion* **30**, 408 (1974).
21. J. R. GALVELE, in *Predictive Capabilities in Environmentally Assisted Cracking* (ed. R. RUNGTA) p. 273. The American Society of Mechanical Engineers, New York (1985).
22. N. CABRERA and N. F. MOTT, *Rep. Progr. Phys.* **12**, 163 (1949).
23. T. R. BECK, *J. Electrochem. Soc.* **129**, 2500 (1982).
24. N. SATO and M. COHEN, *J. Electrochem. Soc.* **111**, 512 (1964).
25. P. I. MARSHALL and G. T. BURSTEIN, *Corros. Sci.* **23**, 1219 (1983).
26. A. T. FROMHOLD, Jr, *Theory of Metal Oxidation, Vol. I Fundamentals—Series Defects in Crystalline Solids*, (eds S. AMELINCKX, R. GERVERS and J. NIHOUL). Vol. 9. North-Holland Publishing Co., New York (1976).
27. T. E. EVANS, in *Passivity of Metals* (eds R. P. FRANKENTHAL and J. KRUGER), p. 410. The Electrochem. Soc. Inc., New Jersey (1978).
28. M. FLEISCHMAN and H. R. THIRSK, *Adv. Electrochem. Eng* (ed. P. DELAHAY) Chapter 3, p. 123. John Wiley & Sons, New York (1963).
29. S. SZKLARSKA-SMIALOWSKA, in *Localized Corrosion* (eds R. W. STAEHLE, B. F. BROWN, J. KRUGER and A. AGRAWAL), p. 312. National Association of Corrosion Engineers, Houston (1974).
30. M. G. ALVAREZ and J. R. GALVELE, *Corrosion* **32**, 285 (1976).
31. J. R. GALVELE, *Corros. Sci.* **27**, 1 (1987).
32. R. N. PARKINS, *Corros. Sci.* **20**, 147 (1980).

STRESS CORROSION CRACKING OF α-BRASS IN PHOSPHATE, TRIPHOSPHATE AND PYROPHOSPHATE SOLUTIONS

R. B. REBAK* and J. R. GALVELE

Comisión Nacional de Energía Atómica, Departamento Materiales, Avda. Libertador 8250, Buenos Aires 1429, Argentina

Abstract—The constant potential slow strain rate technique was used to study the susceptibility of α-brass to stress corrosion cracking (SCC) in phosphate, triphosphate and pyrophosphate solutions. α-Brass was found to be immune to SCC in alkaline Na_2HPO_4 solutions, but susceptible to SCC in alkaline $Na_4P_2O_7$ and $Na_5P_3O_{10}$ solutions. Only intergranular cracking was observed. The presence of Cu^{2+} ions in the corrosive environment expanded the range of electrode potentials where SCC was found. At constant potential, the presence of Cu^{2+} ions had no effect on crack velocity. The Cu^{2+} ions acted by reducing the IR drop in the crack, thus allowing for higher electrode potentials at the tip of the crack. The present results fit better into a surface-mobility SCC mechanism than into an anodic dissolution mechanism.

INTRODUCTION

ALPHA-BRASS is susceptible to stress corrosion cracking (SCC) in a wide range of corrosive environments. The degree of aggressivity, from the SCC point of view, is well documented for nitrite solutions,[1-3] and for ammoniacal solutions.[4-6] Brass has also been reported to show SCC in the following aqueous solutions: alkalis,[7-8] pyrophosphates,[7] acetates,[8] formiates,[8] carbonates,[7-8] citrates,[8] tartrates,[8] nitrates,[7-9] acid sulphates,[10] chlorates[11] etc.

The case of phosphate derivative solutions is of interest, because of the scarcity of information. Bobylev[7] reported SCC of brass in pyrophosphates, as confirmed by Shiga and Hoshino,[12] who also reported SCC in tripolyphosphates. Kawashima *et al.*[9] on the other hand, reported that α-brass was immune to SCC in orthophosphate solutions. All these measurements were made either at an open circuit potential, or, as it was the case with orthophosphate solutions, at a single potential value. For a better understanding of the SCC mechanism of brass in these solutions, it would be useful to have information on the rate of crack propagation, the function of the electrode potential, and the morphology of the cracks.

The purpose of the present work is to make a comparative study of SCC of α-brass in the three following environments: sodium triphosphate solutions, sodium pyrophosphate solutions, and sodium orthophosphate solutions. In the first two solutions stable complexes with Cu^{2+} ions are formed,[13] while in the third one insoluble compounds are formed with the same cation.[14]

The most relevant reactions between the environment and copper ions are the following, for the above-mentioned solutions[13] (see Table 1).

* On leave from the Universidad Nacional de Misiones, Facultad de Ciencias Exactas, Químicas y Naturales.

Manuscript received 10 July 1988.

83

TABLE 1. REACTIONS OF COPPER IONS

H_3PO_4 Hydrogen phosphate (phosphoric acid) H_3L

Metal ion	Equilibrium	Log K	
H^+	$HL/H.L$	10.79	(1)
	$H_2L/HL.H$	6.46	(2)
Cu^{2+}	$MHL/M.HL$	3.3	(3)
	$MH_2L/M.H_2L$	1.3	(4)

$H_4P_2O_7$ Hydrogen diphosphate (pyrophosphoric acid) H_4L

Metal ion	Equilibrium	Log K	
H^+	$HL/H.L$	7.43	(5)
	$H_2L/HL.H$	5.41	(6)
Cu^{2+}	$ML/M.L$	7.6	(7)
	$ML_2/M.L^{2}$	12.45	(8)

$H_5P_3O_{10}$ Hydrogen triphosphate (triphosphoric acid) H_5L

Metal ion	Equilibrium	Log K	
H^+	$HL/H.L$	8.61	(9)
	$H_2L/HL.H$	5.69	(10)
Cu^{2+}	$ML/M.L$	9.36	(11)

Constant potential slow strain rate tests confirmed that brass shows intergranular SCC in pH 10 triphosphate and pH 10 pyrophosphate solutions, while no cracking was found, at the same pH values, in orthophosphate solutions. The presence of dissolved Cu^{2+} ions in the media enhanced the SCC process, and the results were analysed from the point of view of the surface mobility SCC mechanism.[15]

EXPERIMENTAL METHOD

The polarization curve measurements and most of the constant potential slow strain rate tests (SSRT) were performed on 0.08 cm diameter wires, and in de-aerated solutions. The chemical composition of the wires was (in weight percent): 63.3% Cu; 0.02% Pb; <0.005% As; 0.005% Al; 0.003% Sn; 0.007% P; <0.01% Fe; 0.0003% Mg; 0.01% Ni; 0.001% Ag; 0.005% Si; balance Zn. A few SSRT were performed with 0.3 cm diameter, 1.5 cm length, cylindrical tensile test samples in non-de-aerated solutions. The composition of these samples was: 61.7% Cu; <0.002% Al; 0.005% Pb; <0.002% Si; <0.002% Cr; 0.02% Fe; 0.02% Ni; <0.05% Ca; <0.0005% Mn; <0.005% Ti; <0.02% V; <0.0002% Mg; 0.005% Ag and balance Zn. No significant differences were found between the results on the wire samples and those on the cylindrical test samples.

All the samples were degreased with acetone, vacuum annealed for 24 h at 450°C, and water-quenched. Prior to the experiments, the samples were chemically polished in 55% (in volume) phosphoric acid plus 20% nitric acid plus 25% acetic acid, washed with water, rinsed with alcohol and dried in hot air.

The strain rate used in the SSRT was 2×10^{-6} s^{-1}, and the measurements were made at room temperature (approx. 21°C).

All the measurements were made under potentiostatic control, and the potential was controlled either with a Wenking ST 72 or a LYP M5 potentiostat. The measurements were made in conventional glass three-electrode cells, with a capacity of 80 cm^3. The potentials were measured through a Luggin capillary, with a mercurous sulphate reference electrode, and are reported in the normal hydrogen electrode (NHE) scale. The de-aeration of the solutions was done with nitrogen, prepurified by the Gilroy and Mayne technique.[16]

The solutions were prepared with distilled water and Reagent Grade chemicals from Alfa Products. Due to solubility limitations, the concentration of the solutions used was 0.2 M. When necessary, the pH of the solution was increased by addition of a concentrated NaOH solution. The pH chosen was high enough to obtain maximum complex stability of the Cu^{2+} ions, as expected from equations (5), (7) and (8) for diphosphate solutions and from equations (9) and (11) for triphosphate solutions.

The solutions used were: 0.2 M Na_2HPO_4, pH 10.5; 0.2 M Na_2HPO_4 + 0.05 M $CuSO_4$, pH 10.6; 0.2 M $Na_4P_2O_7$, pH 10.1; 0.2 M $Na_4P_2O_7$ + 0.05 M $CuSO_4$, pH 10.1; 0.2 M $Na_4P_2O_7$ + 0.1 M $CuSO_4$, pH 10.0; 0.2 M $Na_5P_3O_{10}$, pH 10.0; 0.20 M $Na_5P_3O_{10}$ + 0.05 M $CuSO_4$, pH 9.0.

After fracture, the corroded samples were observed under a Philips SEM 500 scanning electron microscope. Afterwards the samples were mounted for metallographic sectioning, the length of the longest crack was measured, and from the straining time a mean crack velocity (V_p) was calculated.

Polarization curves were measured on the wire samples, in a conventional three-electrode glass cell, with an 80 cm^3 capacity. In this case the solutions were de-aerated, and the temperature was kept at 25°C with a Haake F3S thermostat. Quasi-potentiostatic curves were obtained by changing the potential in 20 mV steps, and recording the current after a 2 min exposure to each potential.

EXPERIMENTAL RESULTS

Polarization curves

Figure 1 shows typical quasi-stationary polarization curves for α-brass in the following solutions: 0.2 M Na_2HPO_4 (pH 10.5), 0.2 M Na_4P_2O- (pH 10.1) and 0.2 M $Na_5P_3O_{10}$ (pH 10.0). Typical corrosion potentials (E_c) in the same solutions are also shown in Fig. 1. E_c increased with the molecular weight of the solution anion, the values found being: −0.150 V(NHE) in the Na_2HPO_4 solution, −0.105 V(NHE) in the Na_4P_2O- solution, and −0.075 V(NHE) in the $Na_5P_3O_{10}$ solution. When the potential was increased above E_c, the current density showed a sharp increase, reaching a constant value some 200 mV above the corrosion potential. The value at which the current density was stabilized was clearly related to the solubility of the copper compounds formed on the metal surface. In the case of a Na_2HPO_4 solution, where insoluble $Cu_3(PO_4)_2 \cdot 3H_2O$ was probably formed, the maximum current density found was around 2×10^{-5} A cm^{-2}. While both in Na_4P_2O- and in $Na_5P_3O_{10}$ solutions, where soluble cupric complexes were formed, the limiting current densities were, respectively, 5 and 2.5×10^{-3} A cm^{-2}.

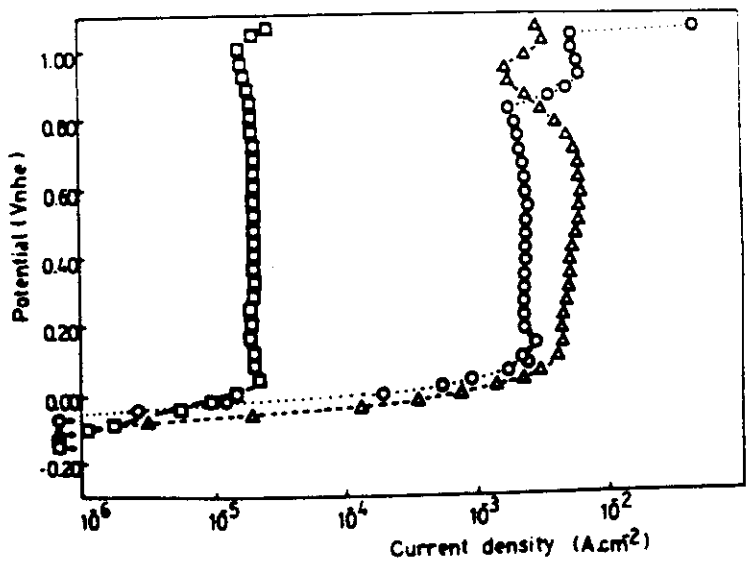

FIG. 1. Typical quasi-stationary anodic polarization curves for α-brass in the following de-aerated solutions: □ 0.2 M Na_2HPO_4, pH 10.5; △ 0.2 M $Na_4P_2O_7$, pH 10.1; and ○ 0.2 M $Na_5P_3O_{10}$, pH 10.0; at 25°C. Symbols with arrows: corrosion potential values.

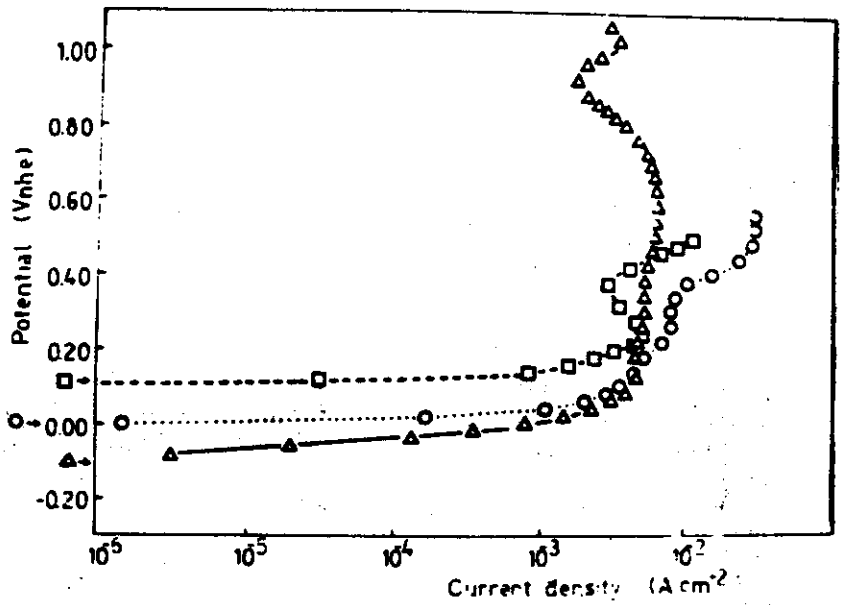

FIG. 2. Effect of dissolved Cu^{2+} ions on the anodic polarization curves of α-brass in de-aerated pyrophosphate solutions at 25°C. △ 0.2 M Na_4P_2O-, pH 10.1; ○ 0.2 M Na_4P_2O- + 0.05 M $CuSO_4$, pH 10.1; □ 0.2 M Na_4P_2O- + 0.1 M $CuSO_4$, pH 10.0. Symbols with arrows: corrosion potential values.

Figures 2 and 3 show the effect of cupric ions on the polarization curves of brass in the above mentioned solutions. As shown in Fig. 2, the addition of 0.05 M $CuSO_4$ to a pH 10.1, 0.2 M, Na_4P_2O- solution shifted the value of the corrosion potential from −0.105 V(NHE) up to 0.000 V(NHE); and if the $CuSO_4$ concentration was increased to 0.1 M, the corrosion potential increased to 0.110 V(NHE). During the quasi-potentiostatic polarization curve measurements, in both solutions, the current showed a sharp increase and it reached values above 10^{-3} A cm^{-2} at potentials only 40 mV above the corrosion potential. The surface of the samples showed severe corrosion (Fig. 4). The samples were covered with brown corrosion products which, at higher potentials, turned into a white jelly-like corrosion product.

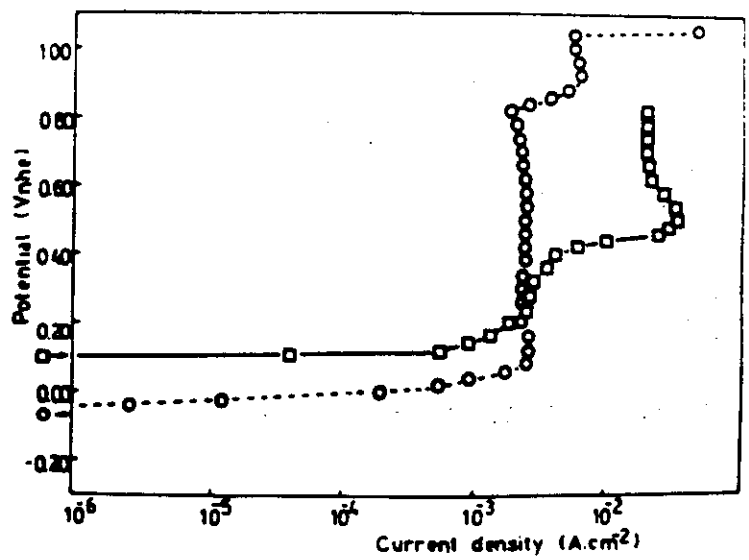

FIG. 3. Effect of dissolved Cu^{2+} ions on the anodic polarization curves of α-brass in de-aerated triphosphate solutions at 25°C. ○ 0.2 M $Na_5P_3O_{10}$, pH 10.0; □ 0.2 M $Na_5P_3O_{10}$ + 0.05 M $CuSO_4$, pH 9.0. Symbols with arrows: corrosion potential values.

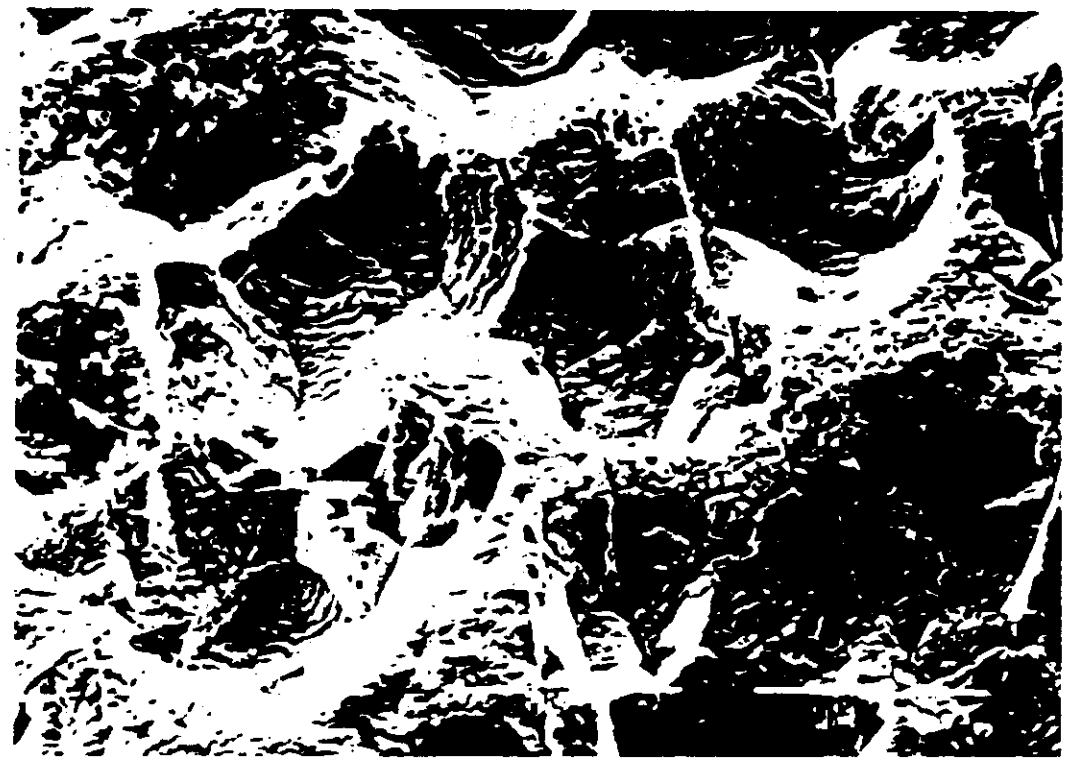

FIG. 4. Corroded brass surface, at the end of a polarization curve measurement in a 0.2 M $Na_4P_2O_7$ + 0.05 M $CuSO_4$, pH 10.1, solution. Dashes: 10 μm.

FIG. 7. Stress corrosion cracks on a passive surface. α-Brass strained in a 0.2 M $Na_4P_2O_7$ solution, pH 10.1. Potential: −0.100 V(NHE). Strain rate: 2×10^{-6} s^{-1}. Exposure time: 43 h 10 min. Dashes: 10 μm.

FIG. 8. Stress corrosion cracking plus generalized dissolution. α-Brass strained in a 0.2 M $Na_4P_2O_7$ solution, pH 10.0. Potential: 0.100 V(NHE). Strain rate: 2×10^{-6} s^{-1}. Exposure time: 45 h 30 min. Dashes: 10 μm.

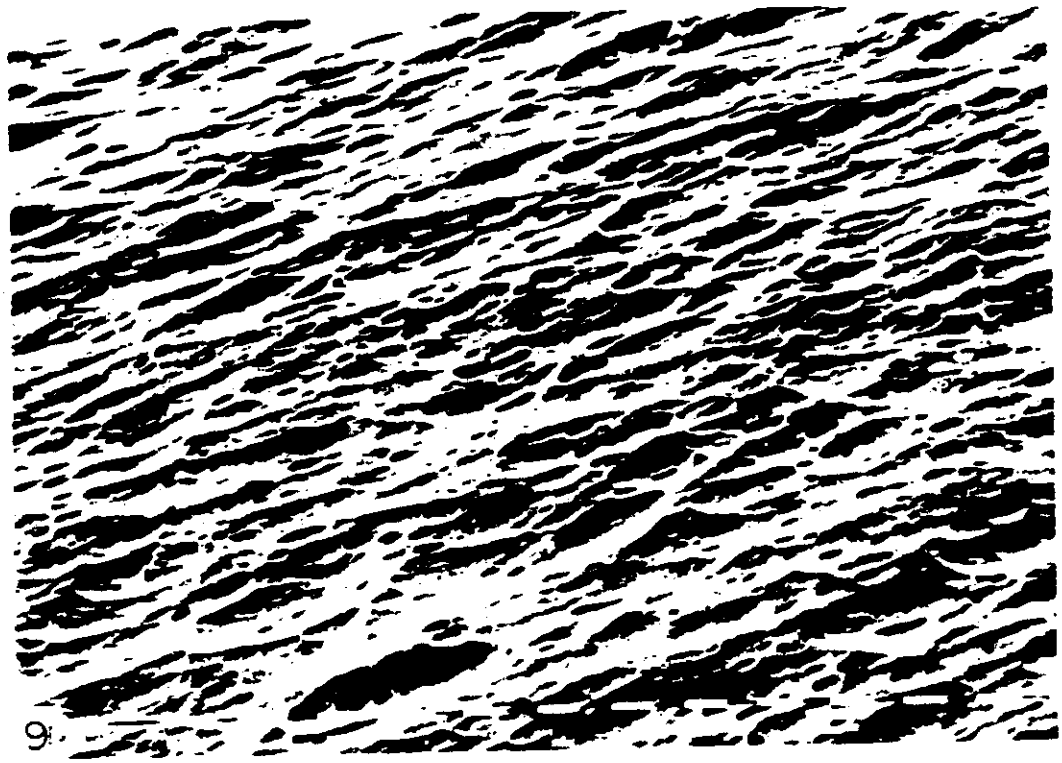

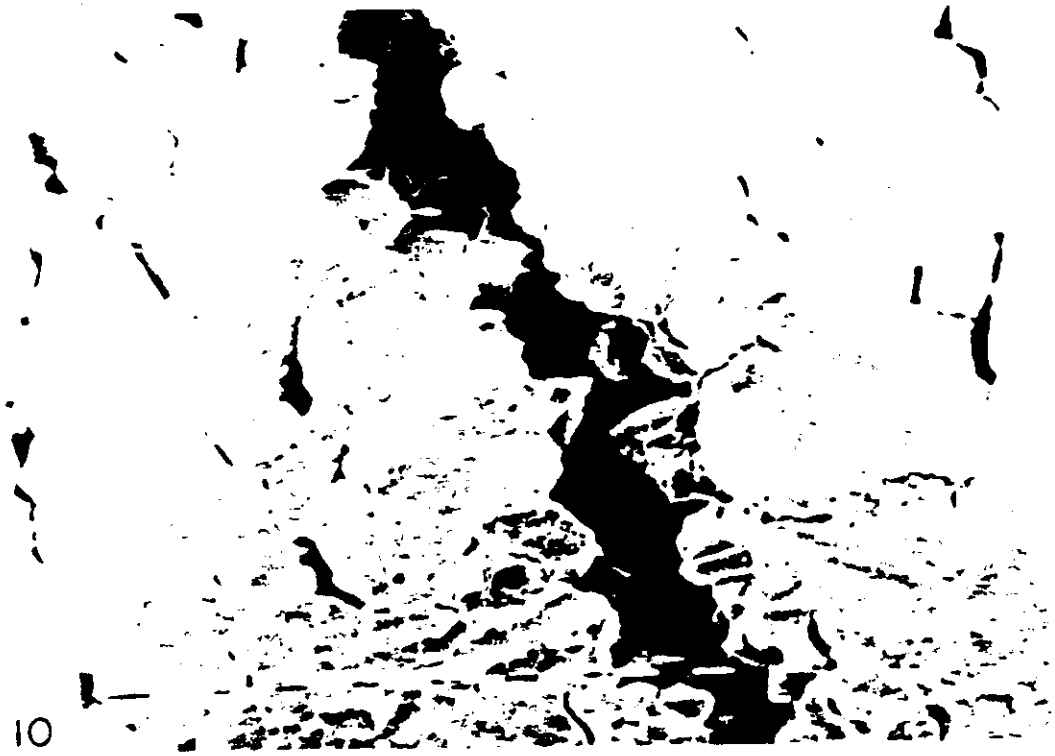

FIG. 9. Generalized corrosion on an α-brass sample strained at 0.200 V(NHE), in a 0.2 M $Na_4P_2O_7$, pH 10.1, solution. Strain rate: 2×10^{-6} s^{-1}. Exposure time: 42 h 24 min. Dashes: 10 μm.

FIG. 10. Intergranular stress corrosion cracking plus copper electrodeposition on an α-brass sample strained at 0.000 V(NHE) in a 0.2 M $Na_4P_2O_7$ + 0.05 M $CuSO_4$ solution, pH 10.1. Strain rate: 2×10^{-6} s^{-1}. Exposure time: 46 h 30 min. Dashes: 10 μm.

FIG. 12. Expansion of the SCC range due to the increase in the Cu^{2+} ion concentration. Intergranular stress corrosion cracking plus copper electrodeposition on an α-brass sample strained at 0.080 V(NHE) in a 0.2 M $Na_4P_2O_7$ + 0.1 M $CuSO_4$ solution, pH 10.0. Strain rate: 2×10^{-6} s^{-1}. Exposure time: 22 h 30 min. Dashes: 100 μm.

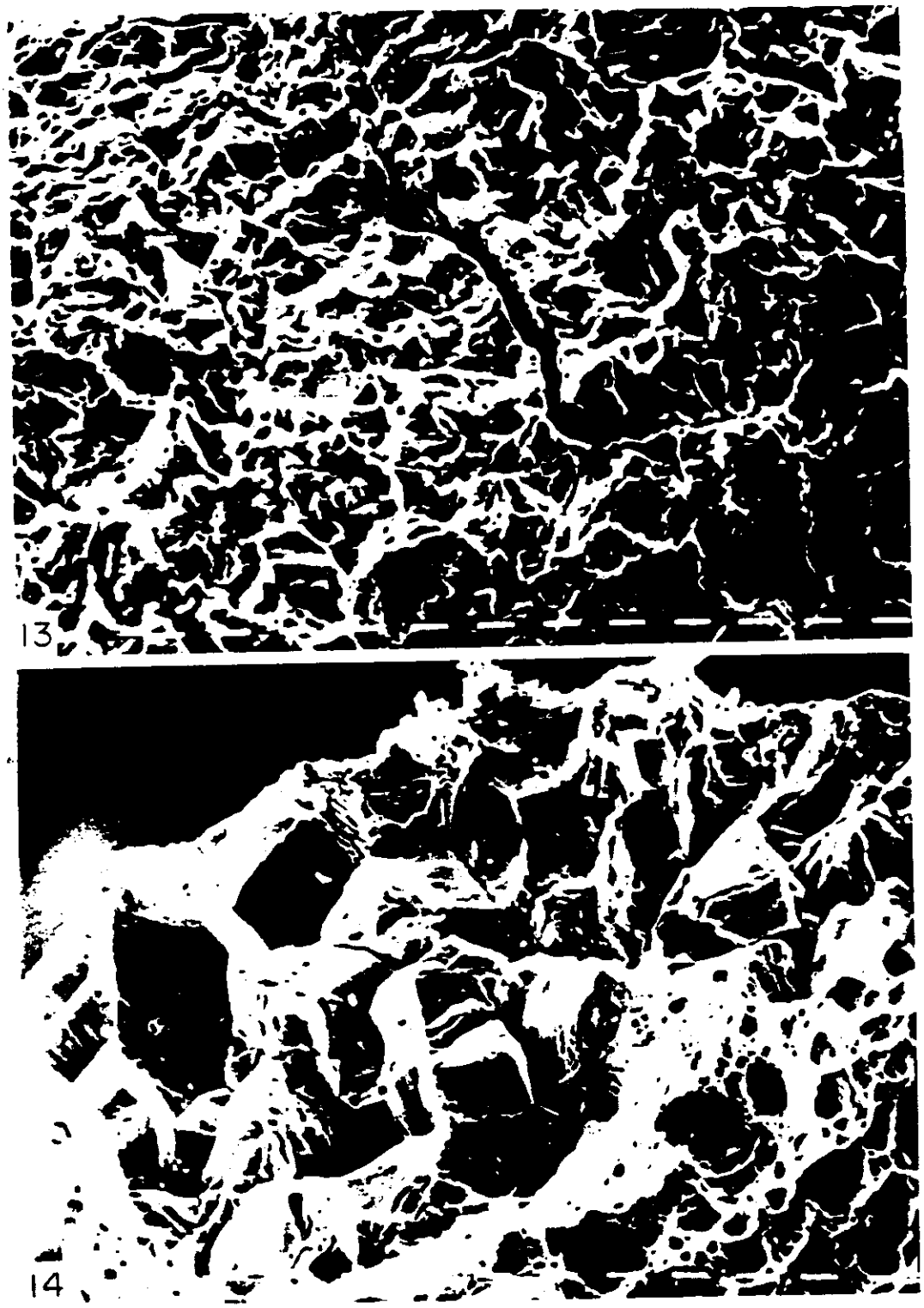

FIG. 13. Generalized dissolution plus cracking on a brass wire sample strained in a 0.2 M $Na_4P_2O_7$ + 0.1 M $CuSO_4$, pH 10.0, solution at 0.200 V(NHE). Strain rate: 2×10^{-6} s^{-1}. Exposure time: 14 h 20 min. Dashes: 10 μm.

FIG. 14. Fracture surface of an α-brass wire strained in a 0.2 M $Na_4P_2O_7$ + 0.1 M $CuSO_4$, pH 10.0, solution at 0.080 V(NHE). Strain rate: 2×10^{-6} s^{-1}. Exposure time: 22 h 30 min. Dashes: 10 μm.

When 0.05 M $CuSO_4$ was added to a 0.2 M $Na_5P_3O_{10}$ solution (Fig. 3) the corrosion potential of brass increased from −0.075 V(NHE) to 0.1 V(NHE). If the brass sample, in the 0.2 M $Na_5P_3O_{10}$ + 0.05 M $CuSO_4$, was polarized to a potential above the corrosion potential, active dissolution of the sample was observed. The sample was covered with brown corrosion products, and the current reached a maximum of 0.500 V(NHE). Above this potential, loosely adherent white jelly-like corrosion products were observed on the samples, and at the end of the polarization run, the surface of the samples showed generalized corrosion, with preferential grooving along the grain boundaries.

Slow strain rate tests

Parkins' technique of constant potential slow strain rate tests was used for the brass samples in the above phosphorus containing solutions. After fracture, the samples were metallographically sectioned and a mean crack velocity was calculated. No cracking was detected in the pH 10 Na_2HPO_4 solutions after slow straining tests between −0.10 V(NHE) and 0.40 V(NHE). Figure 5 shows the potentials tested and the minimum crack velocities detectable through these experiments. If there was any SCC susceptibility, at the tested conditions the cracks should have propagated at velocities lower than 3×10^{-11} m s^{-1}. The addition of 0.05 M $CuSO_4$, which led to insoluble cupric compounds, had no effect on the SCC susceptibility of brass in the 0.2 M, pH 10.6, Na_2HPO_4 solution.

As shown in Fig. 6, brass suffered SCC in 0.2 M Na_2P_2O- solutions. Cracking was detected at the corrosion potential, −0.100 V(NHE), and the crack velocity increased with the potential increase, up to 0.100 V(NHE). No cracking was found in Na_4P_2O- solutions above 0.100 V(NHE). The specimens strained at −0.100, −0.050 and 0.000 V(NHE), showed abundant intergranular cracking on otherwise clean and uncorroded surfaces (Fig. 7). At 0.050 and 0.100 V(NHE) intergranular cracking was also found (Fig. 8), but generalized corrosion of the surfaces was also observed. At 0.200 V(NHE), on the other hand, generalized corrosion replaced the SCC process, as shown in Fig. 9.

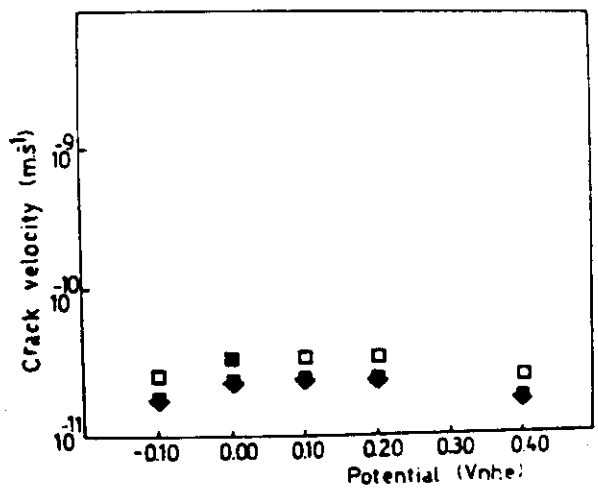

FIG. 5. Constant potential slow strain rate experiments for α-brass in orthophosphate solutions. □ 0.2 M Na_2HPO_4, pH 10.5; ■ 0.2 M Na_2HPO_4 + 0.005 M $CuSO_4$, pH 10.6. No cracks were observed at the end of the tests. The symbols show the minimum crack velocities detectable under the present experimental conditions. Strain rate: 2×10^{-6} s^{-1}. Approximate exposure time: 50 h.

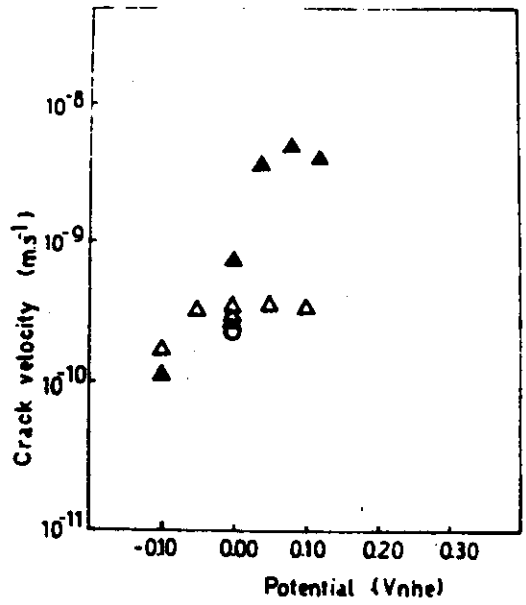

FIG. 6. Crack velocity values measured for α-brass strained in pyrophosphate solutions. △ 0.2 M $Na_4P_2O_7$, pH 10.1; ▲ 0.2 M $Na_4P_2O_7$ + 0.05 M $CuSO_4$, pH 10.1; ○ 0.2 M $Na_4P_2O_7$ + 0.05 M Na_2SO_4, pH 10.3. Strain rate: 2×10^{-6} s^{-1}. At constant potential, the presence of Cu^{2+} ions had no effect on crack velocity.

Figure 6 shows also the effect, on the SCC process, of the addition of 0.05 M $CuSO_4$ to the 0.2 M $Na_4P_2O_7$. To make sure that the effects observed were only due to cupric ions, and not to the sulphate ions, a test was run in a 0.2 M $Na_4P_2O_7$ + 0.05 M Na_2SO_4 solution. The behaviour of brass in this solution was the same as in the 0.2 M $Na_4P_2O_7$ solution.

In the presence of 0.05 M $CuSO_4$, intergranular SCC was found below the corrosion potential, 0.00 V(NHE). Simultaneously with the cracking, copper deposition was observed on the brass surface (Fig. 10), the lower the potential the heavier the deposition. In the experiments run at potentials above the corrosion potential, 0.040, 0.080 and 0.120 V(NHE), intergranular cracking was also found, but in this case the cracking was accompanied by generalized dissolution. The dissolution rate was higher, the higher the potential. In all these cases intergranular cracking was found. Figure 6 shows that the presence of copper ions in the $Na_4P_2O_7$ solution expanded the range of SCC susceptibility, but without changing the cracking rate. The crack velocities found in the copper containing solutions appeared to be an extrapolation of the values found in the absence of copper. By increasing the potential, the crack velocity increased, up to a point where abundant dissolution was observed. Any further increase in the potential produced an increase in the rate of generalized dissolution, without any noticeable changes in the crack velocity.

In a separate set of experiments the effect of varying the Cu^{2+} ion concentration, on SCC susceptibility, was studied. Figure 11 shows the mean crack velocities measured in a 0.2 M $Na_4P_2O_7$ solution with two different Cu^{2+} ion concentrations, 0.05 M $CuSO_4$ and 0.1 M $CuSO_4$, respectively. As shown in Fig. 11, at a given electrode potential, a change in the Cu^{2+} ion concentration had no effect on crack velocity. An increase of the Cu^{2+} ion concentration caused an expansion in the range of potentials where SCC was found, or what is the same, a shift of the potential at which generalized dissolution replaced SCC. As a rule, below the corrosion potential, surface deposition of metallic copper took place simultaneously with cracking

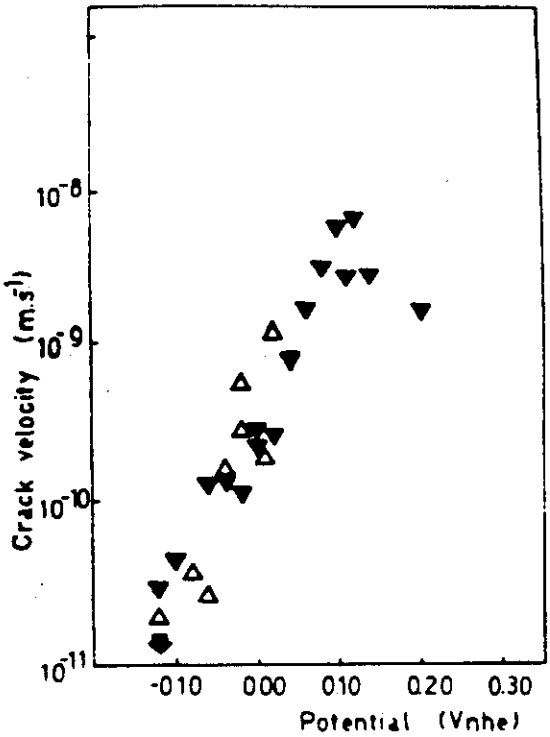

FIG. 11. Effect of Cu^{2+} ion concentration on the crack velocity values measured for α-brass strained in pyrophosphate solutions. △ 0.2 M $Na_4P_2O_7$ + 0.05 M $CuSO_4$, pH 10.1; ▼ 0.2 M $Na_4P_2O_7$ + 0.10 M $CuSO_4$, pH 10.0. Strain rate: 2×10^{-6} s^{-1}. At constant potential, the change in Cu^{2+} ion concentration had no effect on crack velocity.

(Fig. 12), while above the corrosion potential, cracking took place in the presence of generalized dissolution of the alloy (Fig. 13). In every case, the fracture surfaces showed typical intergranular SCC (Fig. 14).

Figure 15 shows the mean crack velocities found for brass strained in a 0.2 M $Na_5P_3O_{10}$ solution, both alone and with the addition of 0.05 M $CuSO_4$. As with the

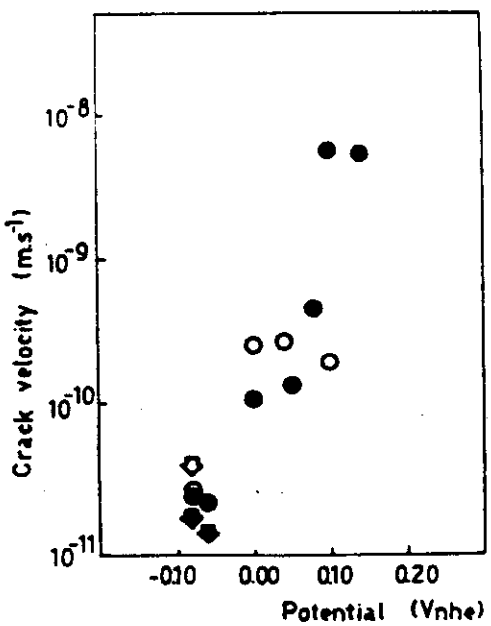

FIG. 15. Crack velocity values measured for α-brass strained in triphosphate solutions. ○ 0.2 M $Na_5P_3O_{10}$, pH 10.0; ● 0.2 M $Na_5P_3O_{10}$ + 0.05 M $CuSO_4$, pH 9.0. Strain rate: $2 \times 10^{-6} s^{-1}$. At constant potential, the presence of Cu^{2+} ions had no effect on crack velocity.

$Na_4P_2O_7$ solutions, intergranular SCC was observed in the $Na_5P_3O_{10}$ solutions. An increase in the potential led to generalized corrosion, and the presence of Cu^{2+} ions expanded the range of SCC susceptibility by increasing the potential at which generalized dissolution started.

DISCUSSION

The present work showed that while brass is immune to SCC in alkaline Na_2HPO_4 solutions, it is susceptible to SCC in both alkaline $Na_4P_2O_7$ solutions and $Na_5P_3O_{10}$ solutions. The stress corroded samples failed by intergranular cracking, and the SCC susceptibility was different for different electrode potentials and Cu^{2+} ion contents of the environment.

Figures 6, 11 and 15 show that the crack velocity, for brass in tri- and pyrophosphate solutions, was potential-dependent up to a certain potential (E_L), different for each solution, above which this dependence was lost. Figures 2 and 3 show that this limiting potential was the potential at which the anodic dissolution reached a value of about 10^{-4} A cm^{-2}. At lower potentials, where the current density was lower, the crack velocity was a function of the potential. On the other hand, at higher potentials, where anodic dissolution was higher, the crack velocity became potential independent. It is also concluded, from Figs 6, 11 and 15 that, at constant potential, the presence of Cu^{2+} ions had no effect on the crack velocity, but it expanded the region of potentials where SCC was found.

Turnbull[17] showed that the potential drop in cracks and crevices, at the corrosion potential, was zero and could increase with the polarization of the sample. At the corrosion potential, the external potential and the potential at the tip of the crack were equal. If the sample was cathodically polarized the IR drop increase was usually small, and there was little difference between the external potential and that at the tip of the crack. On the other hand, when the sample was anodically polarized, leading to the anodic dissolution of the sample, the IR drop showed a sharp increase, and a potential was eventually reached at which further changes in the applied potential had no effect on the potential at the tip of the crack.

The results of the present work, combined with the observations of Turnbull, led to the conclusion that the crack velocity was a function of the potential at the tip of the crack, and that it was affected by the external potential only when those changes were followed by equivalent changes at the tip of the crack.

These observations explain the role of Cu^{2+} ions on the SCC of brass. The addition of Cu^{2+} ions to the $Na_4P_2O_7$ solution and the $Na_5P_3O_{10}$ solution, produced an increase in the corrosion potential. On the other hand, at a given potential, below E_L, the presence of Cu^{2+} ions in the solution had no effect on the crack propagation rate. From the work of Turnbull,[17] it was concluded that the only role of Cu^{2+} ions was to allow higher potential values at the tip of the crack.

Whatever the process, at an atomic level, at the tip of the crack the above observation showed that the process was accelerated by anodic polarization. The simplest explanation seemed to be that anodic dissolution was taking place at the tip of the crack. Nevertheless, this explanation had to be dismissed because of the independence of crack velocity from the Cu^{2+} ion concentration, and because crack propagation was found below the corrosion potential, under conditions where cathodic deposition of copper was taking place.

Another explanation taken into consideration was the surface mobility SCC

mechanism proposed by Galvele.[15] The melting point of the various copper–phosphate compounds was not available, but by comparison with equivalent silver compounds,[14] it seemed reasonable to expect that cupric orthophosphate had a high melting point, while cupric tri- and pyro-phosphates had low melting points. Consequently, as experimentally found, no SCC had to be expected for brass in alkaline Na_2HPO_4 solutions, while SCC susceptibility was to be expected both in $Na_5P_3O_{10}$ solutions and in $Na_4P_2O_7$ solutions.

As for the effect of the electrode potential on crack velocity, two alternative explanations should be considered. It has been reported that surface diffusion, and hence crack velocity, are a function of the surface coverage of the low melting point compound.[15] In aqueous environments, where the low melting point compound is usually formed by anodic reaction of the metal with the environment, an increase in the potential should lead to an increase in coverage, and in consequence an increase in crack velocity. On the other hand, the surface mobility mechanism for SCC[15] assumes that crack propagation takes place by emission of adatoms from the tip of the crack. These adatoms should be similar to those produced in the underpotential deposition of metals. The literature in this field[18] mentions that these adatoms are partly ionized. If this was the case in SCC, the production of those partly ionized adatoms would involve a charge transfer process, and should be favored by anodic polarization. Further experiments will be necessary to test the validity of these two alternatives.

CONCLUSIONS

(1) α-Brass is immune to SCC in alkaline Na_2HPO_4 solutions, while it is susceptible to SCC in alkaline $Na_5P_3O_{10}$ and $Na_4P_2O_7$ solutions.

(2) All the fracture surfaces show intergranular cracks.

(3) The presence of Cu^{2+} ions in the corrosive environment expand the range of potentials where SCC is observed.

(4) At a given potential, the crack velocity is independent of the Cu^{2+} concentration of the corrosive solution.

(5) The Cu^{2+} ions, when present in the solution, cause an increase in the corrosion potential. Since the IR drop in the cracks is zero at the corrosion potential,[17] the result is that the electrode potential attainable at the tip of the crack is higher in the presence of the Cu^{2+} ions, than in their absence.

(6) The present results are better explained by the surface mobility SCC mechanism[15] than by a mechanism based on anodic dissolution.

Acknowledgements—The present research has been supported by the Programa Latinoamericano de Lucha Contra la Corrosión OEA-CNEA, and by the Conseio Nacional de Investigaciones Científicas y Técnicas, Argentina.

REFERENCES

1. M. G. Alvarez, C. Manfredi, M. Giordano and J. R. Galvele, *Corros. Sci.* **24**, 769 (1984).
2. V. K. Gouda, S. M. Sayed and H. A. El-Sayed, *Proceedings of the 9th International Congress on Metallic Corrosion*, Vol. 1, p. 153. National Research Council, Toronto, Canada (1984).
3. R. B. Rebak, R. M. Carranza and J. R. Galvele, *Corros. Sci.* **28**, 1089 (1988).
4. E. Mattsson, *Electrochim. Acta* **3**, 279 (1961).
5. E. N. Pugh, W. G. Montague and A. R. C. Westwood, *Trans. Am. Soc. Metals* **58**, 665 (1965).
6. H. E. Johnson and J. Leja, *Corrosion* **22**, 178 (1966).

7. A. V. BOBYLEV, in *Intercrystalline Corrosion and Corrosion of Metals Under Stress* (ed. I. A. LEVIN), p. 298. Consultants Bureau, New York (1962).
8. R. N. PARKINS and N. J. H. HOLROYD, *Corrosion* **38**, 245 (1982).
9. A. KAWASHIMA, A. K. AGRAWAL and R. W. STAEHLE, in *Stress Corrosion Cracking—The Slow Strain-Rate Technique* (eds G. M. UGIANSKY and J. H. PAYER), p. 266. American Society for Testing and Materials, Philadelphia (1979).
10. H. W. PICKERING and P. J. BYRNE, *Corrosion* **29**, 325 (1973).
11. M. SAENZ de SANTA MARIA and J. C. SCULLY, *Corros. Sci.* **23**, 753 (1983).
12. S. SHIGA and M. HOSHINO, in *Conf. on Environmental Degradation of Engineering Materials in Aggressive Environments*, p. 201. Bracksburg, Vancouver (1981).
13. R. M. SMITH and A. E. MARTELL (eds), *Critical Stability Constants*, Vol. 4, *Inorganic Complexes*. Plenum Press, New York (1976).
14. R. C. WEAST (ed.), *Handbook of Chemistry and Physics*, 54th Edn. CRC Press, The Chemical Rubber Co., Cleveland, Ohio (1973–1974).
15. J. R. GALVELE, *Corros. Sci.* **27**, 1 (1987).
16. D. GILROY AND J. E. O. MAYNE, *J. appl. Chem.* **12**, 382 (1962).
17. A. TURNBULL, *Corros. Sci.* **23**, 833 (1983).
18. K. JÜTTNER and W. J. LORENZ, *Z. Phys. Chem. Neue Folge* **122**, 163 (1980).

Corrosion Science, Vol. 27, No. 6, pp. 631–635, 1987
Printed in Great Britain

0010–938X/87 $3.00 + 0.00
Pergamon Journals Ltd.

SHORT COMMUNICATION

EMBRITTLEMENT OF COPPER BY THE SURFACE MOBILITY MECHANISM

G. L. BIANCHI and J. R. GALVELE*

Departamento Materiales, Comision Nacional de Energía Atómica,
Avda. Libertador 8250, Buenos Aires (1429), Argentina.

Abstract – Experimental evidence supporting the surface mobility mechanism for embrittlement of metals was found. Embrittlement of high purity copper was observed during slow strain rate tests in argon contaminated with CuCl, at 200° C. As reported in the literature such environment substantially increases the surface self-diffusivity of copper.

According to the surface mobility mechanism,[1,2] stress corrosion cracking, liquid metal embrittlement and hydrogen embrittlement of non-hydride forming metals have, at an atomic level at the tip of the crack, a common mechanism. The surface mobility mechanism sustains that crack propagation is due to the capture of vacancies by the stressed lattice, at the tip of the crack. The rate controlling step is the rate of movement of vacancies or adatoms along the surface of the crack. The effect of the environment is to change the surface self-diffusivity of the metal or alloy. The surface mobility mechanism[2] predicts that embrittlement should be observed on tensile stressed metals, at temperatures below 0.5 T_m (T_m being the melting point of the metal, in K), and in environmental conditions that allow high surface mobility.

The aim of the present work is to test the above prediction. Delamare and Rhead[3] studied the surface self-diffusion of high purity copper in the presence of various surface contaminants. They exposed copper samples under conditions where only one monolayer of the surface contaminant was deposited on the metal. To this purpose the contamination of the metal was produced just by the vapour pressure of the contaminating salt present in the same furnace (Fig. 1). Delamare and Rhead found that if in the furnace, the argon atmosphere was contaminated with CuCl, the surface self-diffusivity of copper increases by about four orders of magnitude. The surface mobility mechanism predicts embrittlement of copper, if stressed in argon contaminated with CuCl, at

Manuscript received 9 April 1987.

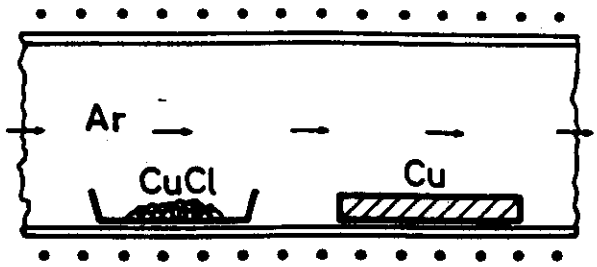

FIG. 1. Experimental method used by Delamare and Rhead[3] for measuring surface self-diffusivity of copper in the presence of various contaminants.

temperatures below 0.5 T_m.

Figure 2 shows the experimental technique used in the present work. Circular section tensile test pieces of 99.999 % copper were slowly strained at 2.3 x 10^{-6} s^{-1}, at 200°C, both in pure argon and in argon contaminated with CuCl. The CuCl used was purified by the same method applied by Delamare and Rhead.[3]

Copper samples strained in pure argon, at 200°C, failed with a reduction in area of 75 to 78 %. Observed under the scanning electron microscope, the fracture surfaces showed dimples typical of a ductile failure. The surface of the samples showed severe plastic deformation. There was no evidence of any type of cracking on the strained samples.

The straining experiments were repeated in a furnace where crystals of pure CuCl were present. In this case the copper samples were exposed to argon contaminated

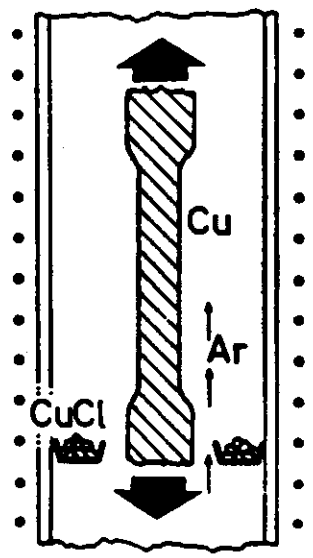

FIG. 2. Slow strain rate experiments with high purity copper in argon contaminated with CuCl vapour, at constant temperature.

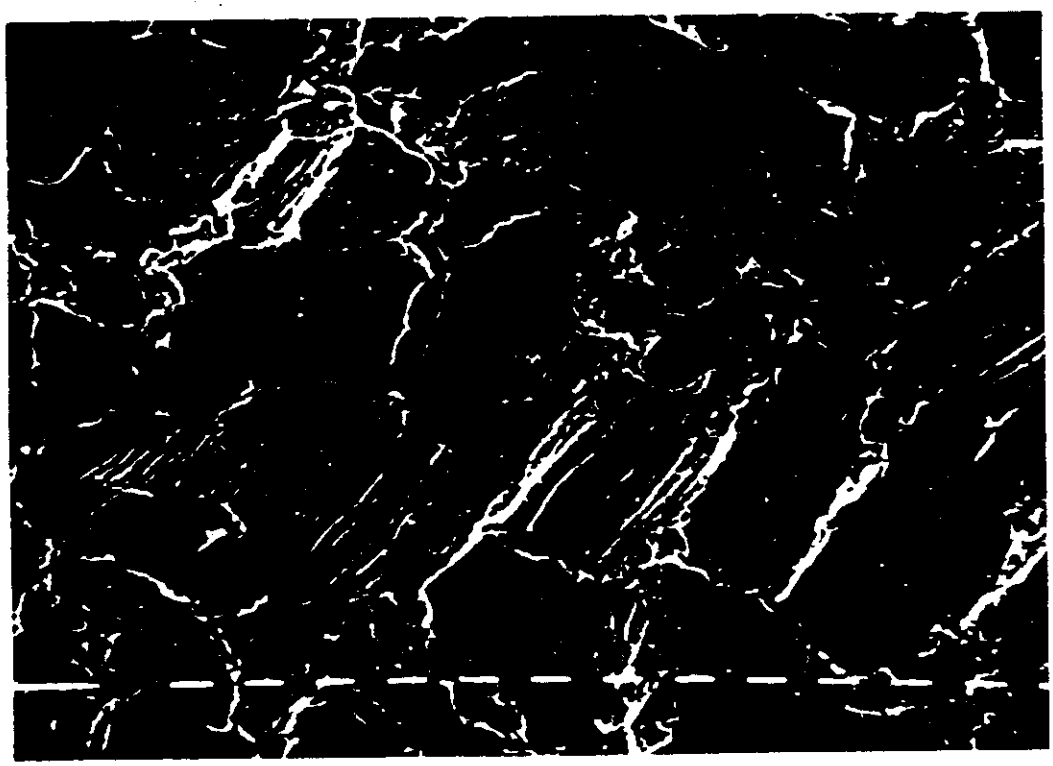

FIG. 3. Intergranular cracks on 99.999 % copper strained in argon contaminated with CuCl vapour. Temperature: 200°C. Strain rate: 2.3 x 10^{-6} s^{-1}. Dashes: 10 µm.

with CuCl vapour. The vapour pressure of the contaminant was that of equilibrium at 200°C. A rough estimate of its value would be 10^{-4} mm Hg.[4,5] These copper samples failed after a shorter exposure time, and the reduction in area observed in these experiments was only between 55 and 59 %. Intergranular cracks were observed on the fracture surface, and abundant cracking was found on the surface of the strained samples. Figure 3 shows the surface of a copper sample strained in argon contaminated with CuCl. The cracks observed were mainly intergranular, but incipient transgranular cracks were frequently found.

The absence of cracks in the samples strained in pure argon indicates that processes like creep cracking were absent at the experimental conditions used in the present work. Cracks like those in Figure 3 are the result of the action of the environment, i.e.: the presence of CuCl vapour. From the work of Delamare and Rhead,[3] such a change in the environment is known to induce a very high increment in the surface mobility of copper. As expected from the surface mobility mechanism for embrittlement of metals, pure copper showed embrittlement in such environment.

Unless the presence of CuCl vapour in argon, at 200°C, has an effect on copper other than that described by Delamare and Rhead,[3] the conclusion of the present work is that the surface mobility mechanism is valid as a metal embrittlement mechanism, and that it could be used to predict the embrittlement susceptibility of metals and alloys in various environments.

Acknowledgements - The present research has been supported by the Programa Latinoamericano de Lucha Contra la Corrosión OEA-CNEA, and by the Consejo Nacional de Investigaciones Científicas y Técnicas, Argentina.

REFERENCES

1. J. R. GALVELE, J. electrochem. Soc. 133, 953 (1986).
2. J. R. GALVELE, Corros. Sci. 27, 1 (1987).
3. F. DELAMARE and G. E. RHEAD, Surf. Sci. 28, 267 (1971).
4. C. J. SMITHELLS and E. A. BRANDES (eds.), Metals Reference Book, 5th edn. Butterworths, London (1978).
5. R. C. WEAST (ed.), Handbook of Chemistry and Physics, 54th edn., CRC Press, The Chemical Rubber Co., Cleveland, Ohio (1973-1974).

Printed in Great Britain

EXPERIMENTAL CONFIRMATION OF THE SURFACE MOBILITY–STRESS CORROSION CRACKING MECHANISM: Ag–15Pd, Ag–15Au AND Ag– 30Cd ALLOYS IN HALIDE AND SULPHATE CONTAINING SOLUTIONS

G. S. DUFFÓ and J. R. GALVELE

Comisión Nacional de Energía Atómica, Departamento Materiales, Avda. del Libertador 8250, Buenos Aires-1429, Argentina

Abstract—The stress corrosion cracking susceptibility of Ag–15Pd and Ag–15Au alloys was studied in 1 M KCl, KBr, KI and Na_2SO_4 solutions. These studies were complemented with measurements on an Ag–30Cd alloy in 1 M KCl, HCl and 10% $FeCl_3$ solutions, where only de-alloying was detected; and on an Ag–15Pd alloy in iodine-saturated organic solvents, where crack velocities similar to those in a 1 M KI solution were measured. The predictions of the surface mobility–SCC mechanism were supported by the present experimental results. De-alloying was found to be either a parallel or a competing process rather than the cause of SCC since de-alloying is dependent on surface mobility.

INTRODUCTION

ACCORDING to the surface mobility–SCC mechanism,[1] environmentally induced crack propagation is due to the capture of vacancies by the stressed lattice, at the tip of the crack. The rate controlling step is the rate of movement of adatoms along the surface of the crack, and the role of the environment is to change the surface self-diffusivity of the metal or alloy. This mechanism predicts environmental embrittlement on tensile stressed metals, at temperatures below 0.5 T_m (T_m being the melting point of the metal, in K), and in environmental conditions that allow high surface mobility.

Correlations between the predictions of this mechanism and the available stress corrosion cracking (SCC) information have already been pointed out.[1] Experimental evidence supporting this mechanism has been reported in four recent publications. Bianchi and Galvele[2] found embrittlement of high purity copper in argon contaminated with CuCl, at 200°C, where high surface mobility had previously been measured.[3] Duffó and Galvele[4] reported the SCC of Ag–Pd and Ag–Au alloys at electrochemical potentials at which low melting point compounds were formed on the alloy surface. By means of this mechanism Manfredi, Maier and Galvele[5] were able to explain the potential-dependent transition from intergranular to transgranular SCC on AISI 304 in $MgCl_2$ solutions. Furthermore, Duffó, Maier and Galvele[6] reported that the dependence on temperature of SCC for AISI 304 stainless steel in LiCl solutions was equal to that predicted by the surface mobility mechanism.

When developing the surface mobility–SCC mechanism,[1] it was pointed out that silver alloys were of high academic interest because of the high number of low melting point compounds to be found in silver. Many of these compounds belong to the

Manuscript received 26 January 1989.

Ag/AgCl reference electrode family, so that abundant literature is available on their electrochemical behaviour.[7] The fact that these silver compounds are sparingly soluble is an additional advantage, because their presence on the corroded surfaces can be confirmed by *ex situ* surface analysis.

The SCC susceptibility of silver alloys is well documented in the literature.[8–13] Unfortunately, to our present interest, the number of environments tested is limited, and no crack velocities have been available.

The electrochemical behaviour of silver alloys has received wide attention in the last few years, either because of the mechanistic interests in the de-alloying processes or because of the possible practical applications of some of the silver alloys in dentistry.[14–18]

In the present work Ag–15Pd, Ag–15Au and Ag–30Cd alloys were studied in various environments. It was found that the predictions of the surface mobility–SCC mechanism,[1] were supported by the present experimental results, and it was also found that de-alloying could either be a parallel or a competing process rather than the cause for SCC, because of its dependence on surface mobility.

EXPERIMENTAL METHOD

The samples used were 0.08 cm diameter wires of Ag–15Pd (at.%), Ag–15Au (a/o), and Ag–30Cd (a/o). The chemical composition of the alloys is given in Table 1.

The specimens of both Ag–15Pd and Ag–15Au were etched for a few seconds in conc. HNO_3 solution, degreased with acetone, annealed for 1 h in argon at 800°C and air cooled. Prior to the measurement the surface of the samples was cleaned by immersion in 50% HNO_3, rinsed with both distilled water and acetone, and dried with hot air. The wires of Ag–30Cd were degreased with acetone, annealed for 1 h in argon at 600°C and air cooled. Previous to the measurements, the Ag–Cd specimens were degreased with acetone and dried with hot air.

Most of the work is based on constant potential slow strain rate tests (SSRT). The cell used was described in a previous paper.[19] The solutions used were 1 M KCl, KBr, KI and Na_2SO_4. They were prepared with analytical grade reagents and bi-distilled water. A few experiments were performed with the Ag–Cd alloy in 1 M HCl, 1 M KCl and in 10% $FeCl_3$ solutions. The electrode potentials were measured through a Luggin capillary with a saturated calomel electrode for the KCl, HCl and $FeCl_3$ solutions, and a

TABLE 1. CHEMICAL COMPOSITION (IN W/O) OF THE ALLOYS USED IN THE PRESENT WORK

	Ag–30Cd	Ag–15Pd	Ag–15Au
Cd	29.4	<0.05	ND
Al	<0.002	<0.002	0.002/0.05
Pb	0.005/0.02	<0.005	ND
Si	0.0005/0.002	~0.0005	~0.005
Fe	<0.002	0.002/0.005	~0.02
Mg	<0.0002	<0.0002	~0.0005
Cu	0.05/0.2	~0.05	0.05/0.2
Pd	ND	15.6	ND
Ir	ND	<0.01	ND
Pt	ND	<0.01	ND
Au	ND	0.003/0.01	24
Sn	ND	ND	<0.005
Cr	ND	ND	<0.002
Ni	ND	ND	<0.005
Ag	balance	balance	balance

ND: Not detected.

mercurous sulphate electrode for the other solutions. All the potentials are reported in the normal hydrogen electrode (NHE) scale. All the experiments were performed at room temperature.

A few slow strain rate experiments were performed in toluene and benzene saturated with iodine, all of them analytical grade reagents.

The intermediate strain rate technique (ISRT)[20] for electrochemical prediction of SCC susceptibility was tested on Ag–15Pd samples strained in a 1 M KCl solution. The strain rates used were 1.6×10^{-2} and $2.2 \times 10^{-3}\ s^{-1}$. The current changes during straining were recorded, and the current density on the freshly exposed metal was calculated. With this value, and by applying Faraday's law, a crack propagation rate (c.p.r.) was calculated. The details of this technique were described in a previous publication.[20]

A LYP Electronica potentiostat and millivoltmeter and a Taccusel EPL2-20G recorder were used for the present work. The solutions were de-aerated in a scrubber connected to the cell. Nitrogen, pre-purified according to the Gilroy and Mayne method,[21] was bubbled through the solution and the cell, and after a 60-min de-aeration period, the solution was introduced into the cell. Afterwards, the specimen was allowed to reach a steady potential for 15 min. Then the chosen potential was applied to the static sample for 15 min while the current was being recorded, and finally the wire was strained to fracture at the desired strain rate. The cell was coupled to the moving grip of the straining machine through a pulley to prevent any new metal surface entering the cell during the stretching of the wires. During the slow strain rate tests an initial strain rate of $2.6 \times 10^{-6}\ s^{-1}$ was used, except for the Ag–30Cd alloy, for which a strain rate of $1 \times 10^{-6}\ s^{-1}$ was used.

After fracture, the specimens were observed under a scanning electron microscope (Philips SEM 500) and then metallographically mounted and sectioned in order to measure the crack depth. From the length of the longest crack and the straining time, a mean c.p.r. was calculated.

The anodic polarization curves were measured potentiokinetically starting from a potential 50 mV lower than the corrosion potential and at a potential scanning rate of 0.5 mV s^{-1}. Before starting the measurements, the samples were allowed to reach a stationary potential by exposition to the solution for 1 h at open circuit potential, under a stream of purified nitrogen. These measurements were performed with a PARC 173 potentiostat with a PARC 175 potential scanner and recorded with a Houston Instrument–*XY* recorder. A conventional three electrode glass cell with a capacity of 80 cm^3 was used.

EXPERIMENTAL RESULTS

Polarization curves

Anodic polarization curves were measured for Ag–15Pd in the KCl, KBr, KI and Na_2SO_4 solutions. Figure 1 shows the anodic polarization curve for the Ag–15Pd alloy in a 1 M KCl solution. For the sake of comparison the polarization curve for pure (99.99%) silver, is also included.

As reported by other authors,[16] the presence of palladium in silver caused a slight increase in the corrosion potential of the alloy (Fig. 1). The shift in the corrosion potential was a function of the halide present in the solution. In the chloride containing solution the shift was 0.05 V, while in the bromide containing solution it was 0.11 V and in the iodide solution 0.17 V.

Above the corrosion potential, the polarization curve showed a current maximum, followed by a low current region and finally a current increase was observed, leading to current density values close to those of pure silver.

The behaviour of Ag–15Pd in a 1 M KCl solution was studied by analysis of both the surface products and the solution. Samples of Ag–15Pd were exposed for 22 h, at constant potential, in a 1 M KCl solution. The potentials chosen were 0.4 and 0.6 V(NHE), the first in the pseudo-passive region, and the second after the second current increase. At the end of the experiments Auger-surface-analyses of the samples were performed and the solutions were chemically analysed. After the exposure at 0.4 V(NHE) no Pd was detectable in the solution, while by Auger analysis surface enrichment of Pd was observed. At 0.6 V(NHE), on the other hand, dissolved Pd was detected in the solution, and the amount of Pd found indicated a

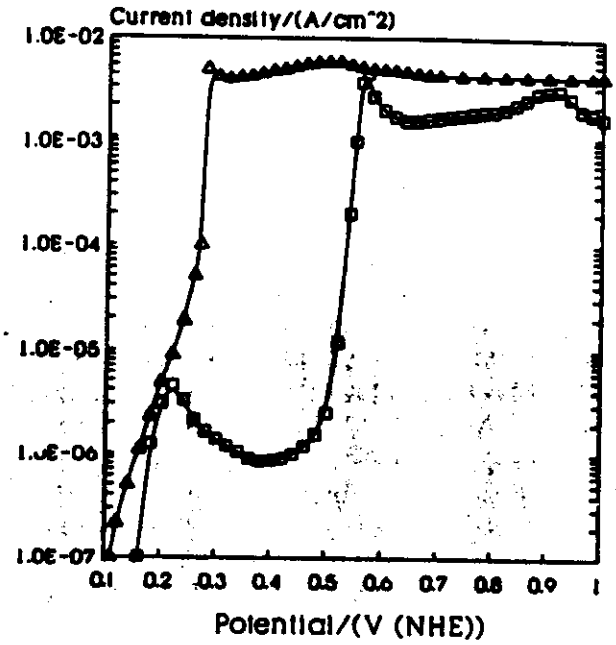

FIG. 1. Anodic polarization curves of Ag–15Pd and Ag 99.99% in 1 M KCl solution. △: Ag 99.99. □: Ag–15Pd.

quasi-stoichiometric dissolution of the alloy. Simultaneous dissolution of silver and palladium was taking place at this potential. These results are coincident with those reported by Rambert and Landolt[14] for Ag–Pd alloys in a 12 M LiCl solution.

The first part of the polarization curve, with surface accumulation of Pd, is a typical region (a), according to Pickering's classification of alloy polarization curves.[22] The current increase observed at higher potentials was probably enhanced by a reaction of the type:

$$Pd + 4\,Cl^- = (PdCl_4)^{2-} + 2e$$

and silver and palladium were simultaneously dissolved, i.e. Pickering's region (c). According to the same author, the combination of region (a) plus region (c) leads to Type II polarization curves. As shown below, Type I polarization curves, i.e. region (a) plus region (b) (selective dissolution) were found for Ag–30Cd and for Ag–15Au, both in a 1 M KCl solution.

By increasing the potential the anodic current increased up to a second plateau where the control was due to the transport of ions across the silver halide film covering the electrode.[23] This type of behaviour was found in all the three halide solutions tested.

The shape of the polarization curves in sulphate solution was different from that found in the halide solutions. In a Na_2SO_4 solution (Fig. 2), the current density above the corrosion potential remained low for a wide potential span, without the presence of current peaks, and afterwards showed a current increase, but not as sharp as in halide solutions.

Figure 3 shows a typical polarization curve for Ag–15Au in a 1 M KCl solution. According to Rambert and Landolt's work,[15] the transition from selective to simultaneous dissolution occurs at 10% of noble metal for Ag–Pd alloys and at above 20% for Ag–Au alloys. Then the current breakdown in Fig. 3 is due to the selective dissolution of Ag, region (b) in Pickering's classification.

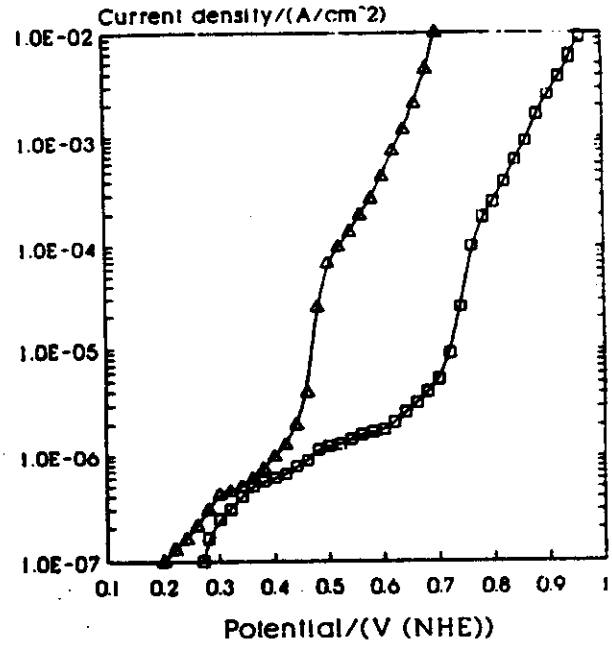

FIG. 2. Anodic polarization curves of Ag–15Pd and Ag 99.99% in 1 M Na_2SO_4 solution. △: Ag 99.99. □: Ag–15Pd.

The polarization curves for Ag–30Cd, in all the solutions tested in the present work, are very similar to those for pure silver. Surface analyses of the corroded samples showed selective dissolution of Cd. This selective dissolution was particularly severe on the strained specimens, as described below.

Slow strain rate tests: Ag–15Pd *alloy in aqueous solutions*

Wire samples of Ag–15Pd alloy were strained to rupture, at constant potential and with an initial strain rate of 2.6×10^{-6} s^{-1}, in 1 M KCl, KBr, KI and Na_2SO_4

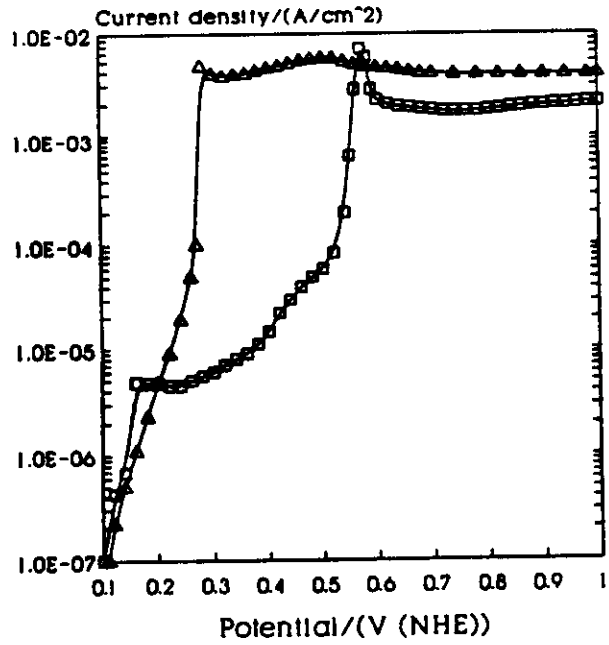

FIG. 3. Anodic polarization curves of Ag–15Au and Ag 99.99% in 1 M KCl solution. △: Ag 99.99. □: Ag–15Au.

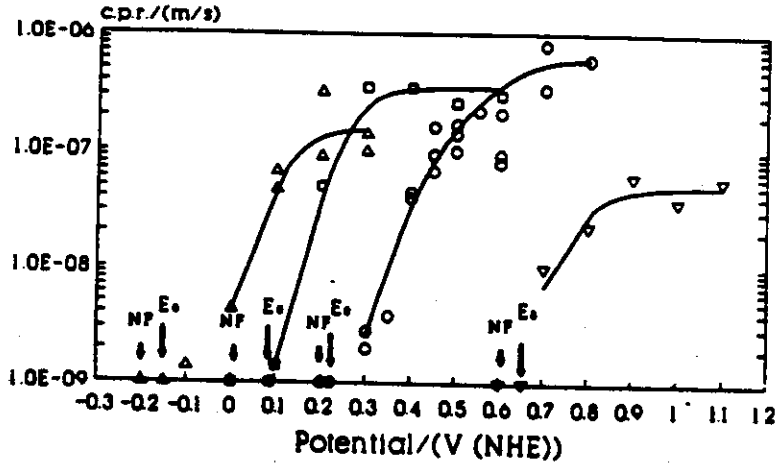

FIG. 4. Crack propagation rate as a function of the electrode potential for Ag–15Pd wires strained in various solutions △: 1 M KI; □: 1 M KBr; ○: 1 M KCl; ▽: 1 M Na_2SO_4. Strain rate 2.6×10^{-6} s^{-1}. E_0: formation potential for the respective silver compound. NF: no cracks detectable after the straining test.

solutions. Stress corrosion cracking was found in all the solutions tested. The crack velocities measured are shown in Fig. 4. The crack velocity was a function of the potential, and decreased with the potential of the sample, as this approached the formation potential of the respective silver compound ($E_{0\,Ag/AgCl} = 0.222$ V, $E_{0\,Ag/AgBr} = 0.087$ V, $E_{0\,Ag/AgI} = -0.150$ V and $E_{0\,Ag/Ag_2SO_4} = 0.653$ V). No cracking was detectable below this potential. When the potential was increased above E_0 the crack velocity increased, reaching its maximum value at an overpotential of *ca* 0.2 V above E_0. Above this potential the crack velocity remained practically constant.

The fracture surfaces showed typical intergranular cracking, as shown in Fig. 5. In a few fractographs traces of an apparently incipient transgranular cracking were detected, but the identification was not conclusive. The fracture surfaces and the surface of the strained wires showed a granular deposit, as shown in Fig. 5. EDAX analysis identified these corrosion products as the respective silver halide or silver sulphate. The density of the coverage of the metal surface by these corrosion deposits was a function of the potential. While at low overpotentials only few isolated crystals of the silver compound were detectable, at high overpotentials the surface of the samples was fully covered by them.

The wires strained at high overpotentials showed extensive cracking and practically no reduction in area. The maximum crack velocities measured ranged from 5.9×10^{-8} m s^{-1} for the 1 M Na_2SO_4 solution up to 7.9×10^{-7} m s^{-1} for the 1 M KCl solution. As shown in Fig. 4, the maximum crack velocities measured were a function of the environment, and the velocities decreased in the following order: 1 M KCl > 1 M KBr > 1 M KI > 1 M Na_2SO_4.

Slow strain rate tests: Ag–15Au *alloy in aqueous solutions*

Since palladium is known to form stable hydrides[24] which could eventually lead to the embrittlement of the Ag–Pd alloy, a separate set of experiments was performed on Ag–15Au wires. The aim of these experiments was to make sure that the above results were not due to a specific action of palladium in the silver alloy.

FIG. 5. Typical example of the intergranular fracture surfaces found in the present work. Ag–15Pd wire strained at constant potential in 1 M KCl solution. Strain rate: 2.6×10^{-6} s^{-1}. Potential: 0.6 V(NHE). Dashes = 1 μm.

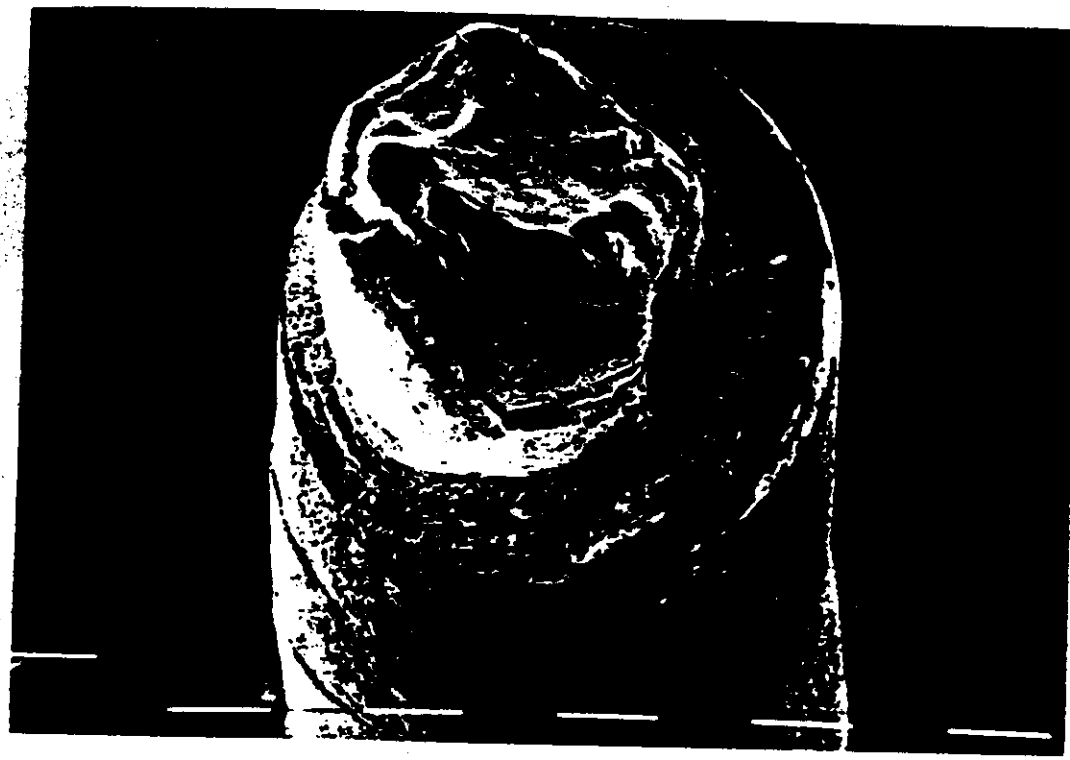

FIG. 7. Typical fracture surface of Ag–30Cd wire strained, at constant potential, in 1 M HCl solution. Cracks are limited to the de-alloyed porous silver layer. Potential 0.770 V(NHE). Strain rate: $1 \times 10^{-6} s^{-1}$. Dashes: 100 μm.

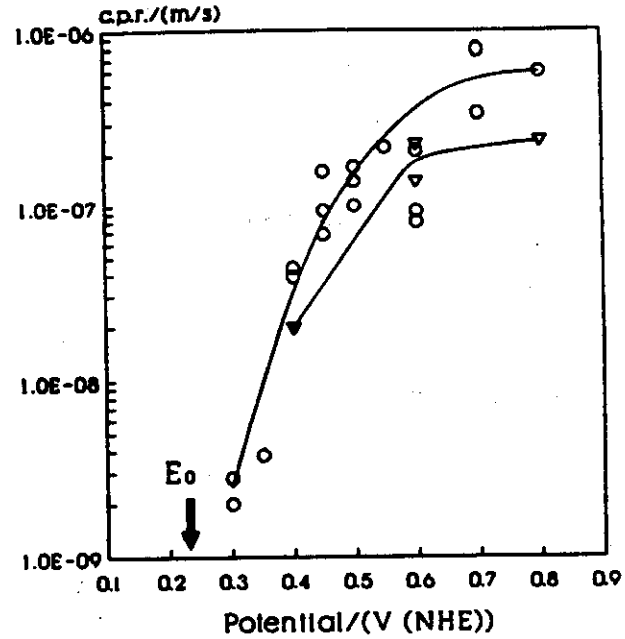

FIG. 6. Comparison of crack propagation rates as a function of the electrode potential for Ag–15Pd (○) and for Ag–15Au (▽) wires strained in 1 M KCl solution. Strain rate $2.6 \times 10^{-6}\,s^{-1}$.

Slow strain rate tests were performed with Ag–15Au wires in a 1 M KCl solution at various potentials. As shown in Fig. 6, the crack velocities observed for Ag–15Au were very similar to those found for Ag–15Pd at the same electrode potential and in the same solution. In separate experiments[25] crack velocities measured with Ag–15Au in various environments, and at various strain rates, were very similar to those found for Ag–15Pd. The fractured Ag–15Au samples showed the same intergranular cracking and an accumulation of silver compounds equivalent to that found with the Ag–15Pd alloy.

Slow strain rate tests: Ag–15Pd *alloy in non-aqueous solutions*

It could be argued that due to the use of aqueous solutions the SCC reported above for Ag–15Pd could be due either to a specific action of the water molecules, or to the entrance of hydrogen into the alloy. To test this possibility a few slow strain rate experiments were performed in non-aqueous solutions.

As a result of the action of the environment, the surface mobility–SCC mechanism requires a low melting point compound to be formed on the metal surface. There is no limitation to the way this compound is formed. It could be formed in a gaseous environment, as reported by Bianchi and Galvele,[2] in an aqueous solution with the compounds formed by an electrochemical reaction as shown above, or in non-aqueous solutions, provided the surface compounds are formed by a chemical reaction.

Evans[26] has shown that silver iodide films grow when silver metal is exposed to the action of iodine dissolved in chloroform. In the present work, toluene and benzene were preferred to the chloride-containing solvent used by Evans. When wires of Ag–15Pd were strained at $2.6 \times 10^{-6}\,s^{-1}$ in pure toluene or in pure benzene, straining was interrupted after 30 h, without traces of cracking. On the other hand, when the Ag–15Pd wires were strained in iodine saturated toluene (approx. 0.14 M I_2) or in iodine

saturated benzene (approx. 0.47 M I_2) the wires broke in less than 2 h straining, and intergranular SCC was found. The corroded samples showed crystals of corrosion products on the surface, which by EDAX analysis were shown to be AgI. The crack velocities found were 7×10^{-8} m s^{-1} in the iodine saturated toluene, and 6×10^{-8} m s^{-1} in the iodine saturated benzene. As shown in Fig. 4, the c.p.r. values found in the non-aqueous solutions were very close to the maximum c.p.r. found in an aqueous 1 M KI solution.

Slow strain rate tests: Ag–30Cd *alloy*

Samples of Ag–30Cd alloy were strained in 1 M KCl, 1 M HCl solutions, at constant potential, and in 10% $FeCl_3$ solution, at open circuit potential, with an initial strain rate of $1 \times 10^{-6} s^{-1}$. Contrary to what was expected from the literature,[8,9,12] no stress corrosion cracking was found for Ag–30Cd in the above mentioned solutions. As shown in Fig. 7, severe de-alloying was observed, and any cracks found were restricted to the de-alloyed region, which, as shown by microprobe analysis, consisted of a thick porous layer of silver. Previous workers must have mistaken the cracks of the de-alloyed layer as stress corrosion cracks.

As shown in Fig. 8, the de-alloying rate, for the Ag–30Cd straining wires, was a function of the potential. It started, as it was the case with SCC, above the equilibrium potential for AgCl formation, and increased with the potential, the de-alloyed front propagation rate being about two orders of magnitude lower than the crack velocity measured for Ag–15Pd under the same experimental conditions. Most probably, as shown by Polan, Popplewell and Pryor,[27] for Cu–Zn alloys, the straining of the wires accelerated the de-alloying process.

Intermediate strain rate tests: Ag–15Pd *in a* 1 M KCl *solution*

The ISRT was found to be very useful in the prediction of SCC susceptibility when anodic dissolution was supposed to be the rate controlling step.[20] In the present work

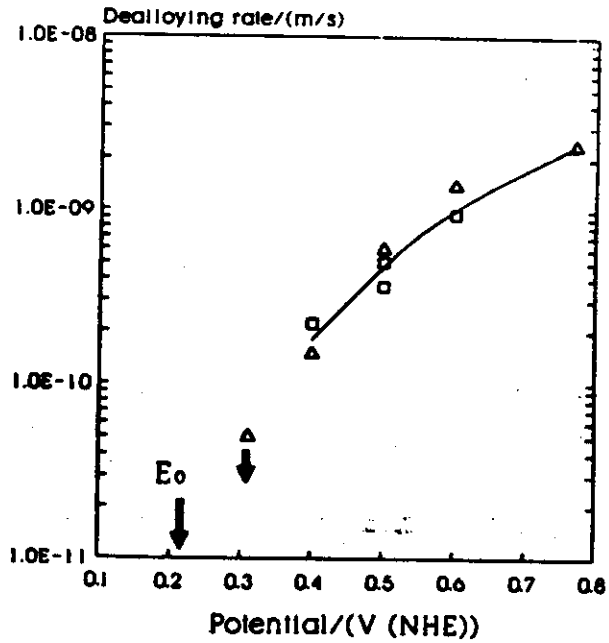

FIG. 8. The rate of de-alloying, under constant potential and slow strain rate, for Ag–30Cd wires strained in 1 M HCl (□) and in 1 M KCl (△) solutions. Strain rate: $1 \times 10^{-6} s^{-1}$. E_0: formation potential for AgCl.

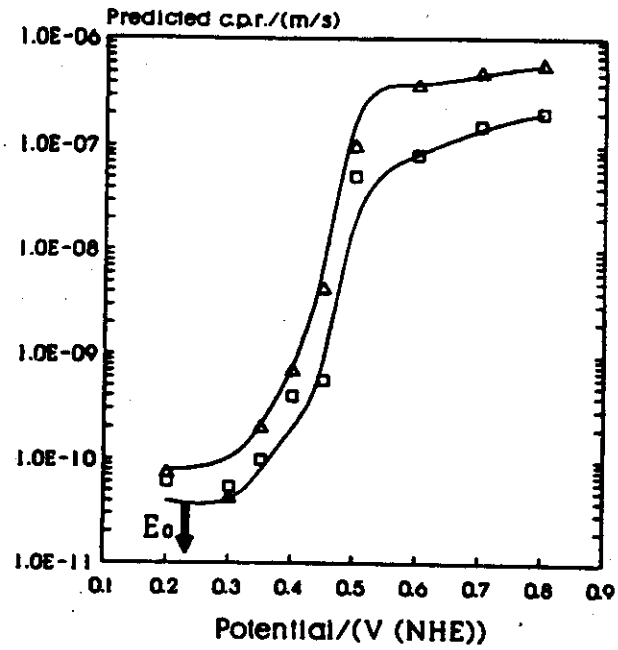

FIG. 9. Crack propagation rates predicted by the Intermediate Strain Rate Technique, for Ag–15Pd in 1 M KCl solution. Strain rates used: △: $1.6 \times 10^{-2}\ s^{-1}$; □: $2.2 \times 10^{-3}\ s^{-1}$. E_0: formation potential for AgCl.

it was applied on Ag–15Pd samples strained in a 1 M KCl solution. The strain rates used were $1.6 \times 10^{-2}\ s^{-1}$ and $2.2 \times 10^{-3}\ s^{-1}$. Figure 9 shows the crack propagation rates predicted by this technique.

Figure 10 shows a comparison between the ISRT predicted values and those measured by the SSRT. While for the maximum c.p.r. values coincidence is found between prediction and measurement, a gross deviation is found at lower potentials.

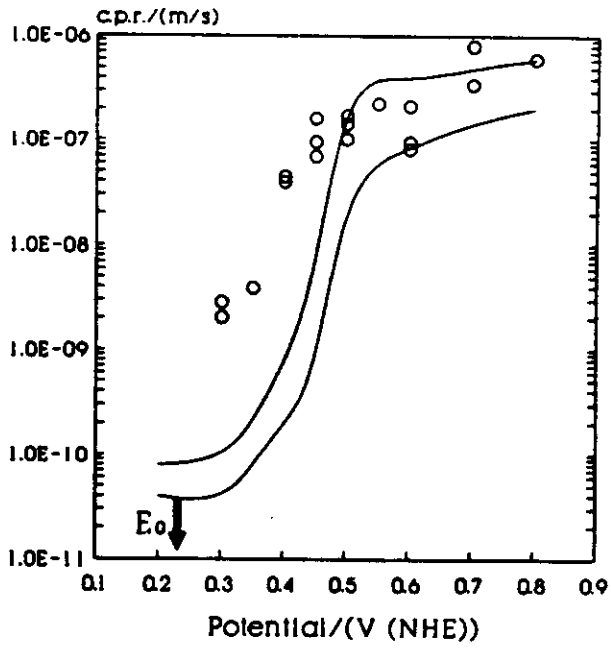

FIG. 10. Comparison between c.p.r. values predicted by ISRT (—) and those measured by SSRT (O). Ag–15Pd in 1 M KCl solution. E_0: formation potential for AgCl. No satisfactory correlation is found between the predicted and the measured values.

At these potentials the ISRT grossly underestimates the c.p.r. values. A similar discrepancy was recently reported for the intergranular SCC of stainless steels in $MgCl_2$ solutions.[5] As was the case with austenitic stainless steel, it was concluded that anodic dissolution does not give an appropriate account of the intergranular SCC of Ag–15Pd in a 1 M KCl solution.

DISCUSSION AND CONCLUSIONS

SCC is frequently associated with de-alloying[22,28] and since the alloys tested in the present work showed different types of dissolution behaviour, to check how such a behaviour correlates with SCC susceptibility would be useful.

Some authors have associated selective dissolution, region (b), with the occurrence of SCC.[22] Figure 11 shows the correlation between the c.p.r. and the polarization curve for Ag–15Pd alloy in 1 M KCl solution. The c.p.r. is observed to start increasing as soon as the electrode potential surpasses the formation potential of AgCl, and it keeps increasing up to a maximum value of about 0.6 V(NHE). This range of potentials encompasses the region (a) of Pd surface enrichment, and the region (c) of simultaneous Ag–Pd dissolution. From Fig. 11 there is no indication that the SCC process was affected by this change in the alloy dissolution behaviour. It seems that the presence of palladium on the alloy surface had no effect on the c.p.r. Most probably it favoured the SCC process by reducing the anodic reaction in region (a). A strong anodic reaction in this region, as it is the case with pure silver (Fig. 1), would compete with the SCC process by blunting the cracks.

A similar conclusion should be drawn for Ag–15Au in a 1 M KCl solution, as shown in Fig. 12. In this case, as mentioned above, selective dissolution is present, region (b). Nevertheless, SCC was found at potentials lower than the breakdown potential. In the present case we are dealing with intergranular SCC, but a similar observation of SCC below the breakdown potential was reported by Lichter *et al.*[29]

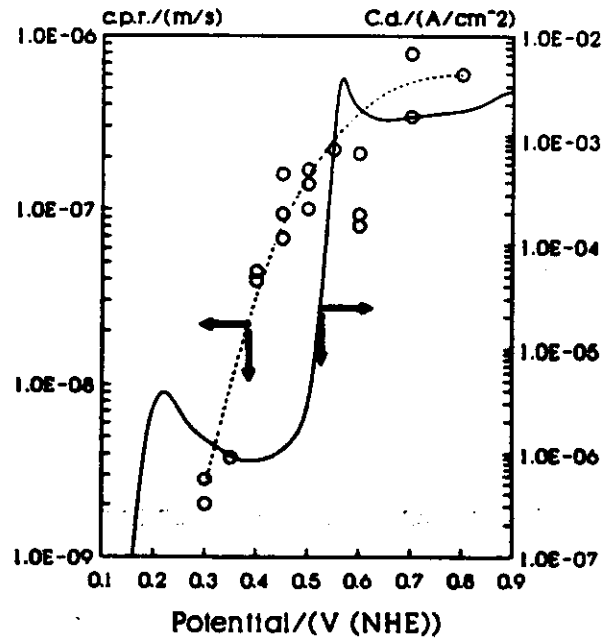

FIG. 11. Correlation between the crack propagation rate (O) and the polarization curve (—) for Ag–15Pd alloy in 1 M KCl solution. SCC was found before the current increase due to simultaneous dissolution (Pickering's region c).

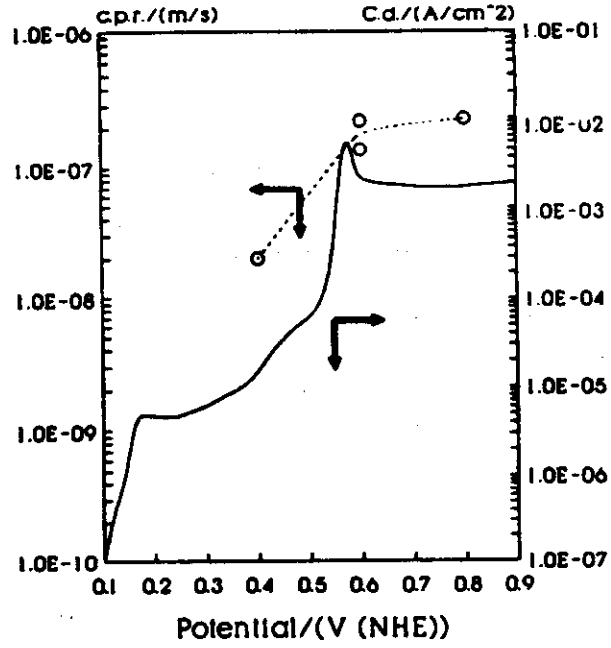

FIG. 12. Correlation between the crack propagation rate (O) and the polarization curve (—) for Ag–15Au alloy in 1 M KCl solution. SCC was found before the current increase due to selective dissolution (Pickering's region b).

for transgranular SCC in Cu–Au alloys. As for Ag–30Cd in a 1 M KCl solution, even though region (b) was present, no SCC was detected in that region.

From the computer modelling of the de-alloying process, made by Sieradzki *et al.*[30] it is evident that surface diffusion is an important step in this process. As predicted by the surface diffusion–SCC model,[1] the solutions used in the present work are those that would give maximum surface mobility to the alloy. If surface mobility is a necessary condition for de-alloying and for SCC, it should be concluded that both will be present either as parallel or as competing processes. From the above results it is concluded that when the enhanced surface mobility is induced for the less noble metal, as it was the case with Ag–15Pd and Ag–15Au alloys, SCC should be expected. On the other hand, if the enhanced surface mobility is induced for the more noble metal, as it was the case with Ag–30Cd alloy, only de-alloying will be found. In this case de-alloying will compete with SCC.

Let us see now how the results of the present work fit with the predictions of the surface mobility–SCC mechanism.[1] From a qualitative point of view the predictions of this mechanism have been satisfied. As shown in Fig. 4, SCC was found only under those electrochemical conditions where low melting point surface compounds, leading to high surface mobility, were formed on the alloy surface. In the case of silver alloys, SCC susceptibility was not a specific property of the alloying element, since it was found in alloys with Pd and with Au. When the alloying metal was less noble than silver, as it was the case with Ag–30Cd, no SCC was found because of the competing action of the de-alloying process.

The importance of the surface compound was shown by the use of iodine-containing non-aqueous solutions. Provided the low melting point compound was present on the alloy surface, no matter how it was produced, SCC took place.

For the demonstration of the validity of the surface mobility–SCC mechanism, the predictions should also be fulfilled at a quantitative level. According to the

surface mobility–SCC mechanism,[1] the crack propagation rate is given by the following equation:

$$\text{c.p.r.} = \frac{D_s}{L}\left[\exp\left(\frac{\sigma a^3}{kT}\right) - 1\right] \tag{1}$$

where D_s($m^2\ s^{-1}$) is the surface self-diffusion coefficient; L is the diffusion path, typically 10^{-8} m; a is the atomic diameter, in m, σ the maximum stress at the tip of the crack, in N m^{-2}, k the Boltzman constant, in J K^{-1}, and T the absolute temperature, in K. The D_s values were estimated with the following equation, based on the publications both of Gjostein[31] and of Rhead:[32,33]

$$D_s = 7.4 \times 10^{-2} \exp - (30T_m/RT) + 1.4 \times 10^{-6} \exp - (13T_m/RT) \tag{2}$$

where R is the gas constant (R = 1.987 cal $mole^{-1}\ K^{-1}$), T the absolute temperature and T_m the melting point of the surface compound, both in K.

In the present work all the c.p.r. measurements were performed at a very low strain rate: $2.6 \times 10^{-6} s^{-1}$. At the same time, the c.p.r. values found were usually very high. This combination of factors led to fractured samples with almost negligible plastic deformation. Consequently it was considered adequate to take for σ the value $\sigma_{0.2}$ = 62.4 MPa measured for the Ag–15Pd samples. The value taken for the atomic size was that for silver $a = 2.88 \times 10^{-10}$ m. As for the D_s values induced by each silver compound, the following melting points were used in eq. (2): AgBr: 432°C; AgCl: 455°C; AgI: 558°C and Ag_2SO_4: 652°C.

From the above values and eqs (1) and (2), the c.p.r. values predicted by the surface mobility–SCC mechanism,[1] were calculated and they are shown in Fig. 13, where they are compared with the maximum c.p.r. values measured in the present work.

As shown in Fig. 13, the surface mobility–SCC mechanism predicts quantitatively the c.p.r. values for Ag–15Pd in 1 M KI and 1 M Na_2SO_4 solutions. For 1 M KCl and 1 M KBr solutions, where higher c.p.r. values were expected, the system seems to have reached a saturation limit. This saturation value is easily explained when the electrochemical reactions taking place inside the cracks are taken into account.

As shown in Fig. 4, and as reported in a previous publication,[4] SCC is found, in each of the environments tested, only above the formation potential of the respective silver compound. This shows that the presence of those low melting point silver compounds is a necessary condition for SCC to occur. Those compounds, in aqueous solutions are formed by the following reaction:

$$n\text{Ag} + \text{X}^{n-} = \text{Ag}_n\text{X} + ne^-. \tag{3}$$

Since these compounds must be present at the tip of the crack, two processes must take place inside the cracks. The first one, as indicated by eq. (3), is a charge transfer reaction, that will start at the equilibrium potential, E_0, and will become faster as the positive overpotential gets higher. The second is the transport, by diffusion and migration, of the X^{n-} ions from the bulk solution to the site inside the crack where the charge transfer reaction is taking place. This site is not necessarily the tip of the crack. It most probably is a few atomic distances away, since the Ag_nX compound can move along the crack by surface diffusion.

The surface mobility–SCC mechanism,[1] requires at least a monolayer of Ag_nX to be present at the tip of the crack. In aqueous solutions the formation of such a

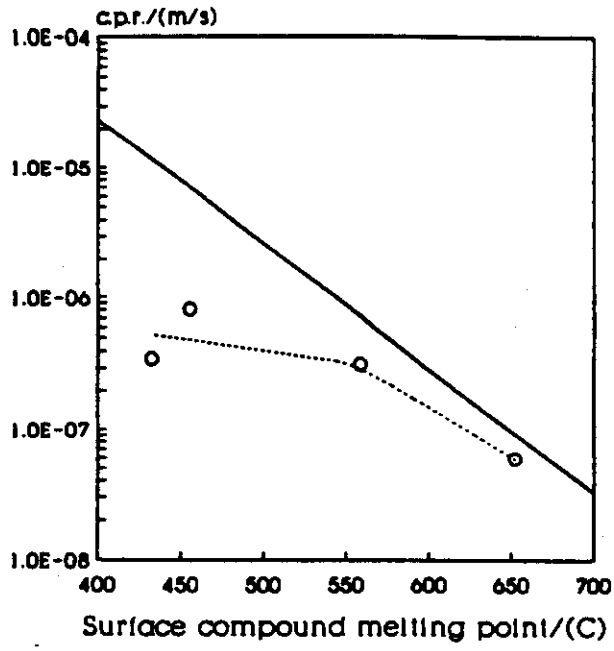

FIG. 13. C.p.r. as a function of the surface compound melting point for silver alloys. σ = 62.4 MPa. Temperature = 25°C. Comparison between the values predicted by the surface mobility–SCC mechanism[1] (—) and the maximum c.p.r. values measured for Ag–15Pd alloy in 1 M KCl, 1 M KBr, 1 M KI and 1 M Na_2SO_4 solutions (○). The measured values follow the predicted values up to the point where diffusion overvoltage becomes the rate controlling step.

monolayer involves the circulation of an anodic current and the transport of X^{n-} ions along the crack. As the crack propagates, it generates some new metal surface to be covered by the Ag_nX monolayer. The higher the c.p.r. the higher the current and the faster the transport of ions required. From electrochemical kinetics[34] it is well known that processes of this type cannot increase without limit, because the diffusion overvoltage becomes the rate controlling step. In other words, in aqueous solutions, the c.p.r. in Fig. 13 will follow the theoretical values only up to a limit above which the process will become limited by diffusion overvoltage.

The equation for diffusion overvoltage is:[34]

$$\eta = \frac{RT}{nF} \ln\left(1 - \frac{i}{i_d}\right) \tag{4}$$

where i_d is the limiting current, which is given by the following equation:

$$i_d = -Z_a\left(1 + \left|\frac{Z_a}{Z_b}\right|\right)\frac{FD_aC_a}{\delta}, \tag{5}$$

Z_a being the charge of the anion and Z_b that for the cation. It was assumed that $Z_a = -1$; and that $|Z_a/Z_b|$ is equal to 1. In the present calculations $n = 1$ and the following conservative assumptions were made to correlate the value of i with that of the c.p.r. It was assumed that only a monolayer of Ag_nX was being formed. Figure 5 showed that thicker layers were formed on the crack surfaces, and hence higher i values were involved. The other conservative assumption made was that $\delta = 0.01$ cm. This is the thickness of the diffusion layer in a stagnant solution, and in the present case it is assumed that this value involves this diffusion layer plus the depth of the crack. Other

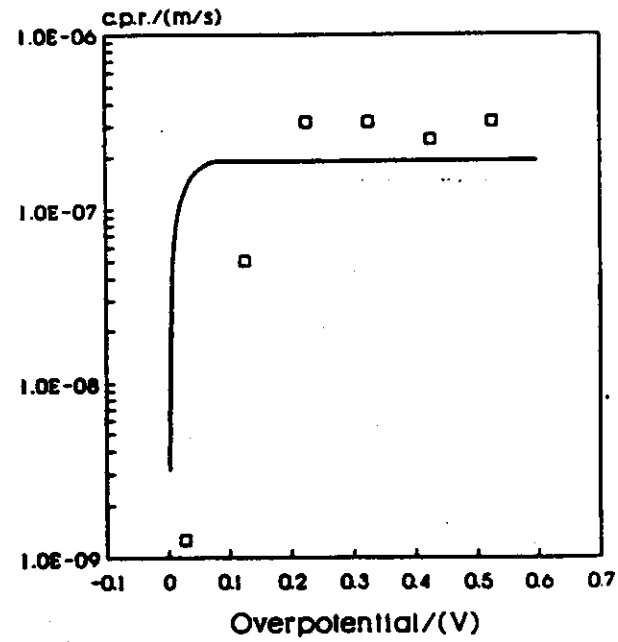

FIG. 14. Maximum crack velocity allowed by diffusion overvoltage (—) compared with the c.p.r. values measured for Ag–15Pd alloy in 1 M KBr solution (□). It is shown that the maximum c.p.r. measured is limited by the diffusion overvoltage.

values considered were: $D_a = 10^{-9}$ m^2 s^{-1} and $C_a = 1$ M. With these values the maximum c.p.r. allowed by diffusion plus migration of X^{n-} ions was calculated, and is shown in Fig. 14, where it is compared with the c.p.r. values measured for Ag–15Pd in a 1 M KBr solution. The results in Fig. 14 confirm that the limiting value observed in Fig. 13 was due to diffusion overvoltage.

The following conclusions are drawn from the present work:

(1) SCC of Ag–15Pd and Ag–15Au in 1 M KCl, 1 M KBr, 1 M KI and 1 M Na_2SO_4 solutions follows the predictions of the surface mobility–SCC mechanism.[1]

(2) The SCC found was not due to a specific action of Pd present in the alloy, since the same crack propagation rates, under the same experimental conditions, were found for Ag–15Pd and Ag–15Au alloys.

(3) SCC was not due to the entrance of hydrogen into the alloy or to the presence of water in the environment, since the crack propagation rates found for Ag–15Pd in iodine saturated toluene or benzene were equal to those in a 1 M KI solution.

(4) No evidence was found of de-alloying being the cause of SCC. Cracking was found in all the three regions of alloy dissolution described by Pickering.[22]

(5) De-alloying and SCC could be parallel or competing processes. When the surface compound induces high surface mobility on the more noble metal, only de-alloying is found, while when the action takes place on the less noble metal, coexistence of de-alloying and SCC could be found. On the other hand, the surface mobility–SCC mechanism,[1] does not require de-alloying for the existence of SCC, a point that was confirmed by the fact that pure metals could show SCC.[2,35]

Acknowledgements—The present research has been supported by the Programa Latinoamericano de Lucha Contra la Corrosión OEA-CNEA, and by the Consejo Nacional de Investigaciones Científicas y Técnicas, Argentina.

REFERENCES

1. J. R. Galvele, *Corros. Sci.* **27**, 1 (1987).
2. G. L. Bianchi and J. R. Galvele, *Corros. Sci.* **27**, 631 (1987).
3. F. Delamare and G. E. Rhead, *Surf. Sci.* **28**, 267 (1971).
4. G. S. Duffó and J. R. Galvele, *Corros. Sci.* **28**, 207 (1988).
5. C. Manfredi, I. A. Maier and J. R. Galvele, *Corros. Sci.* **27**, 887 (1987).
6. G. S. Duffó, I. A. Maier and J. R. Galvele, *Corros. Sci.* **28**, 1003 (1988).
7. D. J. G. Ives and G. J. Janz (eds), *Reference Electrodes. Theory and Practice*, p. 179. Academic Press, New York (1961).
8. L. Graf, in *Proc. Conf. Fundamental Aspects of Stress Corrosion Cracking* (eds R. W. Staehle and A. J. Forty), p. 187. NACE, Houston (1959).
9. N. Ohtani and R. A. Dodd, *Corrosion* **21**, 161 (1965).
10. L. Graf, in *Proc. 2nd Int. Congr. Metallic Corrosion*, p. 89. NACE, Houston (1966).
11. L. Graf and J. Budke, *Z. Metallkunde* **46**, 378 (1955).
12. L. Graf and N. Wieling, *Z. Metallkunde* **63**, 379 (1972).
13. L. Graf, *Z. Metallkunde* **66**, 749 (1975).
14. S. Rambert and D. Landolt, *Electrochim. Acta* **31**, 1421 (1986).
15. S. Rambert and D. Landolt, *Electrochim. Acta* **31**, 1433 (1986).
16. S. Sastri, T. Vaidyanthan and K. Mukherjee, *Metall. Trans.* **13A**, 313 (1982).
17. H. Kaiser and H. Kaesche, *Werks. Korros.* **31**, 347 (1980).
18. T. Vaidyanathan and A. Prasad, *J. Dent. Res.* **60**, 707 (1981).
19. J. R. Galvele, S. M. de De Micheli, I. L. Muller, S. B. de Wexler and I. L. Alanis, in *Localized Corrosion* (eds R. W. Staehle, B. F. Brown, J. Kruger and A. Agrawal), p. 580. NACE, Houston (1974).
20. J. R. Galvele, in *Predictive Capabilities in Environmentally Assisted Cracking* (ed. R. Rungta), p. 273. The American Society of Mechanical Engineers, New York (1985).
21. D. Gilroy and J. Mayne, *J. appl. Chem.* **12**, 382 (1962).
22. H. W. Pickering, *Corros. Sci.* **23**, 1107 (1983).
23. V. Birss and G. Wright, *Electrochim. Acta* **27**, 1439 (1982).
24. H. K. Birnbaum, in *Environment-sensitive Fracture of Engineering Materials* (ed. Z. A. Foroulis), p. 326. The Metallurgical Society of AIME, Warrandale (1979).
25. G. S. Duffó and J. R. Galvele, to be published.
26. U. R. Evans, *The Corrosion and Oxidation of Metals: Scientific Principles and Practical Applications*, p. 774. E. Arnold, London (1960).
27. N. W. Polan, J. M. Popplewell and M. J. Pryor, *J. electrochem. Soc.* **126**, 1299 (1979).
28. K. Sieradzki and R. C. Newman, *Phil. Mag.* **A51**, 95 (1985).
29. B. D. Lichter, W. F. Flanagan, J. B. Lee and M. Zhu, in *Conf. Environment Induced Cracking of Metals*, NACE-ASM, Kohler, Wisconsin (3–7 October 1988).
30. K. Sieradzki, R. R. Corderman, K. Shukla and R. C. Newman, *Phil. Mag.* in press.
31. N. A. Gjostein, in *Surfaces and Interfaces–I* (eds J. J. Burke, N. L. Reed and V. Weiss), p. 271. Syracuse University Press (1967).
32. G. E. Rhead, *Surf. Sci.* **15**, 353 (1969).
33. G. E. Rhead, *Surf. Sci.* **22**, 223 (1970).
34. K. J. Vetter, *Electrochemical Kinetics*, p. 170. Academic Press, New York (1961).
35. K. Sieradzki, R. L. Sabatini and R. C. Newman, *Metall. Trans.* **15A**, 1941 (1984).

Printed in Great Britain

Pergamon Press plc

SHORT COMMUNICATION

SURFACE MOBILITY-STRESS CORROSION CRACKING MECHANISM OF STEELS FOR STEAM TURBINE ROTORS

J. R. GALVELE

Gerencia de Desarrollo, Comisión Nacional de Energía Atómica
Avda. Libertador 8250, Buenos Aires (1429), Argentina

Abstract - Crack velocities measured by Magdowski and Speidel for steels in hot water, covering a wide range of temperatures, Yield Strength and impurity levels, were compared with the Surface-Mobility Stress-Corrosion-Cracking Mechanism predictions. A very good correlation was found between the predicted and the measured values.

According to a recently published Stress Corrosion Cracking (SCC) mechanism, based on surface mobility,[1] metals such as iron, copper, nickel, etc. are susceptible to SCC in high purity water because of their relatively low melting points. Since surface mobility is a function of the melting point of the metal, it was shown that, for the above mentioned metals, surface mobility in hot water is high enough to lead to a measurable crack propagation rate (c.p.r.). This type of failure was called <u>intrinsic SCC susceptibility</u> to distinguish it from SCC induced by specific environments, and consequently called <u>specific SCC susceptibility</u>.[1]

The surface mobility-SCC mechanism,[1] predicts that the c.p.r. will be given by the following equation:

$$c.p.r. = \frac{Ds}{L}\left[\exp\left(\frac{\sigma . a^3}{k . T}\right) - 1\right] \qquad [1]$$

where $D_s(m^2 s^{-1})$ is the surface self-diffusion coefficient; L, the diffusion path, typically 10^{-8} m; a, the atomic diameter, in m; σ, the maximum stress at the tip of the crack, in $N m^{-2}$; k the Boltzmann constant, in $J K^{-1}$; and T the absolute temperature, in K. The D_s values were estimated with the following equation, based on the publications both of Gjostein[2] and of Rhead.[3,4]

$$D_s = 7.4 \times 10^{-2} \exp-(30\ T_m/RT) + 1.4 \times 10^{-6} \exp-(13\ T_m/RT) \qquad [2]$$

where R is the gas constant (R=1.987 cal $mole^{-1} K^{-1}$), T the absolute temperature and T_m either the melting point of the metal (intrinsic SCC) or that of the surface compound (specific SCC), all in K.

The intrinsic SCC of iron can be evaluated through equations

[1] and [2] using the melting point of iron (1539°C + 273) as T_m; a = 2.5 x 10^{-10} m; and T being the water temperature. There could be some uncertainty about the value of σ, particularly when, as in the present work, comparisons are made with fracture mechanics tests. Nevertheless, good correlations have been shown[1] between the values of equation [1] and the c.p.r. values found in zone II of a fracture mechanics c.p.r./K_I curve, when the Yield Strength (Y.S.) values are used for σ.

Magdowski and Speidel[5] have recently published an extensive work on the SCC behaviour of steels in hot water. Their measurements are of particular interest because they give abundant information on the effects of Y.S. and T on the c.p.r. for a wide variety of steels. The authors studied thirteen different steels, including the 3.5NiCrMoV and 2CrNiMo type steels and modern "clean steels", with lower contents of impurity elements. Their study covered more than thirty different Y.S. values, ranging from 614 MPa up to 1420 MPa, and temperatures from below 0°C up to 288°C. They found that alloying and trace elements, like Mn, Si, Mo, Ni, P and S had no influence on the c.p.r. of steels in hot water.

Fig. 1 shows the effect of temperature on the c.p.r. for 600-800 MPa and 1040 MPa steels. The lines show the values predicted by equation [1] for σ values of 700 MPa and 1040 MPa. Fig. 2 shows the experimental and the theoretical values for a steel with Y.S.=1140 MPa. At temperatures below 60°C, a c.p.r. increase due to hydrogen is observed. The effect of hydrogen is accounted for by the surface mobility-SCC mechanism,[1] through appropriate changes in equation [1]. In the case of Fig. 2 the hydrogen effect was calculated using a value of 0.53 for α; nevertheless, hydrogen embrittlement falls outside the scope of the present work.

Magdowski and Speidel found that there are two different effects of Y.S. on c.p.r., a moderate one at low strength levels, and a strong one at high strength levels. The first one is attributed to SCC, while for the second the authors suggest an accelerating effect due to hydrogen. Fig. 3 shows that equation [1] very well predicts the effect of Y.S. on c.p.r., for the first part of the curve. In all the cases studied, the values predicted for 288°C were higher than those measured. This is probably due to an acceleration on the kinetics of the iron oxide film formation process, which would lead to D_s values lower than those predicted by equation [2].

Figs. 1, 2 and 3 therefore prove that equation [1] gives a satisfactory prediction for the SCC of steel in hot water. One

tentative conclusion from this coincidence would be that steels are stress corroded in hot water by a surface mobility mechanism, and that intrinsic SCC susceptibility is involved. A second conclusion is that equation [1] could be a convenient tool for predicting c.p.r. values for regions where no experimental data are available.

REFERENCES

1. J. R. GALVELE, Corros. Sci., 27, 1 (1987).
2. N. A. GJOSTEIN, in Surfaces and Interfaces-I (eds. J. J. Burke, N. L. Reed and V. Weiss), p. 271. Syracuse University Press (1967).
3. G. E. RHEAD, Surf. Sci., 15, 353 (1969).
4. G. E. RHEAD, Surf. Sci., 22, 223 (1970).
5. R. M. MAGDOWSKI and M. O. SPEIDEL, Metall. Trans., 19 A, 1583 (1988).

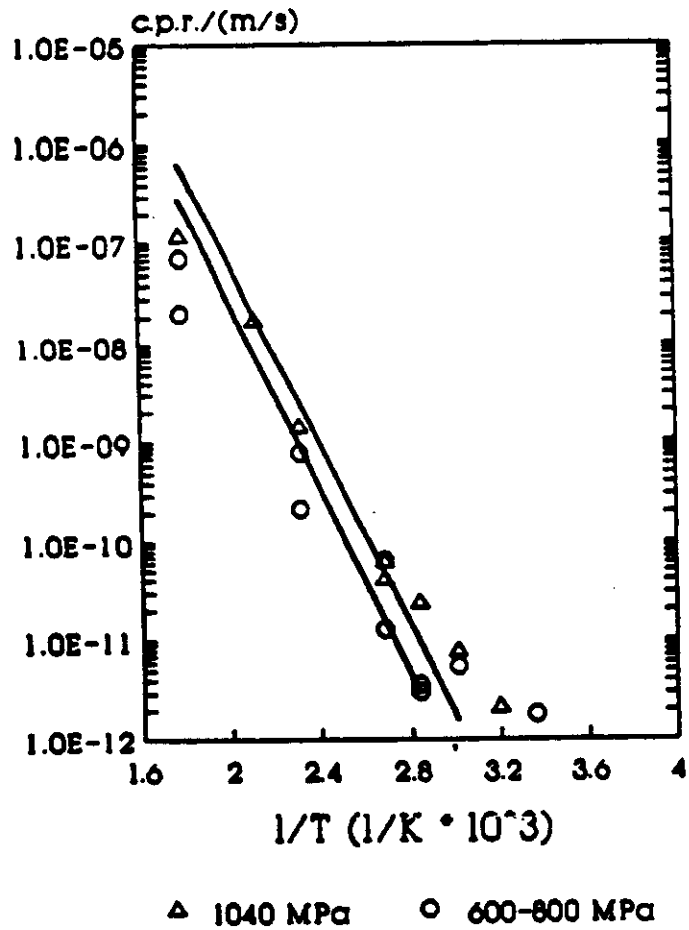

FIG.:1 Effect of temperature on c.p.r.. Points: experimental results by Magdowski and Speidel.[5] Lines: values predicted by Eq.[1]. Upper line: 1070 MPa; lower line: 700 MPa.

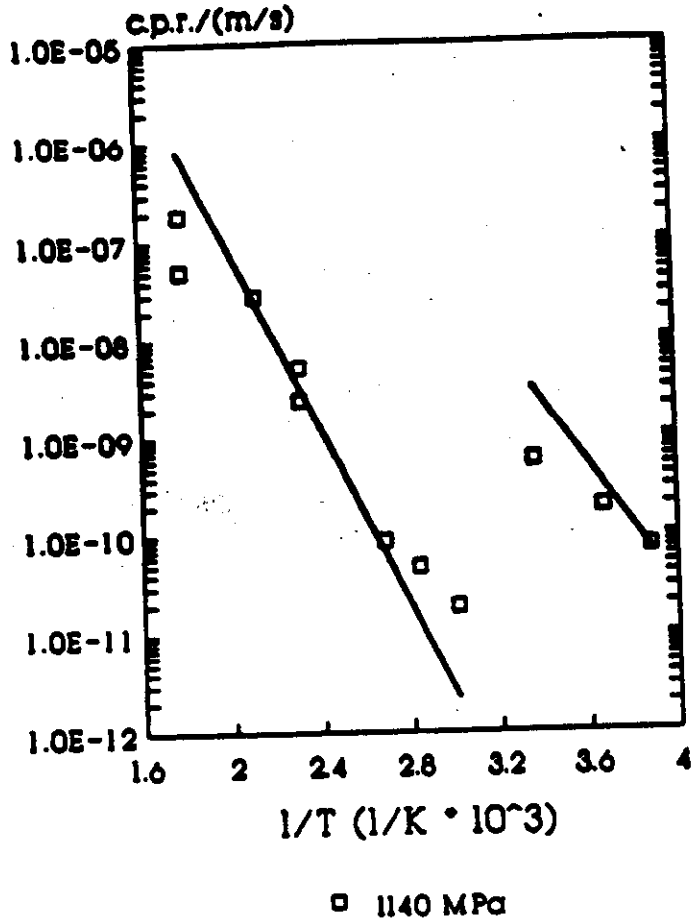

FIG.:2 Effect of temperature on c.p.r. Points: experimental results by Magdowski and Speidel.[5] Lines: values predicted by Eq.(1). High c.p.r. values, at low temperatures, are due to hydrogen embrittlement.

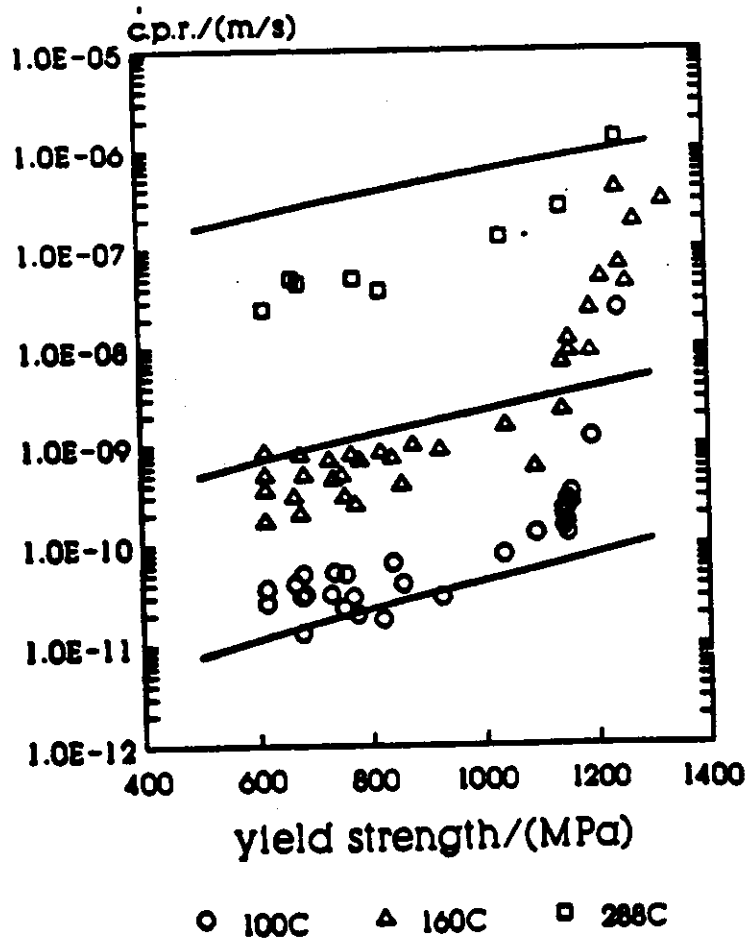

FIG.:3 Effect of Y.S. on c.p.r. Points: experimental results by Magdowski and Speidel.[5] Lines: values predicted by Eq.(1). Deviations are observed for very high Y.S. values and also at 288°C.